Development and Evaluation of Ag-TiO_2 Nano-photocatalysts for the removal of natural organic matter and pharmaceuticals

by

Azar Fattahi

A thesis
Presented to the University of Waterloo
in fulfillment of the
thesis requirement for the degree of
Master of Applied Science
in
Mechanical Engineering

Waterloo, Ontario, Canada, 2019

AUTHOR'S DECLARATION

I hereby declare that I am the sole author of this thesis. This is a true copy of the thesis, including any required final revisions, as accepted by my examiners.

I understand that my thesis may be made electronically available to the public.

Abstract

Increasing the population and growing industries lead to contamination of surface and groundwater and threaten the sustainability of aquatic ecosystems and water resources. Some of the main contributors to water pollution include domestic wastes, industrial discharges, and excess use of pharmaceuticals and personal care products as well as pesticides and fertilizers. The incapability of conventional techniques to remove the contaminants has created a need for innovative water treatment solutions, such as advanced oxidation processes (AOPs).

AOPs are aqueous phase oxidation methods based on the creation of highly reactive chemical species that mineralize organic pollutants. TiO_2 has been widely studied as photocatalysis in AOPs to remove contaminants in water treatment applications. However, the low efficiency under solar irradiation and difficulty in recovering photocatalysis have limited its applications in commercial scale. Doping metals and non-metals to TiO_2 structure is a possible mechanism to increase the efficiency and overcome the limitation of using TiO_2 in water treatment industries.

In the current study, graphene (G) as non-metal and silver (Ag) as a metal dopant were selected to compare the efficiency of photocatalytic reactions of P25 which is the commercial name of TiO_2. It was determined that the rate constant of the reaction using P25-graphene would be 0.36 min^{-1} under the optimum concentration of graphene-oxide 0.48 wt%. However, using the optimum concentration of 1.29 wt% Ag in Ag-doped P25 resulted in a higher rate constant of 1.68 min^{-1}. Thus, P25-1.29 wt% Ag was selected for removal of natural organic matter (NOM) and pharmaceutical compounds.

NOM is the heterogeneous compound formed by the decomposition of microorganisms and their residues in rivers and lakes. These compounds can combine with chlorine in the disinfection process in water treatment plants and form highly carcinogenic byproducts. Photocatalytic degradation of Suwannee River NOM was investigated in this research. P25 and Ag-doped P25 were used as photocatalysis under constant and periodic irradiation of UV and visible light. Total organic carbon (TOC), UV absorbance at 254 nm (UV_{254}) and specific

UV absorbance (SUVA) were used as NOM surrogate parameters to compare the P25 and Ag-doped P25 performance under visible and UV light irradiations. It was found that under the constant illumination of UV light, both P25 and Ag-doped P25 removed about 35% of the TOC in the water matrices, while the removal kinetics was higher using Ag-doped P25. UV_{254} removal for both photocatalysis was about 80% under the UV light. The higher UV_{254} removal than TOC removal illustrates that breaking down the aromatic NOM is more probable using the photocatalysis than mineralizing NOM under the UV light irradiation. Under the visible light irradiation, TOC and U_{V254} removal were about 15% and 20% using both photocatalyst, demonstrating the low efficiency of photocatalytic reactions in removing NOM under the visible light.

The efficiency of Ag-doped P25 and P25 to remove the representative pharmaceuticals in Suwannee River NOM under constant illumination of UV light was compared to visible light. At certain time points, pharmaceuticals were removed from the solution, isolated using solid-phase extraction (SPE) and quantified using liquid chromatography-mass spectroscopy (LC-MS/MS). The removal was measured by comparing the reduction in concentration using the first-order reaction rate constants. Under the UV irradiation, Ag-doped P25 removed o-Atorvastatin, p-Atorvastatin and desvenlafaxine to below the detection limit in 5 minutes. The rate constant of pharmaceutical were higher using Ag-doped P25 than P25. Under the visible light, the rate constants of pharmaceuticals were lower in compare to UV light and there was no significant difference in rate constant of the same compound using P25 and Ag-doped P25.

In summary, this thesis compares the photocatalytic performance of metal and non-metal doped TiO_2 and used the more efficient one (i. e Ag-doped P25) to study the removal of NOM and pharmaceutical compounds from synthetic water solution that mimics wastewater. The irradiation of UV and visible light were compared via constant and periodic illumination. Additional work is required to study the chemistry basis of Ag and TiO_2 behavior in the solutions for better predicting the removal of organic compounds in the water.

Acknowledgements

I would like first to thank my supervisor Professor Y. Norman Zhou for supporting this work and provide the opportunity for me to be part of the Camj group. I want to thank Prof. Mark Servos who granted access to the Water Group to use his laboratory for research and provide supports through valuable discussions.

I would like to thank Dr. Robert Liang for his help and advice during my study. I would like to thank Ivana Jaciw-Zurakowsky, the wonderful teammate and a true friend in the Water Group who trained and helped me in research. I am grateful to Leslie Bragg for all the help in biology lab and in data processing as well as providing the friendly atmosphere for students to work. I would like to thank the co-op students: Sarah kowalczyk, Avnet Kaur and Olivia M. Schneider, for their precious help. An additional thank you goes to NSERC and their support of this project as part of the Strategic Partner Grant.

I would like to thank all my friends in CAMJ and the Servos group in Biology, who kept light perspective on the experience of being a graduate student.

I would like to thank my parents, Maryam and Mohammad, who always encouraged me to follow my dreams and to my brother Arash for the endless love and support.

Finally, I owe a heartfelt gratitude to my husband, Hadi Razmpoosh, who has been a wonderful companion through my studies. Thanks for always believing in me and encourage me to choose what I desire. You always help and uplift my sprit during the tough times and thank you for all the support and love.

Dedication

To my family

List of Figures

Appendices

List of Tables

Appendices

List of Abbreviations

2D: two dimensional

AOP: advanced oxidation process

BET: Brunauer-Emmett-Teller

DBP: Disinfection byproducts

DRS: diffuse reflectance spectroscopy

G: Graphene

GO: Graphene-Oxide

GAC: Granular activated carbon

HMTA: Hexamethylenetetramine or methenamine

HTPA: hydroxyterephthalic acid

HRTEM: High resolution transmission electron microscopy

LC-OCD: Liquid chromatography with organic carbon detection

LED: Light emitting diode

LSPR: Localized surface plasmon resonance

MilliQ: Ultrapure water produced by a Millipore water purification system

NOM: natural organic matter

P25: Standard TiO_2 nanoparticle manufactured by Evonik Degussa

PES: Polyethersulfone

PZC: point of zero charge

ROS: reactive oxygen species

SAED: Selected area electron diffraction

SEM: scanning electron microscopy

SUVA: Specific UV254 absorbance

TEM: Transmission Electron Microscopy

TiO_2: Titanium dioxide

TOC: Total organic carbon

TPA: Terephthalic acid

UV: ultraviolet

UVA: Ultraviolet light between 315 nm and 400 nm

UV_{254}: Ultraviolet light absorbance at 245 nm

UV-LEDs: ultraviolet light emitting diodes

XRD: X-ray diffraction

XPS: X-ray photoelectron spectroscopy

Chapter 1
Introduction

1.1 Background

Population growth is deteriorating the environment in different aspects such as water pollution and drinking water depletion. Lack of clean water resources not only endangers humans but also animals and aquatic species. The conventional water treatment techniques that are being used right now are not capable of removing the different contaminants in the water (e. g. prescription drugs). Moreover, byproducts of the chemicals in conventional treatment techniques with the new man-made compounds can also be harmful and toxic. This makes necessary the development of advanced and innovative treatment approaches to ensure the protection of the environment as well as downstream drinking water intakes.

Advanced oxidation processes (AOPs) are the group of aqueous phase oxidation methods that depend on the production of reactive oxygen species (ROS) such as hydroxyl radicals (·OH) to degrade or destroy the target pollutant. Titanium dioxide (TiO_2) is a semiconductor photocatalyst that is widely used in AOPs based on its chemical stability, environmentally friendly and commercially availability. TiO_2 can produce ROS under the irradiation of light with proper wavelength. The suitable wavelength that resulted in higher TiO_2 photocatalytic efficiency is 385 nm which belongs to the UVA light spectrum [2–5].

In the aqueous medium and in the presence of oxygen species, irradiation of TiO_2 by UV light can excite the electrons to move from the valance band to the conduction band. The produced electrons and holes participate in oxidation and reduction reactions on the surface of the photocatalyst that leads to formation ROS. However, the photo-induced charges can recombine fast and produce energy in the unwanted form like heat. The low efficiency of TiO_2 under the visible light, limit the AOPs in commercial applications in water treatment plants [1, 6].

One way to increase the efficiency of TiO_2 under UV and visible light is by doping it with metal and non-metal elements. Graphene (G) is one of the non-metal dopants that is widely used in photocatalytic applications based on its extraordinary properties such as zero band-gap

energy, large surface area, high electron mobility, and high conductivity. Besides, the low cost and the ease of manufacturing G-based composite materials makes it superior among other carbon allotropes [7-9].

Graphene can enhance the photocatalytic activity of TiO_2 by acting as a 2D surface that helps to create the uniform distribution of loaded TiO_2 nanoparticles in the structure without aggregation. Besides, remarkable electronic properties of graphene would have a positive role in TiO_2 photocatalytic activities. Graphene can prevent the recombination of electron-hole pairs through the formation of heterojunction (Schottky barrier) at the interface of the conjugated π-orbitals of G and TiO_2 conduction band. It can also act as an electron acceptor and trap the excited electrons which reduce the recombination rate by separating electron-hole pairs [10-13].

In addition to non-metallic elements, doping and inserting metallic elements in particular noble metals, can increase the photocatalytic performance of TiO_2. The dispersion of noble metal nanoparticles in semiconductor photocatalysts is known as plasmonic photocatalysis. Noble metals enhance TiO_2 photocatalytic activities by two distinct features: i) acting as electron trap i.e. Schottky junctions, and ii) creating localized surface plasmon resonance (LSPR) which extends the light absorption to the visible light region and improves TiO_2 photocatalytic activity simultaneously [14].

Researchers are interested in using AOPs to remove certain water contaminants from drinking water. Natural organic matter (NOM) and pharmaceutical compounds are two major contaminants in water industries that require the use of novel and advanced techniques for removal. NOM is the mixture of heterogeneous compounds resulted from the decomposition of microorganisms and their residues in rivers and lakes. These compounds are removed in the coagulation step in water treatment plants before the disinfection step. However, the existence of NOM in the disinfection processes can produce carcinogenic and genotoxic by-products. Degradation of NOM using TiO_2 photocatalyst is a multistep process and researchers have found that full decomposition of organic compounds does not happen in the standard time frame normally applied but it can help to degrade the large molecule weight compound to smaller ones [15,16].

Removing pharmaceuticals is another challenge for wastewater treatment plants. Pharmaceuticals are removed in wastewater treatment plants using biological treatments or by activated carbon. However, partial removal of these compounds results in effects on aquatic species i.e. feminizing male fish exposed to the hormones in the birth-controls pills in the rivers and lakes [17-20]. AOPs are attracting attention as a viable option to remove pharmaceuticals from the water. ·OH and superoxide ions ($\cdot O_2^-$) can oxidize and potentially mineralize organic compounds such as pharmaceuticals [17-20]. However, TiO_2 can produce the oxidizing agents under the UV light irradiation and the possibility of solar light as an energy source to start the degradation of NOM and pharmaceuticals in water industry, is still under debate

1.2 Research Objectives

The overall objective of this research was to synthesize the high efficiency TiO_2 based photocatalyst for NOM and pharmaceutical removal under UV and visible light irradiation. Graphene as non-metal and silver as metal dopant to TiO_2 were synthesized using hydrothermal treatment and Ag-TiO_2 was selected for further experiments based on its higher efficiency.

Figure 1-1 shows the brief overview of the research. Chapter 3 is related to improving TiO_2 photocatalytic performance by doping graphene and silver. Chapter 4 and 6 is exploring removal of important water pollutants i.e. NOM (common water parameter) and pharmaceuticals (emerging water pollutant) through use of photocatalysts.

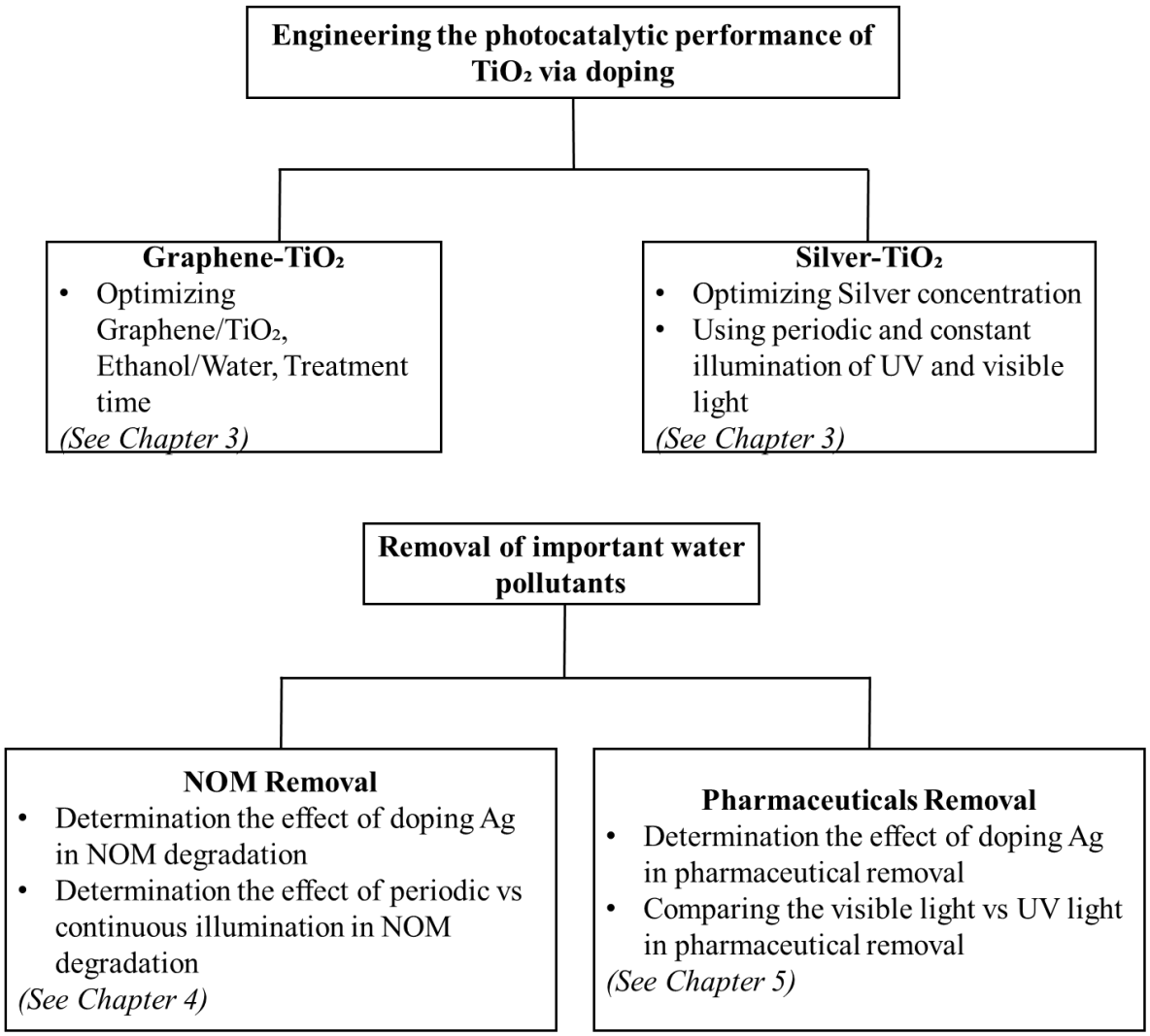

Figure 1-1 Organization framework of research project

1.3 Thesis Organization

This thesis is organized with a literature review and four data/experimental chapters, each describing the major experiments conducted, followed by discussion and analyzing the results and conclusions at the end. A brief overview of each chapter is listed below:

- **Chapter 1. Introduction:** This chapter has an introduction to the thesis and outlines the organization of the thesis.

- **Chapter 2. Literature Review:** This chapter contains a brief introduction to the fundamentals and bases of TiO_2 photocatalysis, doping TiO_2 with graphene and silver, their theory and applications and an introduction about NOM and pharmaceuticals in water and their removal.
- **Chapter 3. Photocatalytic degradation using Ag-TiO_2 and TiO_2-graphene nanocomposite under UV-LED illumination:** This chapter contains the research on doping graphene and silver to improve TiO_2 photocatalytic efficiency under UV and visible light.
- **Chapter 4. Removal of natural organic matter in water using plasmonic photocatalysis under constant and Periodic illumination of UV and visible light:** This chapter outlines the project regarding the removal of NOM from the water using TiO_2 and Ag-TiO_2 and comparetheir efficiency under UV and visible light.
- **Chapter 5. Removal of Pharmaceutical from synthetic water using plasmonic photocatalysis under UV and visible light irradiation:** This chapter outlines the research on removal of pharmaceuticals using TiO_2 and Ag-TiO_2 photocatalysis from synthetic water.
- **Chapter 6. Conclusions and Recommendations:** This chapter includes the general conclusions from and recommendations for future studies.

1.4 Associated Publications

The following publication is associated with this project:

A. Fattahi, R. Liang, A. Kaur, O. M. Schneider, M. J. Arlos, P. Peng, M. Servos, Norman Zhou "Photocatalytic degradation using TiO2-graphene nanocomposite under UV-LED illumination: Optimization using response surface methodology." Journal of Environmental Engineering 7, 103366, 2019
https://doi.org/10.1016/j.jece.2019.103366

Chapter 2 **Literature Review**

2.1 Photocatalysis

In the past decades, photochemistry has not been recognized as science on its own. Up to the beginning of the 20th century, many scientists believed that irradiation behaved in the same way as heating [21]. Giacomo Ciamician was the first scientist who explained the chemical effect of light by separating types of chemical reactions into photochemistry and biochemistry [22]. Further investigations indicated the photochemical reactions as light-forced reactions, while photocatalytic reactions were defined as the group of reactions that accelerate a photoreaction in the presence of a catalyst (Equation. 2-1). However, photocatalysis is being inappropriately used as photoreaction and photolysis [5].

$$\boldsymbol{R + Catalyst \xrightarrow{h\nu} P} \qquad \textbf{(Equation. 2-1)}$$

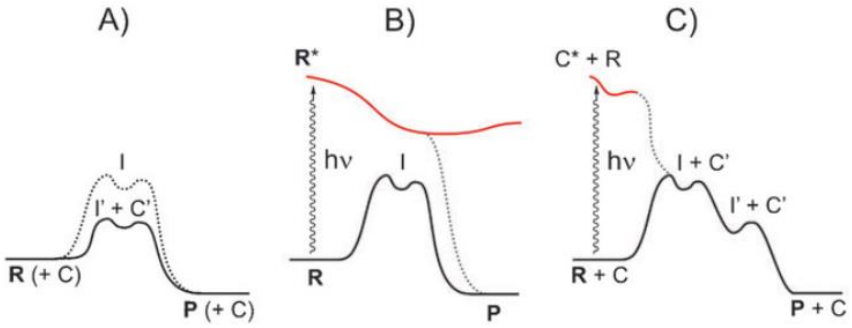

Figure 2-1-1(A) Thermal reaction catalyzed by C via intermediate I`, (B) Photolysis reaction (C) Photocatalyzed reaction [22]

Figure 2-1 illustrates the difference between photolysis and photochemical reactions. Figure 2-1 (A) shows the conversion of reactants (R) to the products (P) using a thermal catalyst. Figure 2-1 (B) shows the photolysis reaction where reagent R actives through the physical reaction e. i. photon energy ($h\nu$) and a reaction occur in the excited surface. In Figure 2-1 (C)

photocatalysts C excites via hv and form C^*. Then it activates the reagent R through chemical reaction i. e. electron transfer and forms I, an intermediate compound such as radical or radical ion. C^* also reacts instantly with R and produces C'. At the end, Intermediate compound, I, transfers to I' and photocatalysts C as well as the product P. So the overall result would be transformation of R to P by absorption of light in the presence of the non-consumed catalyst and spite of photolysis reaction (B), the reaction occurs at the lowest potential surface, the same as thermal reaction [21].

It was considered that photocatalysis could be useful for removing the contaminants in different media including gas, aqueous solution, and pure organic liquid phase. So, they studied extensively by increasing the concerns of water and air pollution. Generally, the photocatalytic reactions happen through the following sections [5, 23]:

1) Transferring the organic contaminants in the aqueous solution to the surface of the photocatalysis
2) Adsorption
3) Reaction in the adsorbed phase (main photocatalytic reaction)
4) Desorption
5) Transferring the product from the interface region

Photocatalysis can be both homogenous and heterogeneous. Meanwhile using heterogeneous photocatalysis i. e solid semiconductors are more common since they are cheaper, stable and recoverable in compare to the soluble ones. When a semiconductor exposes to irradiation possessing higher than their band gap energy E_G ($hv \geq E_G$), the electron would excite in the valance band of the semiconductor and transfer to the conduction band. Thus, holes would appear in the conduction band. Electrons and holes transfer to the surface of the photocatalysis and take part in redox reactions [24]. Figure 2-2 shows the schematics of the photocatalytic reaction.

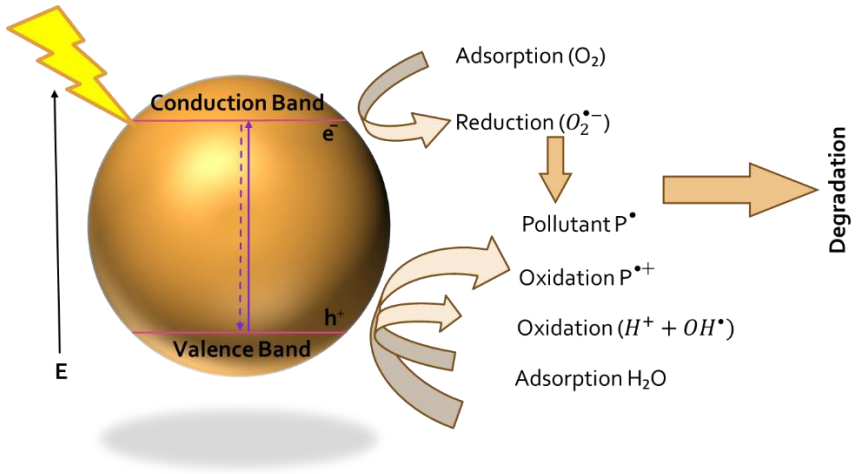

Figure 2-2 Photocatalysis reactions

However, electrons and holes are not lucky enough so stay separately and recombine easily. Fast recombination of electron and holes limit the redox reactions and produce energy in the form of unwanted heat or irradiation. Thus, the long-lived photogenerated charges are responsible for the redox reactions. Scavenged electrons take part in reductive reactions and produce superoxide anions (O_2^-) (Equation 2). Reducible species in the solution can avoid the buildup charge by reacting with electrons [21, 24, 25].

$$\boldsymbol{e^- + O_2 \rightarrow O_2^-} \qquad \textbf{(Equation. 2-2)}$$

Holes in the other hand participate in the oxidative reactions to form very reactive hydroxyl radicals (·OH) (Equation 3) [26]:

$$\boldsymbol{h^+ + H_2O \rightarrow H^+ + \cdot OH} \qquad \textbf{(Equation. 2-3)}$$

According to Table 2-1, ·OH radicals are the main active species in photodegradation reactions that has oxidation power more than most of the oxidants normally used in the water oxidation processes [1]. They decompose organic contaminants by attacking the absorbed contaminant molecules and producing oxidized species. Hydrogen and oxygen atoms in the structure of ·OH radicals form highly reactive species. ·OH radicals react instantly with hydrogen atoms of other compounds and produce harmless products such as H_2O and CO_2 [25, 27].

Table 2-1 Main oxidizing agents used in water treatment with their redox potential [1]

Oxidizing agent	Oxidation potential (V)	Oxidation power*
·OH	2.80	2.06
Ozone	2.07	1.52
Hydrogen peroxide	1.77	1.30
Perhydroxyl radical	1.70	1.25
Permanganate	1.68	1.24
Chlorine dioxide	1.57	1.15
Chlorine	1.36	1
Oxygen	1.20	0.88

* In compare to chlorine's oxidation power which is 1.

The reactivity of ·OH radicals with different water contaminants include bacteria, organic or inorganic compounds, open the new insight in water and wastewater treatment known as Advanced Oxidation Processes (AOPs).

2.1.1 Advanced Oxidation Processes

Conventional water treatment methods like coagulation, precipitation, and biological techniques are not sufficient in removing non-biodegradable organic compounds. The need for secondary treatment and the amount of sludge produced in these processes necessitate the use of more advanced techniques in water purification. Compared to the conventional methods in water treatment, AOP is the process of using different technologies to increase the oxidation power of different contaminants at atmospheric pressure and room temperature. It involves the production of highly reactive ·OH radical species as the strongest oxidant in aqueous media through a combination of chemicals and physical processes shown in Figure 2-3 [1, 6].

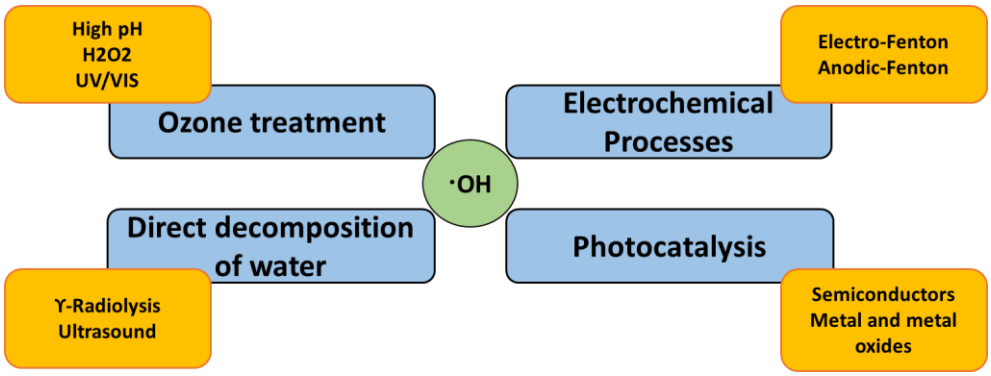

Figure 2-3 ·OH formed through the AOPs

According to Figure 2-3, ·OH can form through the ozone treatment, electrochemical processes, utilizing direct energy source to decompose contaminates and photochemical techniques using semiconductors as photocatalysts [1, 28]. Among the aforementioned methods, metal oxide semiconductors were found as an unparalleled opportunity in water and wastewater treatment due to their suitable band gap position. They can generate ·OH radicals in aqueous medium under UV and visible light irradiation [29]. The photocatalytic efficiency of different semiconductors can compare through the formation of ·OH radicals in the solution. In this regard, Xiang et al, compared the formation of ·OH radicals generated in aqueous media using different semiconductors (Figure 2-4). It was found that among different semiconductors, P25 which is the commercial name of Titanium dioxide (TiO_2) has higher OH-index than other semiconductors, demonstrating that TiO_2 is capable to produce more ·OH radicals and initiate the redox reactions in aqueous media [30].

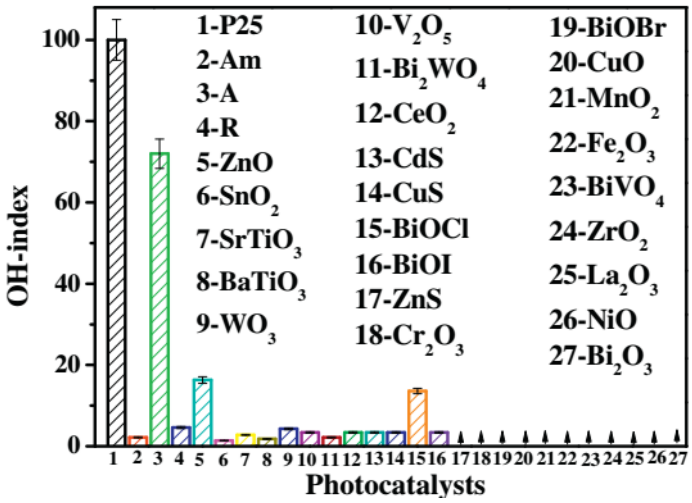

Figure 2-4 Comparison of ·OH-index of various semi-conductors [30]

2.2 Titanium Dioxide

TiO_2 is the most widespread and popular photocatalyst among the semi-conductors. High photocatalytic activity, photo-induced super hydrophilicity, chemical stability are the properties that superior TiO_2 from other semiconductors. These characteristics have been applied in different fields including air and water purification, hydrogen production, metal anticorrosion and antibacterial activity is shown in Figure 2-5 [31].

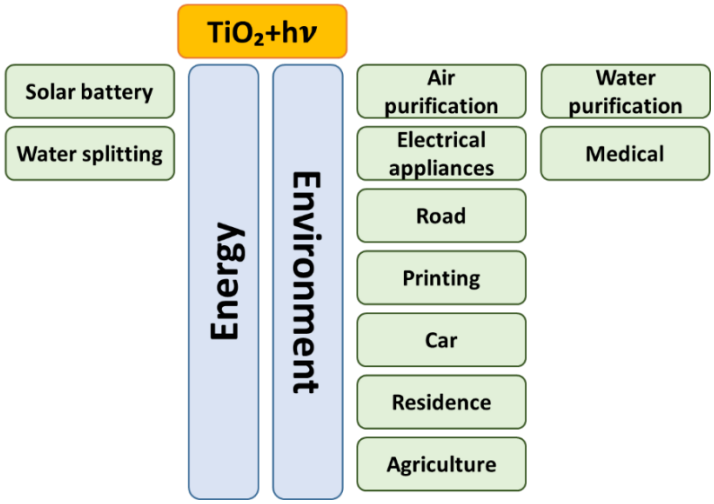

Figure 2-5 Different TiO2 applications in the Environment and Energy field

The photocatalytic properties of TiO_2 are based on the excitation of electrons and holes that happen under the absorption of UV irradiation corresponding to its large band gap. Separated electrons and holes react with electron acceptors and donors that contribute to redox reactions. Equations 2-4 to 2-9 illustrate the reactions that occur in the aqueous solution [2]:

$$TiO_2 + hv \rightarrow TiO_2(e^-_{CB} + hv^+_{VB}) \quad \textbf{(Equation. 2-4)}$$

$$OH^- + hv^+_{VB} \rightarrow \cdot OH \quad \textbf{(Equation. 2-5)}$$

$$O_2 + e^-_{CB} \rightarrow \cdot O_2^- \quad \textbf{(Equation. 2-6)}$$

$$\cdot O_2^- + H^+ \rightarrow \cdot HO_2 \quad \textbf{(Equation. 2-7)}$$

$$2 \cdot HO_2 \rightarrow O_2 + H_2O_2 \quad \textbf{(Equation. 2-8)}$$

$$H_2O_2 + \cdot O_2^- \rightarrow OH^- + \cdot OH + O_2 \quad \textbf{(Equation. 2-9)}$$

UV light can form a superhydrophobic surface on TiO_2 using extra holes. The high portion of the photoinduced holes react instantly with adsorbing water or organic compounds and produce ·OH as explained previously. Yet, there is a small portion of the holes that stuck in oxygen's lattice sites and react with TiO_2, weakening the bonds between the titanium and oxygen ions. Consequently, water molecules intervene in this reaction to produce new OH groups. The new OH groups have high surface energy and are less stable so hydrophilic surface would form (Figure 2-6) [32, 33]. Hydrophilic surface let TiO_2 be useful as self-cleaning and antifogging material for building and mirrors.

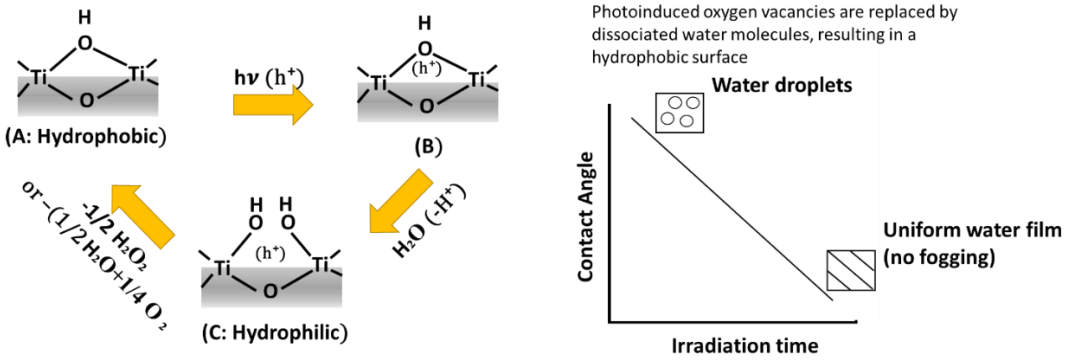

Figure 2-6 Mechanism of photoinduced hydrophilicity [32, 33]

2.2.1 TiO_2 Lattice Structure and Synthesis Methods

Naturally, TiO_2 has three phases: brookite, rutile, and anatase (Figure 2-7) [34]. Brookite has an orthorhombic structure while anatase and rutile have a tetragonal structure. These phases have different photocatalytic activities. Anatase and rutile show higher photocatalytic activity than brookite and are more applicable in environmental remediation. The TiO_2 band gap for different crystal structures is shown in Table 2-2 [35, 36].

Accordingly, anatase has higher bandgap energy than other phases. Higher band gap energy reduces the wavelength of the adsorbed light by anatase which increases the energy level of the valance band to adsorbed higher energy level of redox potential as well as increasing the oxidation power of the electrons and helps the electrons to move faster [36].

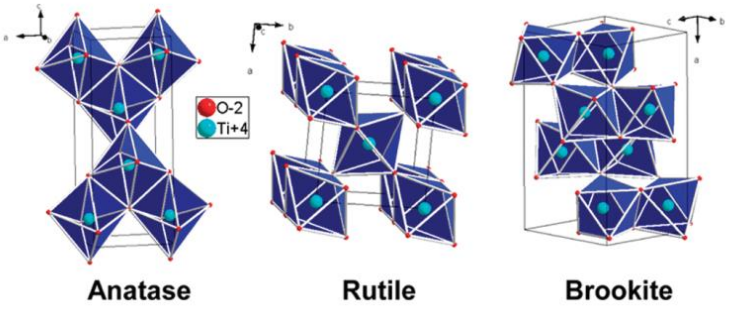

Figure 2-7 TiO_2 phases [34]

Table 2-2 calculated band gap for different phases [36]

TiO_2 phase	Anatase	Rutile	Brookite
Bang gap (eV)	3.20	3.00	3.13

Generally, in photocatalytic researches, P25 is used as the standard of TiO_2 nanomaterials. It's a three mixture of anatase, rutile and amorphous arranged in the complex microstructure, while anatase contains the biggest fraction of about 70% in the mixture. The small size of P25 (21 nm) allows this compound to have high visible light transparency and UV light absorption as well as high adsorption coefficients of the organic compounds on the surface [37-39].

Different methods are available to synthesis TiO_2 nanomaterials including sol-gel, chemical vapor deposition, hydrothermal, spray pyrolysis, etc. Table 2-3 summarize each method with its advantage and disadvantages [40]. In this study, we only focus on the hydrothermal method as it's the facile, inexpensive and environmentally friendly method for the production of different TiO_2 nanomaterials.

Table 2-3 Different TiO2 nanomaterials synthesizing methods

method	Advantages	Disadvantages	Ref.
Hydrothermal	- Simple to operate, reliability, inexpensive - Ability to grow nano to micro size crystals	- The impossibility to observe the crystal as it grows	[41, 42]
Sol-gel	- Simple, homogeny, reliable, reproducible and controllable - Appropriate to deposit on different substrates such as aluminum and stainless steel plates, silica/glass - Adherent to the substrate with complex shapes and large surface to valume	- Costly - High temperature (~ 500 ◦C) and time period required - Thin layer deposition only	[43-46]
Chemical vapor deposition	- Homogenous, pure, repeatable with different rates with high adhesion - Ability to shape differently according to the substrate - Suitable for pipe's inner surface and applicable in different substrates - Ability to coat with other components	- High temperature required - Expensive - Safety issues due to Presence of corrosive gases - Low deposition rates	[47]
Plasma enhanced CVD	- High Adhesion, uniform and low pinhole density - High deposition rate with good mechanical properties - Low temperature require - Applicable for depositing multilayer films - Good step coverage	- Sensitive to temperature - Expensive - High contamination - Safety issue due to toxic by-products formation	[14, 45]

Electrophoretic deposition	- Cheap, homogenous, reliable - High quality including Low porosity and high thickness - Low conductivity and good chemical stability	- Volatile and toxicity - Flammable - High electric field strength - the closeness of suspended particles to the electrodes	[48-50]
Sputtering deposition	- High quality and homogenous film with good adhesion - Easily controllable sputtering speed - suitable for materials with low melting point - convenient manipulation	- High prosity - Plasma contamination - Substrate deterioration due to ionic bombardment	[51]
Spray pyrolysis	- Inexpensive, homogenous with high purity, - Uniform coating in low pressure and temperature - Different substrate applicable - Multilayer fabrication	- Not uniform in thickness	[52, 53]

2.2.2 TiO_2 Energy Band Gap

TiO_2 unique electronic structure is the main reason for its high photocatalytic efficiency among other semiconductors. Semi-conductors possess the empty conduction band and the filled valance band. The distance between the conduction and the valance band is called the band gap. Thus, the requisite energy to stimulate the electrons and transfer them to the conduction band is called the band gap energy (E_{photon}) [54]. The wavelength (**λ**) that provide this energy is related directly to the band gap via Equation 2-10:

$$\boldsymbol{E_{photon} = hc/\lambda} \qquad \textbf{(Equation 2-10)}$$

Substituting the Planck's constant (**h**) by $6.626 \times 10^{-34}\ m^2.k/s$ and light speed (**c**) by 299,792,485 m/s lead us to Equation 2-11 that illustrates the relation between E_{photon} and **λ (m):**

$$\boldsymbol{E_{photon} = 1.98 \times 10^{-25}/\lambda} \qquad \textbf{(Equation 2-11)}$$

When the photons with sufficient energy reach the TiO_2 surface, activation happens. TiO_2 band gap is normally in a range of 3.0-3.2 eV depending on the types of the crystal phases,

corresponds to the wavelength of below 400 nm. In other words, UV light with irradiation lower than 400 nm, can excite the photo-induced charges. The photon energy of 400 nm is equaled to 30,000ºC of thermal energy. This temperature is capable to oxidize all the materials in aqueous media including organic compounds [1].

Meanwhile, UV irradiation that is essential for TiO_2 activation only makes up 5% of the solar energy spectrum, which limits TiO_2 applications under sunlight irradiation. Thus, to utilize the optimum of solar energy, it is desirable to use the semiconductor with the band gap equals 1.35 eV. On the other hand, semiconductors with smaller band gap than TiO_2 are not applicable for water photocatalysis because the photogenerated holes oxidize the semiconductor itself and cause corrosion [3]. In general, in charge generation processes it is necessary to use the semiconductor with a low band gap, thus it can absorb the required photon energy while reducing reflection and scattering of the light [55].

After exciting the photo induced charges, charge separation and recombination are the two phenomena that occur competitively inside the semiconductor. Charge recombination decreases the number of reactive oxidizing agents that produced by emitting light and deactivates the photocatalysts. Efficient charge separation and transportation in the bulk and surface of the semiconductor are essential for photocatalysts in purification processes.

Taking these features into account, there are three essential properties that the semiconductor should have to develop a suitable high- efficiency photocatalytic [55], [56]:

1) Chemical stability
2) Narrow band gap 1.23 eV $<E_g<$ 3.0 eV
3) Highly crystallinity to avoid charges recombination

One of the approaches to increase the absorption spectrum and avoid charge recombination is by doping to create intermediate states and reduce the band gap.

2.2.3 TiO_2 Doping

Doping is the introduction of the foreign atoms to the semiconductor crystal structure. It significantly affects the electronic properties of the semiconductors in the same way as other

defects and imperfections. Generally, doping is divided into n-type and p-type dopants which were defined by the number of outer electrons in dopant. Elements with 3 valance electrons are regarded as p-type, while 5 valance electrons are considered as n-type. P- Doping is more common in the TiO_2 crystals to happen than n doping, as TiO_2 tends to be more oxidative in aqueous media. In other words, the introduction of extra holes is more desirable in TiO_2 crystal structure to decrease the band gap [4, 57].

Figure 2-8 illustrates the reduction in the photocatalysis band gap via metal doping and non-metal doping. $h\nu_1$ is the energy that requires to excite electrons and hole in TiO_2. Metal dopants introduce a new energy level below the conduction band known as the acceptor band and reduce the band gap to the visible light region. In contrast to the metal ions dopants, non-metal ion has less tendency to form donor levels instead, they shift the valance band edge upward and decrease the band gap [55].

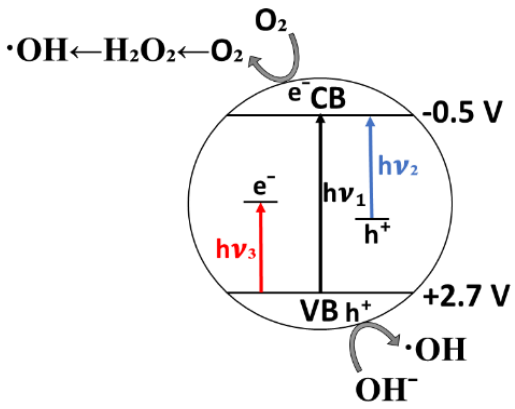

Figure 2-8 TiO_2 dopant with metal ($h\nu_2$) and non-metal dopant ($h\nu_3$)

TiO_2 doping extensively studied by using metal ions including: Al, Ag, Co, Cr, Ce, Er, Fe, Gd, La, Mo, Mg, Os, Pt, Pd, Pr, Rh, Sm, Zn, Zr and non-metal ions including: C, N, S, F, Cl/Br. A list of TiO_2 dopants and preparation methods are explained in Table 2-4.

Table 2-4 Metals and non-metals dopants and preparation methods for doped-TiO_2 photocatalysis

Dopant	Preparation method	Potential application	Ref.
Ag	**Sol gel**: a mixture of $AgNO_3$ and reducing agent ($C_6H_9Na_3O_9$) stirred continuously at 80°C. TIP and HNO_3 added to the solution at 50°C for 24 h (Sol). Sol dried at 105°C for 24 h and calcined at 300°C	Nitrophenol degradation in aqueous media	[58-60]
Fe	**Sputtering deposition**: Ti and Fe with 99.99% purity mixed with Argon and oxygen in the reaction chamber	Wastewater decoloring	[61]
V	**Sol-gel**: a mixture of $C_{10}H_{14}O_5V$ and $C_4H_{10}O$ mixed with a solution containing CH_3COOH in $Ti(OBu)_4$ and hydrolyzed by water generation via CH_3COOH and $C_4H_{10}O$ esterification. The sol dried at 105˚C and then calcined at 400 ˚C for 30 min	Wastewater decoloring	[62]
Au	**Photoreduction/ Sol-gel**: $Ti(OBu)_4$ and ethanol added to $HAuCl_4 \cdot 4H_2O$, CH3COOH and ethanol. The suspension aged for 48 h, dried with vacuum and calcined at 650 ˚C	Wastewater decoloring	[63]
Pt	**Photoreduction**: a mixture of TiO_2, H_2PtCl_6, and methanol irradiated with 125W mercury lamp for 1 h. Pt-TiO_2 separated through filtration and dried up at 100 ˚C for 24 h	Wastewater decoloring	[64]
N	**Oxidation:** Heating TiN at 450-550 ˚C for 2 h in air	Photooxidation of aromatic compounds (e .g. toluene)	[65]
	Sputtering: Annealing anatase TiO_2 in the mixture of 67% NH_3/Ar at 600°C for 3 h	Photooxidation of $C_2H_4O_{(g)}$	[66]
S	**Oxidation:** annealing TiS_2 at 300-600°C	Wastewater decoloring	[67]
N, S	**Sol-gel:** Hydrolysis $Ti(SO_4)_2$ in $NH_{3(l)}$. Gel was centrifuged, washed and dried at 80°C for 10 h in a vacuum and grounded to gain xerogel. The	Volatile compounds photooxidation in the	[68]

	xerogel was calcined at 400-800°C for 3 h in atmosphere	gas phase (e.g. C_3H_6O and CH_2O)	
C	**Sol-gel:** TBOT hydrolyzed with NH_3, ethanol, and water. precipitated TiH_4O_4 was dried at 110°C and calcinated in air at 150-200°C	Degradation of NOx; Wastewater decoloring	[69]
B	**Sol-gel:** Anatase TiO_2 powder was grinding with $C_6H_{15}BO_3$ and calcined in air at 450°C	Photooxidation of C_6H_5OH in the aqueous phase	[70]
P	**Sol-gel:** TIP was hydrolyzed with C_3H_8O and water, and H_3PO_4. Suspension stirred for 2h, centrifuged and dried at 100°C and then calcined at 300°C	C_6H_5OH photooxidation in aqueous media	[71]

The photocatalytic activity of the metal ion dopant is based on its participation as a recombination center or intermediary of interfacial charge transfer. Choi et al. showed that doping with Rh^{3+}, Re^{5+}, Os^{3+}, Ru^{3+}, Fe^{3+} and Mo^{5+} ions effectively enhanced the photocatalytic activity of $CHCl_3$ degradation while doping with Co^{3+} and Al^{3+} reduced the degradation rate. Chen et al also demonstrated that TiO_2 doped with Ni and Fe had higher photocatalytic activity under UV irradiation than TiO_2 alone [72]. However, the photocatalytic activity of the TiO_2-doped under visible irradiation revealed contradictory results. This contrast can be the reason for different operational conditions such as light intensities and chemical parameters like synthesis methods, chemical compounds useful as the probing molecule in the experiments. In this study, we used graphene as non-metal and silver as the metal dopant and exclusively studied the photocatalytic performance of these nanomaterials.

2.2.4 Graphene-TiO_2

Graphene is a popular carbon nanomaterial due to its unique properties. The monolayer, 2D honeycomb lattice of sp^2 bonded carbon atoms creates extraordinary mechanical and electronic properties and makes graphene famous as the strongest and most conductive material known presently [73, 74]. Other than that, graphene has a high specific surface area. The

theoretical specific surface area of individual graphene sheets quantified to be 2630 $m^2.g^{-1}$ [75], which is two times more than the activated carbon uses in water purification [76]. Besides, graphene has a zero-band gap with a work function of -4.42 eV, lower than anatase TiO_2 (-4.40 eV) that ease the excitation of the electrons on graphene's Fermi level of under the irradiation of visible light [77]. This makes graphene a good electron acceptor for TiO_2 while preventing the recombination of electron and holes pairs.

Among graphene's applications, combining graphene with inorganic materials to produce composites or hybrids studied intensively. Graphene can raise TiO_2 photocatalytic properties through the following mechanisms:

1) Graphene's high surface area prepares 2D mats for TiO_2 nanoparticles and facilitates their dispersion while avoiding agglomeration. This property highly affects the application of TiO_2 in water purification and enhance photocatalytic degradation [78]–[80].
2) 2D π-π conjugation net allows great electron mobility (15000 $m^2V^{-1}S^{-1}$) at room temperature. Graphene which is an electron acceptor in graphene-TiO_2 nanocomposite lets the excited electrons to flow at the interface of TiO_2 to graphene. The heterojunction formed at the interface named Schottky barriers separates the excited electron holes pairs and prevents the recombination [81].
3) Zero band gap in graphene offer pre-conditioning for exciting electrons on the Fermi level through infrared and visible irradiation [82].

Figure 2-9 illustrates the mechanism of improving photocatalytic degradation using graphene-TiO_2 nanocomposite. Using graphene would increase the production of ·OH radicals in the aqueous solution and enhance the decomposition of different contaminants.

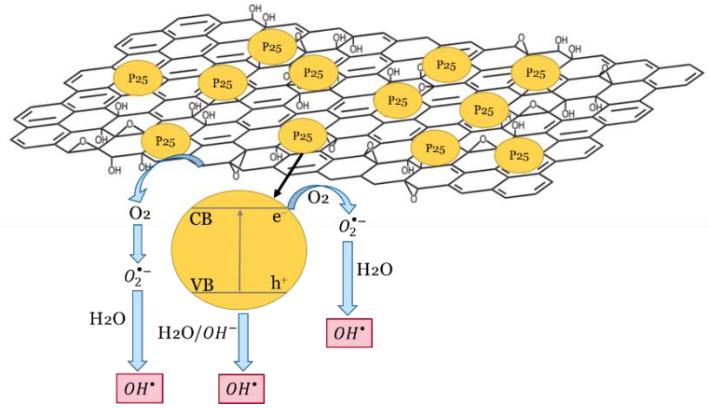

Figure 2-9 Photocatalytic mechanism of TiO_2-graphene

2.2.5 Silver-Titanium Nanocomposite

In addition to non-metallic elements, doping and inserting metallic elements in particular noble metals have a great part in increasing the photocatalytic performance of TiO_2. Dispersion of noble metal nanoparticles into semiconductor photocatalysts known as "plasmonic photocatalysis". Noble metals enhance TiO_2 photocatalytic activities by two distinct features: i) acting as an electron trap (Schottky junctions), and ii) creating LSPR effect which extends the light absorption to the visible light region and improves TiO_2 photocatalytic efficiency simultaneously [83].

The Schottky junctions are the consequence of contacting the TiO_2 and the noble metal. It provides an interior electrical field inside the photocatalyst section and close to the noble metal/semiconductor interface (Figure 2-10). The electrical field provides extra force to move the electrons and holes separately once they created near or inside the Schottky junctions. In other words, Schottky junctions provide a fast path of charge transfer. The interface acts trap centers to activate the reaction sites and participate in the formation of superoxide radical anion ($O_2^{-\bullet}$) [84].

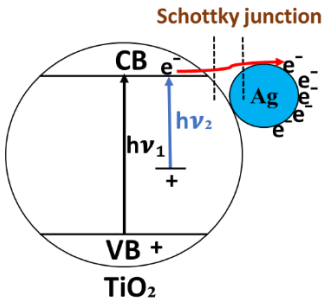

Figure 2-10 Schottky junctions created by doping Ag

The LSPR phenomena happen when the wavelength's frequency suits the resonance conditions of the noble metals. It is explained by the excitation of the conducting electrons with a collective oscillation created by the incident light's electric field. The resulted photoinduced charges form an electrical field near the photocatalytic surface and strongly improves the photocatalyst's visible light adsorption with a low band gap [85].

In addition to the oscillation effect, LSPR can enhance the photocatalytic reactions by generating more charges, heating the neighboring environment that improves reaction kinetics and mass transfer, and also polarizing the non-polar molecule for better adsorption [84]. In the case of Au and Ag, the resonance wavelength can even modify to fall in the visible region depending on the size, shape and local medium [86]. Figure 2-11 shows the LSPR effect in Ag-doped TiO_2.

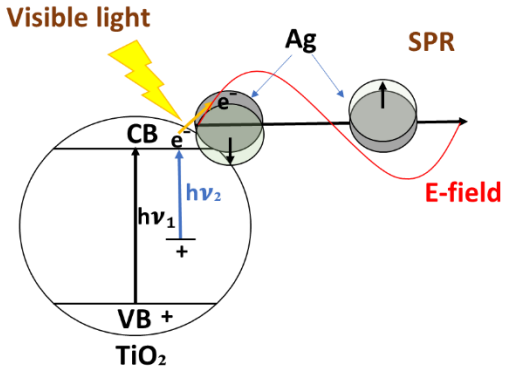

Figure 2-11 LSPR effect under visible light irradiation

Plasmonic photocatalysts have been studied intensively in many fields including surface-enhanced spectroscopy, optics, sensors and bio-sensors, solar cells, medicine, and more recently photocatalytic chemistry for organic molecules decomposition in water treatment [87]. Among the noble metals, Ag is most applicable in water purification due to its high efficiency, corrosion resistance and economically available. In addition to that, silver has antibacterial, anti-mycotic and self-cleaning properties. Silver shows strong cytotoxicity towards a wide range of microorganisms that lead to a bacteriostatic and bactericidal effect [88]. The bactericidal behavior of Ag NPs is related to the LSPR effect that changes the electronic structure of the smaller sized particles on the surface [89].

Figure 2-12 demonstrates the mechanisms of photocatalytic reaction on the surface of Ag/TiO_2 under the UV and visible light illumination. According to Figure 2-12 (a) photo absorption produces strong LSPR at the interface of Ag/TiO_2 which increases the generation of photoinduced charges. Under the UV light irradiation, electrons are excited in the valance band of TiO_2 and transfer to the conduction band where silver captures the free electrons and prevents the recombination of charges. Thus, Holes participate in generating ·OH radicals and electrons generate $O_2^{-\bullet}$. Also, the LSPR effect provides electrons from Ag to TiO_2 via diffusion [88, 89].

Under visible irradiation (Figure 2-12 (b)), electrons generate by the LSPR diffuse to the TiO_2 interface and participate in the generation of $O_2^{-\bullet}$ radicals. The holes that remain in silver from ·OH. Both $O_2^{-\bullet}$ and ·OH play role in photocatalytic degradation of organic molecules [90-92].

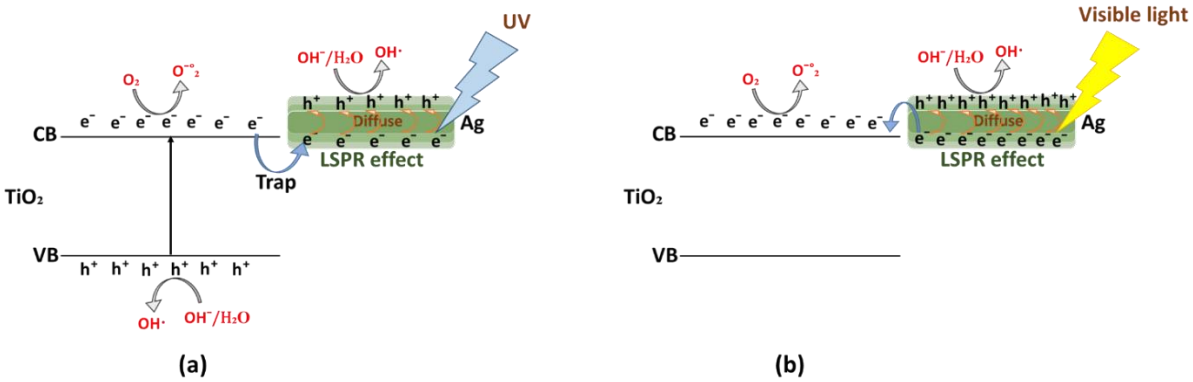

Figure 2-12 Explanation of Ag-TiO_2 mechanism under (a) UV irradiation (b) Visible light irradiation

2.2.6 Kinetics of Photocatalysis

Studies on kinetics of empirical photocatalytic oxidation cannot generalize since each of them provide different reaction rate expressions. Thus, these studies are practical in a limited scope. Table 2-5 illustrates different empirical photocatalytic kinetic expressions.

Table 2-5 Empirical kinetics expression of photocatalytic reaction

Model	Kinetic equation	Eqn	Ref.
Langmuir–Hinshelwood	$r_x = -\frac{kK[X]}{1+K[X]}$	2-12	[93, 94]
Simplified Langmuir-Hinshelwood	$r_x = -kK[X]$	2-13	[95]
Competitive Langmuir-Hinshelwood	$r_x = -\frac{kK[X]}{1+K[X]+\sum_i K_i[Y_i]}$	2-14	[96]
Langmuir-Hinshelwood including light intensity dependence	$r_x = -k'I^n\frac{K[X]}{1+K[X]}$	2-15	[97]
Competitive Langmuir-Hinshelwood including light intensity dependence	$r_x = -k'I^n\frac{K[X]}{1+K[X]+\sum_i K_i[Y_i]}$	2-16	[98]
Langmuir-Hinshelwood including light intensity and humidity dependence	$r_x = -k'I^n[1+f_H([H_2O]-[H_2O]^L)\frac{K[X]}{1+K[X]}$	2-17	[99]
Bimolecular Langmuir-Hinshelwood including light intensity dependence	$r_x = -k'I^n(\frac{K_1[X]}{1+K_1[X]+K_2[H_2O]})(\frac{K_4[H_2O]}{1+K_3[X]+K_4[H_2O]})$	2-18	[100]
Langmuir–Hinshelwood including LVRPA dependence	$r_x = -k'(\int_\lambda e_\lambda d\lambda)^n\frac{K[X]}{1+K[X]}$	2-19	[101]

Quadratic-type	$r_x = -k'[X][O_2](\sqrt{1 + \frac{2\int e^{a}{}_{\lambda} d\lambda}{k'[X][O_2]C_{cat}}} - 1$	2-20	[102]

Results in different experiments show similarities between the photocatalytic degradation rate and Longmuir-Hanshelwood (L-H) kinetics model in Equation 2-12 in Table 2-5. When the concentrations and adsorption constant are low enough (less than 1 mg/L), Equation 2-12 can be simplified to simplified Longmuir-Hanshelwood (Equation 2-13) which known as pseudo-first-order equation [103]. It can rewrite in the following way:

$$\boldsymbol{r_x = ln\frac{C_0}{C} = -kKt = k_{app}t} \quad \textbf{(Equation 2-20)}$$

$$\boldsymbol{C_t = C_0 e^{-k}_{app} t} \quad \textbf{(Equation 2-21)}$$

Where r_x is the reaction rate (mg. l^{-1}.min^{-1}), c and c_0 are the concentration at time t and time 0 (mg.l^{-1}), k is the reaction rate constant (mg. l^{-1}. min^{-1}) and K is the adsorption coefficient of the reactant (l. mg^{-1}). Equation 2-20 shows first-order kinetics, which suits the reactions with low concentrated reactants (ppm ranges). The apparent reaction rate in this model also depends on the initial solute concentrations. Following situations fitted to Equation 2-20 for photodegradation of organic substances [103]:

1) Reactions between two adsorbed compounds
2) Reaction of the adsorbed molecule and a radical species in the solution
3) Reaction between substrate molecule and radicals on the surface in the aqueous media
4) Reactions happen between both of species in the aqueous media

Surface adsorption is necessary for interaction between photo-induced charges and different organic compounds in the solution. Thus, differences in the affinity of adsorption of these compounds can change the reaction rate. ˙OH radicals that are the main active species responsible for the photocatalytic oxidation reactions can act as a reactive intermediate between the organic compound and the photocatalysts. In this case, the reaction rate explains by the rate-limiting step consisting of ˙OH formation or the uniform rate which ˙OH attacks many organics [104].

However, ˙OH has a short lifetime (10^{-9} s) and high activity that prevent its direct diagnosis. Several methods proposed based on introducing the probe molecule in the aqueous solution. The probe molecules reacted with ˙OH and form a quantifiable signal in the long period. These methods include UV/Vis absorption spectroscopy, electron paramagnetic resonance (EPR), and luminescence and fluorescence [30].

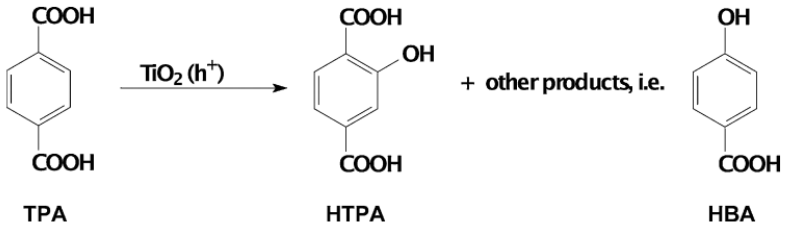

Figure 2-13 Formation of HTPA in a reaction between holes and TPA solution [105]

Terephthalic acid (TPA) is one of the probing molecules that can react with ˙OH and produce a high luminous compound that is used in the detection and measurement of ˙OH. TPA reacts with hydroxyl radical, produces 2-hydroxyterephathalic acid (HTPA) that is the first product of TPA degradation [106]. Figure 2-13 shows the reaction of TPA and TiO_2 and the formation of HTPA. Cernigoj et al. simplified kinetic model for HTPA formation explained in Equation 2-23 [105].

$$\frac{\mathbf{d[HTPA]}}{\mathbf{dt}} = \mathbf{k_1} - \mathbf{k_2}[\mathbf{HTPA}] \qquad \textbf{(Equation 2-23)}$$

Where $[HTPA]$the molar concentration of HTPA, k_1 is is the zero-order HTPA formation rate constant and k_2 illustrates the constant rate of pseudo-first-order of HTPA formation. The difference between k_1 and k_2 is that k_1 belongs to the first minutes of TiO_2 photocatalytic reaction in the TPA solution where the concentration of HTPA is too low and there is an excess of TPA. However, since the concentration of the produced holes and ·OH radicals are constant, it is logical to consider that the HTPA degradation follows pseudo-first-order kinetics [105]. Equation 2-24 is obtained after solving the former equation:

$$[\mathbf{HTPA}] = \frac{\mathbf{k_1}}{\mathbf{k_2}}\left(\mathbf{1} - \mathbf{e}^{-\mathbf{k_2 t}}\right) \qquad \textbf{(Equation 2-24)}$$

2.3 Natural Organic matter

2.3.1 Characteristic of NOM

Natural Organic Matter (NOM) refers to the heterogeneous mixture of carbon-based compounds that form during the decomposition of plants and animal matter. It is abundant in surface water where highly variable in size (from small molecules to macromolecules) and reactivity. Proteins, amino acids, polysaccharides, humic and fulvic acids are the examples of NOM. The concentrations of individual NOM compounds change in different sources and are influenced by the characteristics of the watershed, seasonal changes in temperature and precipitation, long term climate changes and human and animal activities [107].

In addition to the health-related problems, the existence of NOM has a negative effect on the operating unit in water treatment plants. From an aesthetic point of view, NOM can change the water smell, taste, and color. It can cause membrane fouling that engages with a reduction in permeability and increases the backwashing steps which increase the costs. Also in UV disinfection, NOM would cut the UV absorbance in the water and exerting chlorine demand [107].

Although the NOM itself doesn't have any risk to human health, the byproducts of NOM reaction with disinfectants in water treatment plants known as disinfection byproducts (DBPs) are hazardous for human health and are one of the targets in the modern water treatment plants. The presence of NOM in disinfection step, cause the reaction with chlorine and other oxidants and produce halogenated highly carcinogens and teratogens compounds such as Trihalomethanes (THMs) and haloacetic acids (HAAs) [108].

NOM divided into hydrophobic and hydrophilic fractions. The hydrophobic or humic fraction is highly aromatic, it has high molecular weight and large size and is less soluble in water. Therefore, it can easily remove by coagulation even with a low dosage of coagulants. Humic acid and fulvic acid are in this category. Humic acid has dark brown or black and is poor in nitrogen. On the contrary, the hydrophilic or non-humic fraction is less reactive and rich in nitrogen. It consists of carbohydrates, lipids, hydrophilic acids, and amino acids. According to

the researches, non humic fraction reacts with chlorine and produce the THMs in the same way as humic fractions. Each of NOM fractions divided into acidic, alkaline and neutral subgroups [109, 110]. Figure 2-14 summarizes the classification of NOM.

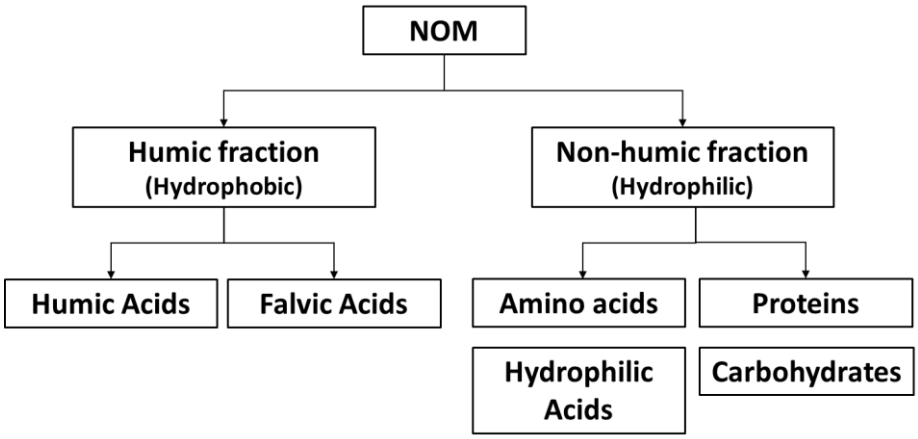

Figure 2-14 Classification of NOM

2.3.2 NOM Removal in Drinking Water Plants

NOM can remove from the surface water through coagulation or adsorption by activated carbon. Although, researchers are interested to use membrane filtration and AOP to remove NOM.

a) Coagulation

Coagulation is the most common way to remove NOM in water industries. In Coagulation, collides such as aluminum and iron are added to water to bond the dissolved species via an electrical double layer and from the repulsive potential field that leads to the production of micro flocs. In the flocculation step, these micro flocks agglomerate and form larger flocs. Large flocks are then removed in clarification step by gravity or buoyancy forces. To remove the remaining flocks, the clean water passes through the filters [111].

However, the effectiveness of coagulation for NOM removal is under debate. 10 to 70% of NOM is removed from raw surface water during coagulation via complexation, precipitation, agglomeration and/or adsorption. The removal depends on the dosage of coagulants, pH, temperature, NOM properties such as particle size and hydrophobicity. The hydrophobic

fraction of NOM is better removed in the coagulation step than hydrophilic [112]. The residuals of the coagulants can recover in water treatment plants. However, practically they are disposed after being used.

b) Adsorption with activated carbon

Activated carbon is the effective adsorbent to remove natural and man-made micropollutants like pesticides, industrial chemicals, taste and odor and algal toxins. However, NOM competes for adsorbing in the porous structure of activated carbon and decreases adsorption sites for other micropollutants. Typically, activated carbon is being used as an additional treatment to remove NOM. Both granula and activated carbon (GAC & PAC) are applied for NOM removal. However, GAC capacity decreases over time and high PAC doses are required to reach the treatment goals [112].

c) Membranes Filtration

Membrane filtration is being used as an alternative to traditional media filters. The most common membranes include microfiltration (MF), ultrafiltration (UF), nanofiltration (NF), and reverse osmosis (RO).

Nanofiltration proved to remove NOM and partially the viruses and hardness with lower operating pressure than other filters. In Canada, nanofiltration are combined with ultrafiltration membranes to remove DBPs in small systems. However, membrane fouling and flux reduction are the main issues in using membranes to remove NOM in water treatment. Water quality, operational parameters, and membrane quality can affect the fouling.

d) AOP

Oxidation via ozonation or AOPs can remove NOM as the advanced method in water treatment plants. It involves the formation of highly reactive radical species at room temperature that can oxidize organic compounds efficiently. They can be used in combination with biological active filters or alone like UV/H_2O_2 and UV/O_3 [110]. Recently, photocatalysts have been found effective in removing NOM which discuses more in the next section.

2.3.3 Photocatalytic degradation of NOM

TiO_2 based photocatalysis can produce ·OH radicals under UV irradiation that can decompose organic compounds including NOM in drinking water. Rate constant in these reactions have been reported to be 5 x 10^8 $M^{-1}S^{-1}$ [113]. The pH and irradiation time, water matrix and photocatalytic particle size are the important variables that affect NOM degradation. Higher pHs and irradiation time would result in a higher degradation rate. However, other compounds in the solution such as bicarbonate, would act as ·OH scavengers and decrease the NOM decomposition [114, 115]. Photocatalytic agglomeration also decreases the effective surface area of the photocatalysts and negatively impact NOM degradation [116].

Based on Liu et al., UV/TiO_2 can break large NOM molecules i.e. hydrophobic fraction into smaller molecules (hydrophilic compounds). However, the intermediates that form after degradation are more resistant to decompose than parent compounds. Liu et al. showed that by increasing the irradiation time, the concentration of hydrophilic compound increased and then decreased demonstrating that the humic fraction of NOM eventually decreases in the solution [109, 117]. Some studied also prove that adsorption of the NOM compounds occurs in the absence of UV irradiation when using TiO_2 that demonstrates the effectiveness of adsorption in NOM removal [117].

2.4 Pharmaceuticals

2.4.1 The occurrence of Pharmaceuticals in Water

By increasing the population, the investment in medical researches increased and led to significant growth in the production and consumption of pharmaceuticals. However, studies showed that chemical disposal from pharmaceuticals manufacturing, hospitals, animal fields, and agricultural activities leave a trace in the environment and find their ways into the sewage systems. Improvements in analytical methods and laboratory instruments allow the detection of pharmaceutical substances in aquatic media that range in micrograms to pictograms per liter [118, 119].

Existence of pharmaceuticals in the aquatic environment can effect both human and other living organisms. For instance, endocrine-active compounds and synthetic hormones are highly active compounds that can interfere with hormone systems. Anticancer drugs may lead to cancer themselves. Antibiotics have been shown to resist some bacteria. In addition to the effect of pharmaceuticals pollution on human health, in the aquatic environment, pharmaceuticals cause fish feminization and developmental delays in small organisms living under the water [120].

Conventional municipal wastewater treatment plants (WWTPs) cannot remove pharmaceuticals mainly because most of them built to remove biodegradable carbon, nitrogen, phosphorus, and microorganisms. Thus, advance processes are required to remove pharmaceuticals. Adsorption with activated carbon, membrane filtration, and biological degradation have been used widely to remove pharmaceuticals. However, low adsorption capacity in activated carbon, membrane fouling in membrane filtration and unpredictability of bacteria's behavior in biological degradation, limit the applications of these methods. AOP is a new way that can degrade the pharmaceutical compounds and is under investigation to be used in wastewater treatment plants.

2.4.2 Using AOP to Remove Pharmaceutical Compounds

High energy in UV irradiation can destroy the microorganism's DNA and RNA and terminate their productive ability. Therefore, it can disinfect the water from harmful microorganisms. The suitable wavelength of UV light is between 250-270 nm. Recently the efficiency of using UV light to degrade the pharmaceutical compounds is tested alone (photolysis processes) or in combination with H_2O_2, H_2O_2/Fe^{2+}, TiO_2 (AOP processes).

In photolysis processes, UV energy can break the bonds in pharmaceutical compounds. In this process, the substrate structure determines whether the compound can absorb the UV light or not. Most of the pharmaceuticals are photoactive, however, UV photolysis is not efficient for all of the pharmaceutical compounds [120].

The compounds with stronger bonds would degrade via oxidation by ·OH radicals produced using H_2O_2, H_2O_2/Fe^{2+}, and TiO_2. In UV/TiO_2 processes, ·OH radicals produce through the separation of electron and hole pairs when UV light irradiated TiO_2. ·OH radicals react unselectively with many pharmaceutical compounds to break the bonds while destroying the toxic by-products formed during UV photolysis [121].

Several parameters affect the generation of ·OH radicals in AOPs. For instance, ·OH radicals are more susceptible to produce in an alkaline environment. The absorbance of UV photons depends on the chemical structure of the pharmaceutical compounds. Suspended particles in the aquatic media might intervene in the penetration of UV light. Presence of other chemicals can interact with ·OH and affect the degradation of pharmaceutical compounds [120].

Chapter 3: **Engineering photocatalytic properties of TiO_2 using silver and graphene as dopant**

3.1 Introduction

TiO_2 is the most popular and promising compound for application in AOPs due to its high chemical and physical stability, non-toxicity and availability. However, commercializing TiO_2 is inhibited because of low quantum yield and limited photo-response range under visible light irradiations. Doping, sensitization, modifying phase and morphology are the strategies that can increase TiO_2 photocatalytic efficiency. Doping with non-metals like graphene and noble metals ions like gold (Au), silver (Ag), platinum (Pt) and palladium (Pd) showed enhancement in photocatalytic activities and photoconversion quantum yield. Noble metals can extend the light absorption in wide bandgap semiconductors to the visible light region with the mechanism known as localized surface plasmon resonance (LSPR) [122].

LSPR is defined as the resonance between the collective motion of conduction (free) electrons at metal surfaces and the incident electromagnetic wave. It can enhance the photocatalytic reactions on nearby semiconductors through the following mechanisms [123]:

1) Electron transfer from the noble metal surface to semiconductor's conduction band.
2) Energy transfer from the surface of noble metal produced by flocculation to the semiconductor that leads to the generation of more photoinduced charges.
3) Increasing the light scattering effect through the noble metal that improves light absorption by the semiconductor. The larger the noble metal particles, the greater the scattering intensity.

In the water treatment field, Ag is given attention due to its antibacterial and non-toxicity properties, photocatalytic activity, surface resonance, surface-enhanced Raman scattering (SERS), and metal enhanced fluorescence (MEF) [122, 124]. Also, the Fermi level of Ag (-4.7 eV) is approximately near the conduction band of TiO_2 (-4.3 eV) that can transfer the light absorption into the visible light region [123].

However, aggregation among Ag nanoparticles can happen while synthesizing Ag-doped TiO_2, which necessitate the optimization of Ag concentration. Ag concentration would influence the electron/hole recombination, separation and electron trapping. Insufficient Ag limits the generation of photo-induced charges while increasing Ag dosage would reduce the electron/holes lifetime by forming extra recombination sites [125]. Consequently, finding the optimum concentration of Ag is a key factor to improve the degradation rate.

In the present study, an effort has been made to investigate the optimum concentration of Ag on the photocatalytic properties of Ag-TiO_2 under UV-LED lights with two different wavelengths (λ=365 nm and λ=405nm) that resemble UV and visible light. A hydrothermal method was used to synthesize the uniform and evenly distributed Ag nanoparticles in the composite. Nanocomposites were dispersed in batch slurry reactors containing terephthalic acid (TPA) as a probing molecule for photocatalytic detection.

3.2 Materials and Methods

3.2.1 Reagents and chemicals

TiO_2 (P25 Aeroxide^{TM}), silver nitrate ($AgNO_3$) and hexamethyleneretramine (HTMA) were used in Ag-TiO_2 synthesis process. TPA solution used as model contaminant in photocatalytic degradation tests. All of the materials were purchased from Sigma-Aldrich (St. Louis, MO). Ultrapure water (Milli-Q® Integral 62 Water Purification System, EMD Millipore, 18.2 mΩ.cm resistivity at 25°C) used during the photocatalytic experiments.

3.2.2 Ag-TiO_2 synthesis

The hydrothermal method was used to synthesis Ag-TiO_2 photocatalysis. To optimize the amount of Ag in photocatalytic degradation tests, different concentrations of $AgNO_3$ and HMTA were added to 1 g P25 in 60 mL aqueous solution according to Table 4-1. The suspension was transferred to 125 mL acid digestion vessel for hydrothermal reaction and heated at 100˚C for 4 h. The resultant compound was separated from the supernatant by washing with ultrapure water and centrifuging at 3600 rpm for 10 minutes for three times. Then the

samples were dried in the furnace at 80˚C overnight. Dried samples were kept in the glass vial for further experiments.

Table 3-1 Different $AgNO_3$ and HTMA concentrations used in synthesizing Ag-doped TiO_2

No.	$AgNO_3$ (mM)	$AgNO_3$ Weight (mg)	Ag weight (mg)	HTMA (mM)	HTMA Weight (mg)	Ag/P25 (wt. %)
1	**0.50**	5.10	3.24	1	8.41	**0.32**
2	**1.00**	10.19	6.47	2	16.82	**0.65**
3	**2.00**	20.38	12.94	4	33.65	**1.29**
4	**10.0**	101.92	64.72	20	168.23	**6.47**

3.2.3 Nanomaterial Characterization

TEM (JEOL 2010F) was used to analyze the surface morphology of Ag-TiO_2 samples. Panalytical MRD X-ray Diffractometer (Cu-K$\alpha_1$radiation and a position sensitive detector) was used to characterize the phases in different samples through XRD. BET surface analyzer (Quantachrome Autosorb iQ) was used to measure the surface area of each sample through outgassing the samples at 200˚C for 24 hours under $N_{2(g)}$. The band gap energies were determined using a Shimadzu UV-2501PC UV-Vis-NIR spectrometer with an integrating Sphere, from diffuse reflectance spectra (DRS). Zeta potential was determined by using Corduan WALLIS zeta potential analyzer with laser doppler electrophoresis. The laser source of 20 mW diode at 635 nm was coupled to an automated optical attenuation system with a measurement angle of 17°. Dynamic light scattering (DLS) was performed using a Cordouan DL 135 Particle Size Analyzer with a 65 mW monomode red laser (λ = 658 nm). A cumulant fit and a Padé-Laplace fit was used to account for mono-disperse and poly-disperse samples. The autocorrelation function for every scan was fitted accordingly. The size of the particles were determined by taking the average size deduced from multiple scans.

3.2.4 Experimental Apparatus

The experimental setup is illustrated in Figure 3-1a, that consisted of two UV-LEDs with different wavelengths; λ=365 nm that resembles the UV light and λ =405 nm that

resembles the visible light. The intensity of the UV and visible light determined to be 2.15×10^4 and 9.06×10^3 $W.cm^{-2}$ .The photocatalytic activity of the nanomaterials investigated in constant illumination of UV light and the visible light as well as different fractions of UV and visible lights. The LEDs controlled by microcontroller (Arduino Uno) and LED current Driver (LEDSEEDUINO) on top of the stir plate. Digital control was used to create a square wave, a signal switched between two wavelengths. Pulsed width modulation (PWM) script was programmed into Arduino microcontroller using the script in Figure 3-1b.

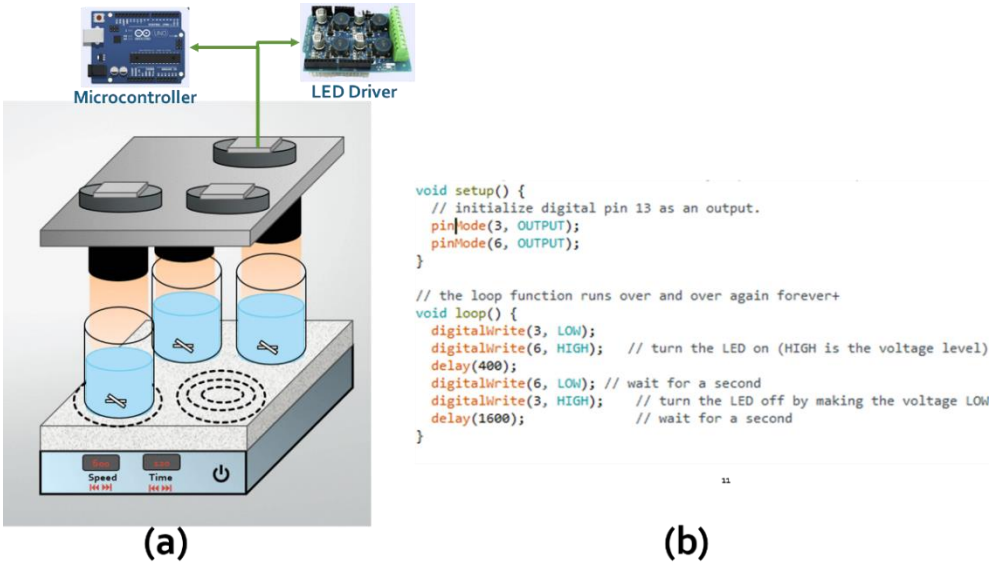


```
void setup() {
  // initialize digital pin 13 as an output.
  pinMode(3, OUTPUT);
  pinMode(6, OUTPUT);
}

// the loop function runs over and over again forever+
void loop() {
  digitalWrite(3, LOW);
  digitalWrite(6, HIGH);   // turn the LED on (HIGH is the voltage level)
  delay(400);
  digitalWrite(6, LOW); // wait for a second
  digitalWrite(3, HIGH);    // turn the LED off by making the voltage LOW
  delay(1600);              // wait for a second
}
```

Figure 3-1 a) Experimental batch reactor with PWM control unit contain microcontroller, LED driver and two LEDs with different wavelengths b) script of coded program using Arduino microcontroller

Different duty cycles and pulse frequencies were tested by changing the on and off time between two wavelengths. The frequencies and duty cycles were calculated using following Equations:

Duty cycles: $\gamma = \frac{t_{405}}{t_{405}+t_{365}}$ **Equation 3-1**

Pulse frequency: $\nu = \frac{1}{t_{405}+t_{365}}$ **Equation 3-2**

Where t_{405} and t_{365} are the length of time when UV-LEDs with λ=405nm and λ=365nm is on. The frequencies and duty cycles are listed in Table 3-2:

Table 3-2 Light profiles for constant and periodic illuminations based on pulsing's duty cycles and frequencies

Duty Cycle (γ)	**$T_{365\ nm}$ (ms)**	**$T_{405\ nm}$ (ms)**	**Light duration (ms)**
Duty cycle experiments at constant frequency			2000 (0.5 Hz)
0%	Continuous illumination of 405 nm		
10%	200	1800	
20%	400	1600	
40%	800	1200	
50%	1000	1000	
60%	1600	400	
80%	1800	200	
100%	Continuous illumination of 365 nm		
Frequency experiments at constant frequency			
50%	10000	10000	20000 (0.05 Hz)
50%	1000	1000	2000 (0.5 Hz)
50%	500	500	1000 (5 Hz)
50%	100	100	200 (1 Hz)

3.2.5 Photocatalytic degradation test

0.831 g TPA added to 6 mM NaOH in 1 L volumetric flask and filled up with milliQ water. 300 mL of the resulting TPA solution was added to 3 beakers, which were covered by aluminum foils to increase the reliability of the experiment. 30 mg of the photocatalyst was added to each beaker accordingly. The experiments were conducted under a dark period for 60 min and after that illumination started according to different duty cycles and frequencies. One mL aliquots were taken at designated time points.

During the photocatalytic reaction, TPA would react with ·OH radicals and produce 2-hydroxyterephthalic acid (HTPA). The formation of HTPA was monitored using the SpectraMax M3 plate reader. Equation 3-3 was used as a kinetic model for HTPA formation [105]:

$$[\boldsymbol{HTPA}] = \frac{\boldsymbol{k_1}}{\boldsymbol{k_2}} \left(\mathbf{1} - \boldsymbol{e}^{-\boldsymbol{k_2 t}}\right) \qquad \textbf{Equation 3 - 3}$$

$[HTPA]$ is the molar concentration of HTPA, k_1 is the zero-order HTPA formation rate and k_2 is the pseudo-first-order kinetic degradation rate. To compare different nanomaterials, only the initial rate constant k_1 (first reaction step) was considered.

3.3 Results and Discussions

3.3.1 Material Characterization

The high annular dark field (HAADF) scanning transmission microscopy (STEM) was used to observe the existence of Ag nanoparticles on the P25 surface. Figure 3-2 demonstrated the bight field and dark field TEM image of P25-0.32 wt% Ag with the lowest Ag concentration. Although Ag nanoparticles did not appear in the bright-field TEM image (Figure 3-2 a), but the contrast in dark field image supported the existence of another element. Therefore, by using EDS mapping we could detect Ag nanoparticles in this sample (Figure 3-2 c-e).

With increasing the silver concentration up to 0.65 wt% Ag, Ag nanoparticles appeared as dark dots on the P25 surface with 1-3 nm length (Figure 3-3 (a)). The distribution of the Ag nanoparticles anchored on the surfaces of P25 increased with increasing Ag^+ ions in precursor suspensions. In other words, the distance between silver nanoparticles in P25-0.65 wt% Ag was larger, and their density was lower in comparison to P25-1.29 wt% Ag. By increasing the Ag concentration to 6.47 wt% Ag, agglomeration was observed on the surface of P25 (Figure 3-3 (c)). The corresponding dark field images indicated that the Ag nanoparticles were attached on the P25 surface separately and the loading density of Ag nanoparticles on the P25 surface increased by increasing Ag concentration (Figure 3-3 d-f).

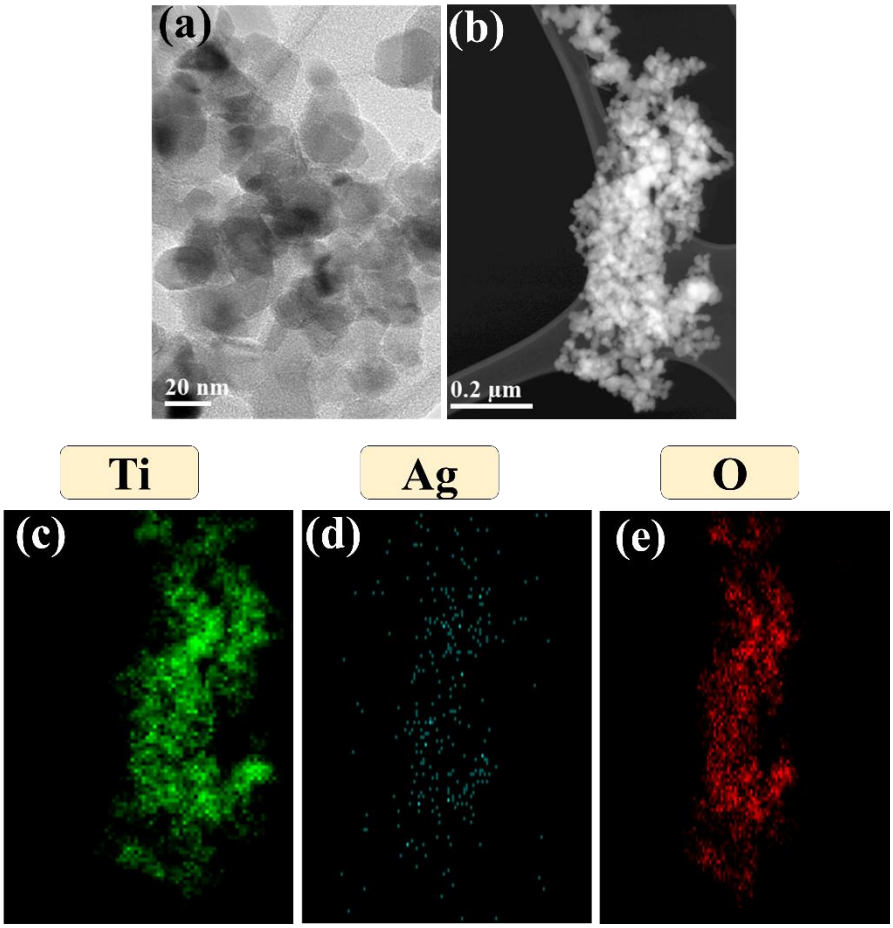

Figure 3-2 TEM image of P25-0.32 wt% Ag a) bright field of b) Dark field c) Elemental mapping of Ti, d) Ag and e) O

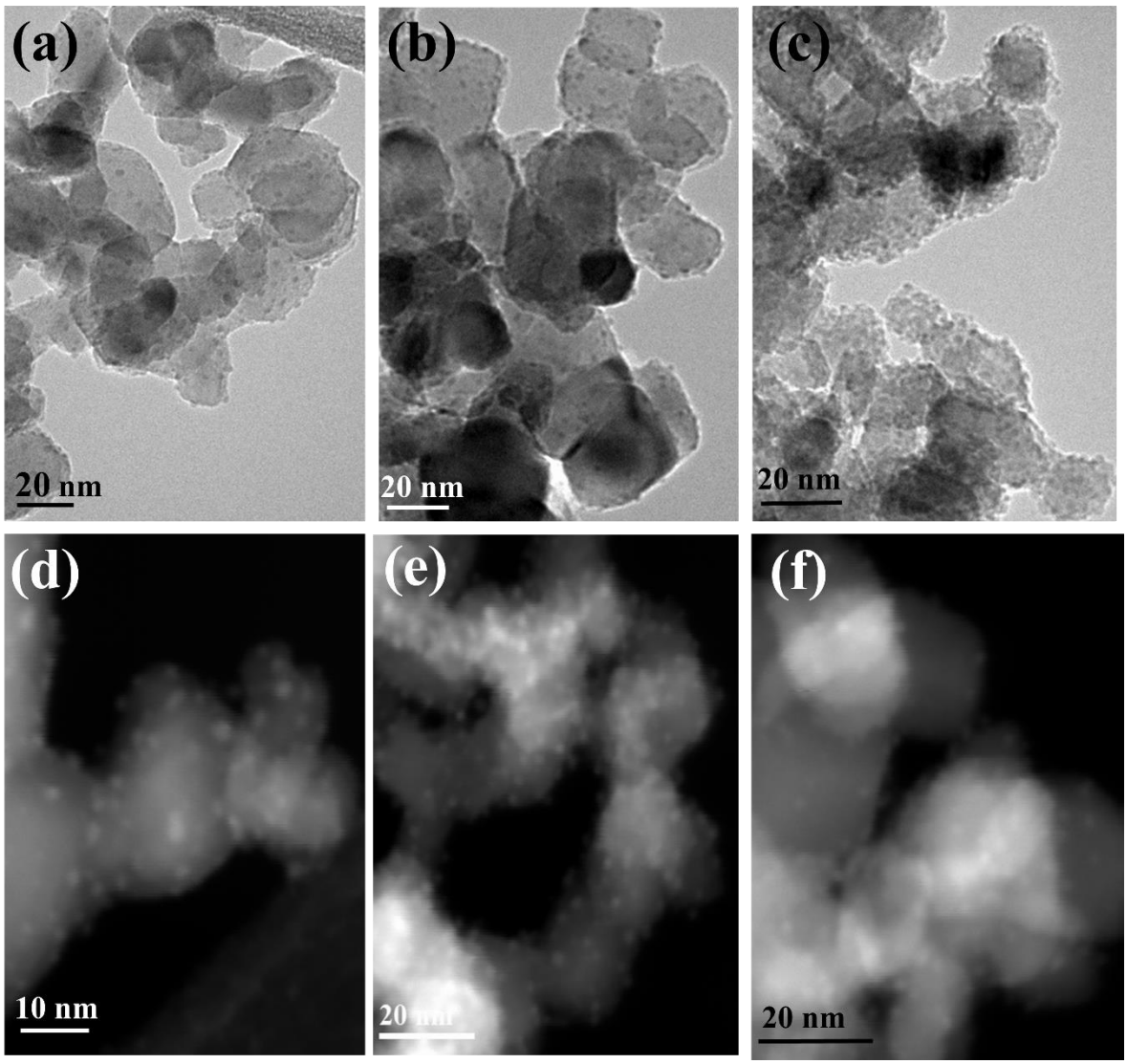

Figure 3-3 Bright field TEM image for a) 0.65 wt% Ag b) 1.29 wt% Ag and c) 6.47 wt% Ag, Dark field TEM image for d) 0.65 wt% Ag e) 1.29 wt% Ag and f) 6.47 wt% Ag

XRD patterns of Ag-p25 samples showed characteristic peaks of both anatase and rutile phases in Fig 3-4. Besides the major reflections of P25 phases, there were two weak peaks located at 44.2 and 64.1˚ in sample P25-6.47 wt% Ag which can be attributed to (111) and (200) reflections of cubic Ag phase. For the samples with smaller amount of Ag, such as 0.32, 0.65

and 1.29 wt% Ag, there was no recognizable peak belonging to Ag due to the detection limitation of XRD technique.

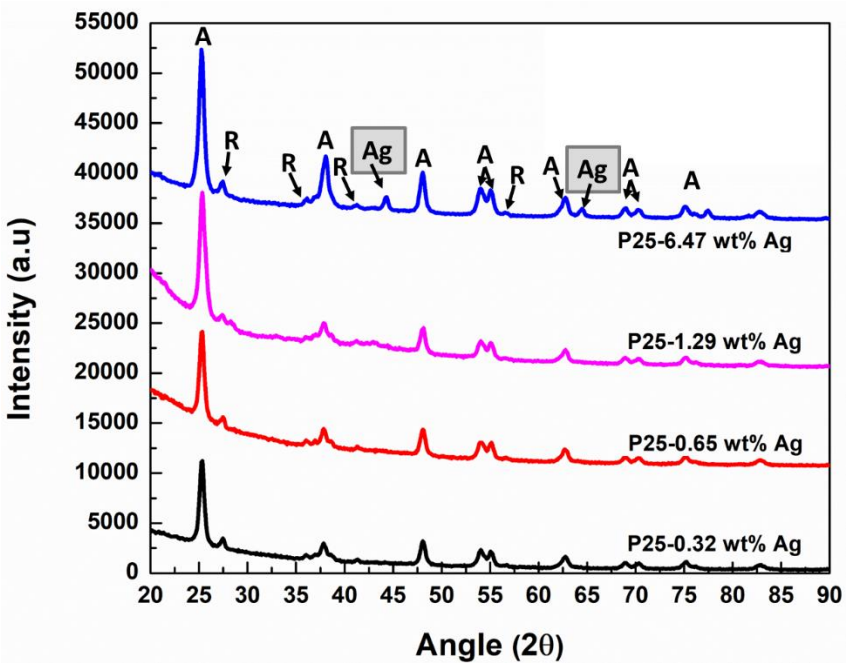

Figure 3-4 XRD patterns of Ag doped P25 with different Ag concentrations

Other characterizations including surface area, zeta potential, band gap, crystal phase and agglomeration size of the samples are summarized in Table 3-3. According to Table 3-3, P25 had the lowest surface area among different samples (57 m^2/g), but it increased by silver doping while, P25-1.29 wt% Ag had the highest specific surface area (113.64 m^2/g). Increasing the silver concentration up to 6.47 wt%, decreased the specific surface area because of agglomeration of silver nanoparticles. The surface charges for bare P25 were found to be -12.5, which increased to -11.77 mV for P25-1.29 wt% Ag and decreased to -18.5 mV by adding silver concentration up to 6.47 wt%.

Table 3-3 Characteristics of P25 and P25-doped silver with different Ag concentrations

Sample	BET Surface Area ($m^2 g^{-1}$)	DFT Pore Volume ($cm^3 g^{-1}$)	Zeta potential in milliQ water (mV)	Band gap (eV)	Agglomeration size (nm) in milliQ water
P25	57	0.12	-12.5	3.08	
P25-0.32 wt% Ag	74.250	0.255	-11.77	3.04	543.17 (Std Dev: 42.8 %)
P25-0.65 wt% Ag	64.605	0.246	-11.77	2.94	623.99 (Std Dev: 10.79 %)
P25-1.29 wt% Ag	113.646	0.285	-11.77	2.86	392.99 (Std Dev: 44.79 %)
P25- 6.47 wt% Ag	60.543	0.202	-18.5	2.96	518.63 (Std Dev: 48.62 %)

The band gap of the samples was determined using the Tauc plots. The band gap energy of P25 was 3.08 eV that is equal to cut off wavelength of 402.53 nm suggesting that P25 is not able to use solar spectrum for photocatalytic activities. The addition of Ag decreased the band gap energy of P25, thus increased the cut off wavelength to visible light region. The mechanism in which Ag enhanced the overall photocatalytic efficiency of P25 might because of scattering the light around the photocatalysis using LSPR energy transfer. Increasing the concentration of silver to 1.29 wt%, reduced the band gap energy to 2.86 eV and increased the cut-off wavelength to 434 nm. However, increasing the Ag loading above the optimal concentration (1.29 wt% Ag), increased the band gap energy due to agglomeration.

The average particle size of P25-doped Ag was measured by DLS to observe the effect of changing Ag concentration in size distribution profile in aqueous solution. Under aqueous conditions, P25 doped Ag nanoparticles could attract other organic compounds in the solution and combined due to electrostatic and van der Waals interactions. The smallest particle size belonged to P25-1.29 wt% Ag. The average particle size of the samples in the solution increased by increasing the silver content to 0.65 wt% and decreased drastically to 392.99 nm by increasing Ag concentration up to 1.29 wt%. By increasing the Ag content up to 6.47 wt%, the average particle size increased to 518.63 nm.

Based on the TEM characterization and Table 3-3, 1.29 wt% Ag was selected as the optimum concentration of silver which can control the crystal growth and agglomeration.

Increasing the Ag concentration further reduce the surface area, increased the band gap energy and agglomeration size.

3.3.2 TPA Degradation using P25-doped Ag photocatalyst under continuous irradiation of UV and visible light

Figure 3-5 shows the TPA degradation of P25 and Ag-doped P25 with different silver concentrations under continuous UV and visible light illumination. HTPA formation rate or rate constant (k_1) indicates the efficiency of photocatalysts in the production of ·OH radicals under light irradiation. According to Figure 3-6, the HTPA formation rate using P25 was 0.9 min^{-1} under UV light. Increasing the Ag concentration increased the rate constant of the reaction. P25-1.29 wt% Ag increased HTPA formation rate up to 1.7 min^{-1}. Increasing the concentration further decreased the rate constant of the reaction. The rate constant of the reaction followed the order: P25-1.29 wt% Ag> P25-0.32 wt% Ag> P25>P25-0.65 wt% Ag> P25-6.47 wt% Ag. Apparently that photocatalytic activity of P25-1.29 wt% Ag was highest and photocatalytic activities of P25-0.65 wt% Ag and P25-6.47 wt% Ag were less than P25 under UV light irradiation.

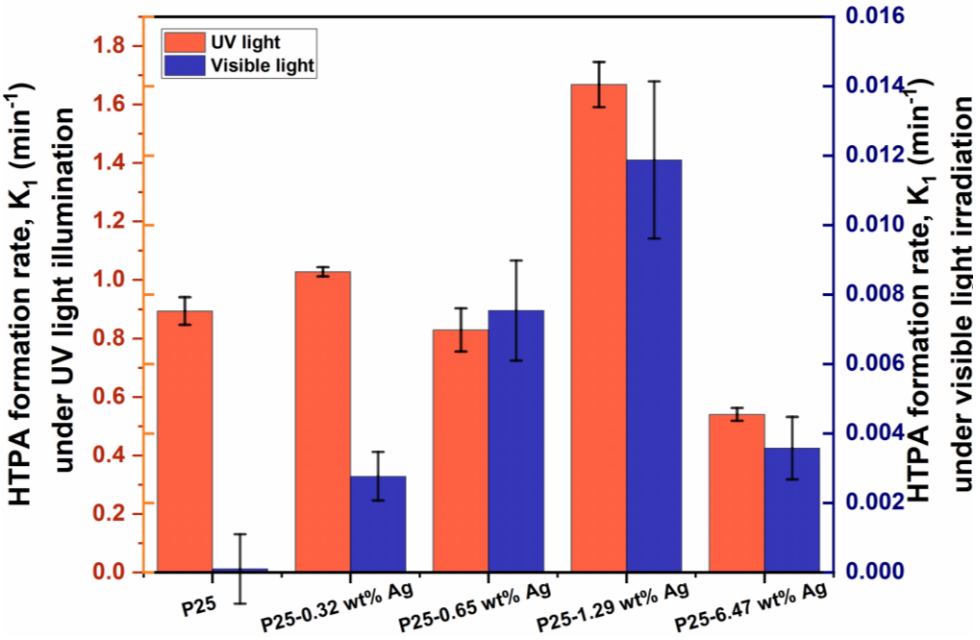

Figure 3-5 TPA degradation of P25 and Ag-doped P25 with different silver concentrations under continuous UV and visible light illumination

Right side of the Figure 3-5 demonstrates the HTPA formation under visible light irradiation. HTPA formation rate for bare P25 was almost zero since the HTPA concentration was below the detection limit in UV-Vis spectroscopy. By doping Ag, the photocatalytic activity of the samples increased under visible light illumination. Rate constant of the reaction using P25-1.29 wt% Ag was highest (0.012 min^{-1}) while rate constant of the reaction using P25-0.32 wt% Ag and P25-6.47 wt% Ag were almost the same and lowest. The rate constant of the reaction using visible light followed this pattern: P25-1.29 wt% Ag> P25-0.65 wt% Ag>P25-6.47 wt% Ag> P25-0.32 wt% Ag>P25.

The performance of different samples under visible light was in accordance with their band gap energy in Table 3-3 and Figure A-1 in Appendix A. The adsorption edge of different samples calculated using Planck's law in Equation 3-4:

$$\boldsymbol{E = \frac{hc}{\lambda}} \qquad \textbf{(Equation 3-4)}$$

Where h and c are the Planck's constant and light speed with 6.626×10^{-34} J.s and 3×10^{8} m/s. Table 3-4 shows the adsorption edge of different samples. The adsorption edge for P25

was 402.53 nm indicating that P25 can only take part in photocatalytic reaction in UV region. By adding silver up to 0.32 wt% Ag and 0.65 wt%, adsorption wavelength increased to 407 and 421 nm. Due to the lower silver concentrations, these samples had lower adsorption capacity in the visible region.

It is expected that by increasing the Ag concentration, the absorption of visible light increases. However, plasmonic field regions might overlap due to agglomeration of Ag nanoparticles and produce spatial charge repulsion. The overlapping ease electron hole pairs recombination and decrease the photocatalytic efficiency [126-128]. Therefore, P25-1.29 wt% Ag provided the suitable band gap position and covered the most available active sites with highest photocatalytic efficiency under both UV and visible light

Table 3-4 Adsorption edge for different samples

Samples	**Band gap (eV)**	**Adsorption edge (nm)**
P25	3.08	402.53
P25- 0.32 wt% Ag	3.04	407.82
P25- 0.65 wt% Ag	2.94	421.7
P25- 1.29 wt% Ag	2.86	433.49
P25- 6.47 wt% Ag	2.96	418.85

The mechanism improving TiO_2 photocatalytic activity using Ag under the UV light is by hindering the e/h pairs through formation of Schottky barriers. The nanoparticles of Ag on the surface of TiO_2 act as electron scavengers since its Fermi level is below the conduction band of TiO_2. When Ag-doped P25 is irradiated under UV light illumination, the photogenerated electrons in the valance band of P25 transfer to the conduction band. Ag nanoparticles on the surface of P25 capture the electrons and separate the electrons and holes. Electrons then transfer to the adsorbed O_2 to generate radical species such as $\cdot OH$. At the same time, holes on P25 surface would react with OH^- and produce reactive oxygen radicals. Consequently, TPA would react with $\cdot OH$ radicals and produce HTPA.

The reduction in photocatalytic activity of P25-6.47 wt% Ag was due to the high density of Ag nanoparticles adhering on P25 surface that occupied the active sites and blocked the UV adsorption. Increasing the density of Ag nanoparticles on P25 surface caused the shielding effect i. e. agglomeration of Ag nanoparticles on P25 surface and reduced the UV absorption [128]. In addition, the high density of Ag nanoparticles might act as recombination centers for separated electron and hole pairs.

The mechanism of photocatalytic activity of P25-doped Ag is different under visible light irradiation. Using the visible light irradiation, the LSPR excites and causes strong localized plasmonic resonance near Ag-P25 interface. Thus e/h pairs generates by optical transitions between the localized electronic states in the band gap of P25. Meanwhile, the heterojunction, Schottky barrier forms at the interface of Ag-P25, hinders the electron transfer form Ag to P25. Yet, owing to the silver high electron oscillating collectivity under the LSPR excitation, electrons come over the Schottky barriers and move from Ag to TiO_2 while holes are captured by the Ag nanoparticles [6].

Density functional theory also specified that silver doping introduces the gap states near or below the minimum conduction band (MCB) and the Fermi level near or in the conduction band. This gap acts as a trap center for photogenerated charges and keeps them separated. Therefore, the electrons on the Ag nanoparticles transfer to P25 conduction band since the electron transfers form Ag to dissolved O_2 is quite slow. The transferred electrons to P25, react with oxygen molecules in the water and form superoxide radicals. Hydroepoxy radicals ($HOO\cdot$) form through the protonation yields and leads to H_2O_2 formation using the trapped electrons. Finally, $\cdot OH$ radicals form which is the strongest ROS during the photocatalytic oxidation of TPA. In addition, holes in the Ag can react with hydroxyl groups (-OH) and water to produce $\cdot OH$ radicals as well [4, 60, 127].

Based on the different mechanisms in photocatalytic degradation using Ag-P25 under UV and visible light irradiation, periodic illumination of UV and visible light was used to increase the photocatalytic efficiency Ag- doped P25 under visible light.

3.3.3 TPA Degradation under periodic illumination of UV and visible light

Silver doping increases the photocatalytic efficiency of P25, but still low degradation rate using Ag-p25 photocatalysts under the visible light (Figure 3-6), limits the application of photocatalysis in water treatment plants. The low photocatalytic activity of Ag-doped P25 might be attributed to inadequate energy required to excite the electrons, slow rate of electron scavenging by O_2, recombination of photoinduced charges and mass transfer control into or from the surrounding medium [129]. One approach to overcome the low photocatalytic efficiency of P25-Ag under visible light is by using periodic illumination of UV and visible light based on their different photocatalytic mechanism.

Under the irradiation of visible light, LSPR excitation causes strong electron oscillations in silver. This phenomena plus the closeness of Ag Fermi level to the conduction band edge of TiO_2, leads electrons to flow from silver to TiO_2 and enable the Ag nanoparticles to capture the holes [122]. Electron movement to TiO_2 is ultrafast, while the electron transfer from silver to adsorbed O_2 is quit slow. Holes in the silver nanoparticles adsorb hydroxyl groups (-OH) and form ·OH radicals [126, 130]. Moreover, under the UV light irradiation, silver nanoparticles act as electronic trap that collect electrons due to Schottky junctions, while holes stay on TiO_2 surface. The enhanced charge separation increases the photocatalytic activity by preventing electron and hole recombination.

The tacit assumption was that when the Ag-doped P25 photocatalysts are illuminated by visible light, Ag nanoparticles are responsible in production of electrons due to strong LSPR. However, by applying periodic illumination of UV light P25 would participate in production of photo-induced charges and increases the charge concentration gradient. Fig 3-7 shows the effect of increasing the UV light duty cycles (at constant frequency) on HTPA formation rate using Ag-doped photocatalysts.

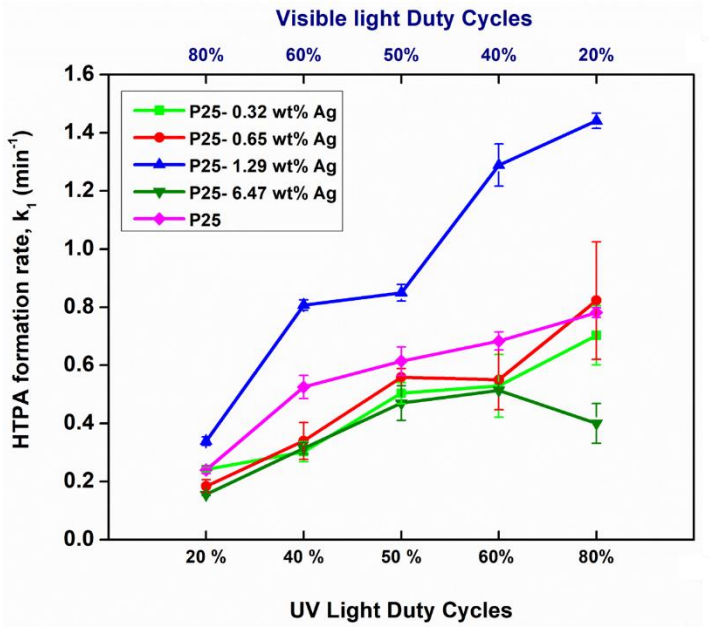

Figure 3-6 Effect of periodic illumination of UV light and visible light on different Ag-doped P25 samples

According to the Figure 3-7 by increasing the UV light duty cycles, HTPA formation rate increased since UV light can promote generation of more electrons and holes. The trend for P25, P25-0.32 wt% Ag, P25-0.65 wt% Ag, P25-6.47wt% Ag was almost the same and photocatalytic activity of P25-1.29 wt% Ag was significantly higher than other photocatalysts due to its higher surface area and lower average particle size (Table 3-3). There was no significant difference between the rate constant of P25-0.32 wt% Ag and P25-0.65 wt% Ag in different duty cycles. In 20% UV light duty cycle, the HTPA formation rate of Ag doped samples was low but still higher than P25. The LSPR effect of Ag nanoparticles might be responsible in enhancing the photocatalytic activity. By increasing the duty cycle, the rate constant increased since increasing the UV light fraction generated more photo-induced charges. The rate constant for the sample P25-6.47 wt% Ag was lowest due to high density of Ag nanoparticles that decreased the available active sites on the surface.

3.3.4 TPA degradation under various frequencies

The HTPA formation rate was quantified under various pulse frequencies ($\boldsymbol{\nu}$=0.05 Hz, 0.5 Hz, 1Hz, 5 Hz) at a constant duty cycle of $\boldsymbol{\gamma}$=50% using Ag-doped P25 samples (Figure 3-8). According to this Figure, the reaction rate constant was uniform using P25-1.29 wt% Ag in different frequencies. The reason might be the large surface area of P25-1.29 wt% Ag that is able to produce enough photo-induced charges for photocatalytic reactions. Other samples showed the same trend in changing the K_1 value by changing the frequencies. Using two-way anova, we indicated that there was no significant difference in HTPA formation rate in 0.05, 1 and 5 Hz. In addition, there is no significant difference in HTPA formation rate using P25-0.32 wt% Ag and P25-0.65 wt% at different frequencies.

Variation of HTPA formation rate by changing the frequency for these samples can be attributed to two mechanisms: (i) increasing the photo-induced charges by longer illumination periods and (ii) breaking up process in P25 nanoparticles that creates new adsorption sites.

Applying long UV exposure time in 0.05 Hz pulse frequency caused the photocatalysts to reach the steady state. The long exposure time, might cause the charge build up and increased electron hole pairs recombination in photocatalysts. Increasing the frequency to 0.5 Hz reduced the charge build up and increased the HTPA formation rate. In 1 Hz frequency, HTPA formation rate decreased again for all the nanoparticles except P25-1.29 wt% Ag which followed the constant trend.

The flocculation in HTPA formation rate under different frequencies using P25, P25-0.32 wt% Ag, P25-0.65 wt% and P25-6.47 wt% may be due to aggregate and disaggregation of nanoparticles in aqueous solution. According to Bahnemann et al. (2004) disaggregation of TiO_2 nanoparticles would occur using intermittent pulsing with sufficient energy [131].

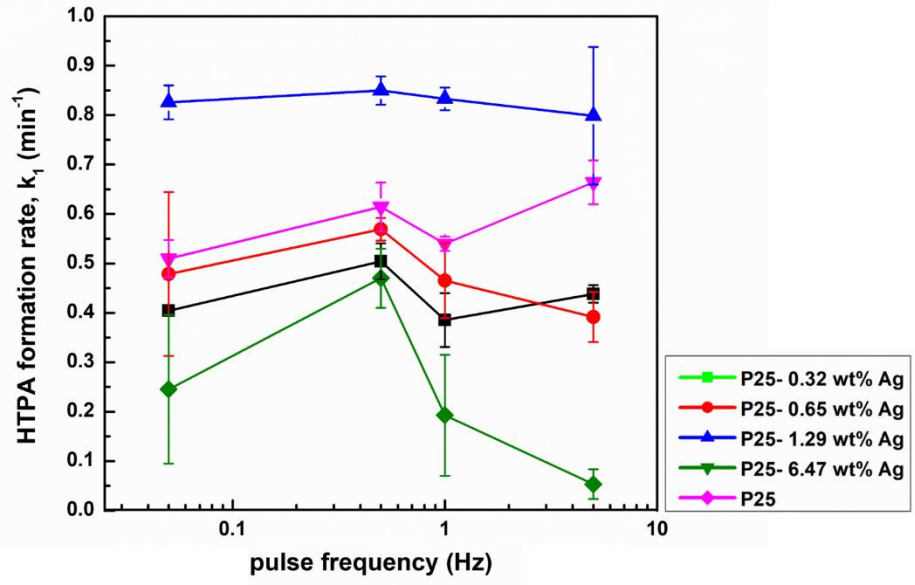

Figure 3-7 HTPA formation rate of P25 and Ag-doped P25 samples with different Ag concentration under constant duty cycle 0f 50% and various frequencies

The HTPA formation of Ag-P25 compared with the optimum HTPA formation of P25-graphene investigated in the previous research by Fattahi et al (2019) [10]. Figure 3-8 illustrates the comparison of HTPA formation rate of P25-graphene and P25 under constant illumination of UV and visible light. According to this Figure, the rate constant of P25-graphene under UV light is about 0.36 min^{-1} which is much higher than P25 (about 0.15 min^{-1}), but lower than P25-1.29 wt% Ag (about 1.66 min^{-1}). The higher rate constant of P25- 1.29 wt% Ag among other photocatalysis, led us to use P25- 1.29 wt% Ag for NOM and pharmaceutical removal.

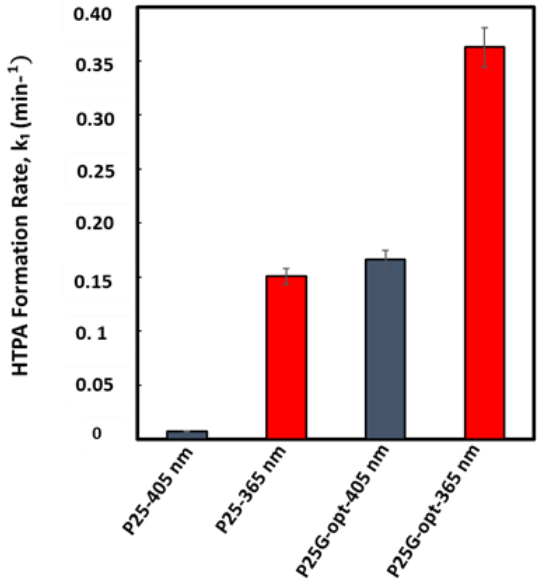

Figure 3-8 HTPA formation rate for P25, P25-graphene under visible light (**λ**=405 nm) and UV light (**λ**=365 nm) [10]

3.4 Conclusions

In summary, Ag doped-P25 nanocomposites with different silver concentration of 0.32, 0.65, 1.29, 6.47 wt% have been synthesized using the hydrothermal method and were tested for degradation of TPA under UV-LED and visible light. Material characterization demonstrated that P25- 1.29 wt% Ag had the highest surface area (113.65 m^2g^{-1}) and lower band gap energy (2.86 eV) among the samples tested. This band gap corresponded to adsorption edge of 433.5 nm, which demonstrated improvement in adsorption under visible light irradiation. Increasing the Ag concentration further, caused agglomeration and decreased the effective surface area of the photocatalysis. The photocatalytic efficiency of the samples was compared under constant UV and visible light irradiation as well as periodic illumination of UV and visible light. The HTPA formation rate for the optimized photocatalysts showed highest rate constant under constant illumination of UV and visible light (1.65 and 0.012 min^{-1}). The effect of periodic illumination of UV and visible light was compared for each sample under constant frequencies and duty cycles. In constant frequency of 0.5 H, increasing the UV light duty cycle, increased

the HTPA formation rate. P25- 1.29 wt% Ag and P25- 6.47 wt% Ag showed the highest and lowest HTPA formation rate among other samples. In constant duty cycle of 50%, HTPA formation rate of the P25- 1.29 wt% Ag was significantly higher than other samples and about 0.8 min^{-1} in different frequencies. Under the same condition, HTPA formation rate of the P25- 6.47 wt% Ag was lower. There was no significant difference in HTPA formation of P25- 0.32 wt% Ag and P25- 1.29 wt% Ag. For other samples, there was no significant change in HTPA formation using 0.05, 1 and 5 Hz.

Chapter 4: **Removal of natural organic matter in water using Ag-TiO_2 photocatalysis under UV-LED and visible light periodic illumination**

4.1 Introduction

Natural Organic Matter (NOM) is complex heterogeneous compound formed through decomposition of microorganisms and their residues in rivers and lakes [132]. The presence of NOM in drinking water leads to operational problems in treatment plants and causes substantial concerns to the water industries. Besides, interaction between NOM and halogen-based disinfectants (i.e. Chlorine) forms disinfection by-products (DBPs) such as Haloacetic acids (HAAs) and Trihalomethanes (THMs) [110]. DBPs cause bladder, colon and rectal cancer as well as reproductive and developmental problems [133].

Thus far, various methods including: coagulation, flocculation, activated carbon adsorption and membrane filtration have been utilized to remove NOM before disinfection process [113]; however, each method has its own downside. Recently the effectiveness of using advanced oxidation processes (AOP) in removing NOM from drinking water is under investigation. AOPs are set of chemical reactions that degrade hazardous organic compounds by generating strong oxidizing species mainly ·OH radicals [16]. TiO_2 is the most popular compound in AOPs since it is chemically stable, environmentally friendly and commercially available. Adsorptive and oxidative abilities of TiO_2, can effectively avoid membrane's fouling and DBPs production through breaking down, adsorbing, altering and mineralizing the large hydrophobic NOM compounds [15, 16, 113].

TiO_2 can degrade the aquatic contaminants in two steps: adsorption that happens in the absence of the lights and degradation that occur in the presence of the lights. In UV light irradiation, the ROS such as ·OH radicals, degrade contaminants that are absorbed on the surface of the photocatalysis. Holes on TiO_2 surface and radicals in the bulk solution degrade the organic pollutants [109].

NOM adsorption on TiO_2 surface is effected by pH and ionic strength. Preferentially, Large and more aromatic NOM compounds adsorb first. In photocatalytic degradation of NOM,

large aromatic NOM compounds break to smaller compounds, which can reduce membrane fouling and DBP formation probability. However, the requisition of UV light (**λ**<400 nm) to generate ·OH radicals and electron/hole recombination, limits the application of TiO_2 in municipal drinking water treatment plants [32, 115]. Visible light adsorption of TiO_2 can be enhanced by decreasing the band gap energy (~3.2 eV) via doping metals and non-metals [32]. Photonic efficiency of TiO_2 also can improve by optimizing the operational parameters like light intensity, pH, catalyst concentration, addition of oxidant, and temperature [134].

In this research we used Ag doping to increase the TiO_2 visible light adsorption. Ag-TiO_2 nanoparticles synthesized using hydrothermal method. We optimized the amount of Ag needed for the highest ·OH radicals production in the solution as discussed in Chapter 3. The optimum Ag-doped P25 sample obtained in pervious chapter, used in the solution containing NOM under UV and visible light. We tested periodic illumination of UV and visible light to increase the photonic efficiency of NOM degradation under visible light. Total Organic Carbon (TOC) and UV absorption at 254 nm (UV_{254}) were used to understand the photocatalytic degradation of NOM.

4.2 Materials and Methods

4.2.1 Reagents and chemicals

Ag doped-P25 nanocomposite synthesized using P25 Aeroxide ^{TM}, $AgNO_3$ and HMTA as described in section 3.2.2. Calcium chloride ($CaCl_2.2H_2O$), Magnesium chloride ($MgCl_2.6H_2O$), Sodium Nitrate ($NaNO_3$), Calcium sulfate ($CaSO_4$), Alginic acid $(C_6H_8O_6)_n$, Sodium bicarbonate ($NaHCO_3$) and Suwannee River NOM were used to make synthetic water for NOM tests. MilliQ water was used for all of the experiments. All chemicals were purchased from Sigma Aldrich.

4.2.2 Ag-doped P25 nanocomposite synthesis and characterization

Ag doped-P25 nanocomposite synthesized using hydrothermal method as described in section 3.2.2. Briefly, different concentrations of $AgNO_3$ and HTMA added to the solution

containing P25. The morphology of the samples obtained by using TEM and XRD. The surface area and band gap of different samples, indicated that the sample with 1.29 wt% Ag has the highest surface area and lowest band gap energy which suits the photocatalytic applications. Thus, P25-1.29 wt% Ag was selected for the NOM experiments.

4.2.3 Water Matrix

Synthetic river water (Synthetic water) was prepared in the lab with Suwannee River NOM in combination with alginic acid and inorganic compounds dissolved in water according to Rosenfeldt and Linden recipe [114]. Table 4-1 describes the preparation of synthetic water. 8 L of fresh water was prepared every day for related experiments.

Table 4-1 Composition of Synthetic water

Stock solutions	**Compound**	**Weigh (g)**	**Storage condition**
Stock A (1L)	$CaCl_2$	0.2264	Store at room temperature
	$MgCl_2$	0.8356	
	$NaNO_3$	0.0412	
Stock B (1L)	$CaSO_4$	0.2954	Store at room temperature
Stock C (100mL)	Suwannee River NOM	0.1024	Store at 4 ^oC.
	Alginic Acid	0.0532	
	NaOH (1 M)	0.25 mL	
Final Synthetic Water (1L)	100 mL Stock A		Store at 4 ^oC.
	333 mL Stock B		
	10 mL Stock C		
	$NaHCO_3$	0.126 g	

4.2.4 Measurement and characterization of NOM

TOC and UV_{254} are the parameters being used to predict DBP formation in the drinking water treatment industry. In current research, TOC was used to quantify NOM as bulk measurement. The samples were run on a Shimadzu TOC-L total organic carbon analyzer equipped with a Shimadzu ASI-L autosampler. The instrument uses a 680˚C combustion catalytic oxidation/NDIR detection method. UV_{254} and specific UV absorbance (SUVA) were used to identify the aromacity of the NOM. UV_{254} measured using fluorescence plate reader

(spectraMax M3, Molecular Device) set with a 254 nm. SUVA was measured by dividing UV_{254} by TOC. Each of these parameters has been used as a backup to analyze the NOM.

4.2.5 NOM Degradation experiments

The experiments were conducted in the same UV-LED set up as in Chapter 3. Constant illumination of UV light and visible light as well as periodic illumination of UV and visible light were tested for each photocatalysts according to the Table 4-2:

Table 4-2 Duty cycles used for constant and periodic illumination at constant frequency of 0.5 Hz

Duty Cycle (γ)	**$T_{365\ nm}$ (ms)**	**$T_{405\ nm}$ (ms)**
0%	0	2000
20%	400	1600
60%	1200	800
80%	1600	400
100%	2000	0

For each Duty cycle, 30 mg of the P25- 1.29 wt% Ag was added to 300 mL of synthetic water matrix in 400 mL beaker and was sonicated for 5 minutes. The solution was mixed continuously using the magnetic stir bar. The experiments consisted of Adsorption and degradation steps. In adsorption, the synthetic NOM water and the photocatalysis stirred for 30 minutes in dark to mix the solution and reach the equilibrium conditions. The period of dark adsorption was selected based on the primary experiments results proving that the TOC removal didn't change between 60 minutes to 30 minutes. After the 30 minutes dark adsorption, the UV-LEDs lamps were turned on and photocatalytic experiments started for duration of 0, 15, 30, 45 and 60 minutes. Each treatment was conducted as an independent experiment in triplicate.

After each time points, the treated water samples were filtered through 0.45 μm polyether sulfone (PES) membrane filters to separate TiO_2 and other particulate matter from the water. The treated water was analyzed for pH, TOC and UV_{254}.

4.3 Results and discussion

4.3.1 NOM removal

TOC defines as the measurement of the mass of organic carbon compounds in the water. However, TOC does not specify the difference in size, aromaticity and the potential to form DBP products. In the other hand, UV_{254} is the indicator for humic substances and aromatic compounds exist in the water and is proven to be better predictor of DBPs than other surrogate parameters [135].

UV irradiation alone is shown to be effective in NOM concentration and DBP formation over the period of days [114, 135]. However, in this research, the maximum time exposure that we used was 60 minutes. So, it is assumed that the variations in degradation were related to Photocatalysis.

4.3.1.1 **Adsorption**

Although its complicated to identify the adsorption mechanism of NOM using TiO_2 nanoparticles, researchers commonly agreed that TiO_2 photocatalysts preferentially adsorb large and aromatic NOM near or at the vicinity of the photocatalysts [116]. In the dark adsorption, the photo-induced redox reactions degrade the NOM adsorbed at the surface of the photocatalysts or the near vicinity of the surface. NOM adsorption and degradation are influenced by the chemical properties such as pH, ionic strength, the presence of divalent ions such as calcium, NOM concentration and type. Particle size can also influence NOM degradation since small particles are more prone to agglomeration and reduce the effective surface area. TiO_2 surface modification such as doping can improve the degradation rate by increasing the number of adsorption sites.

Figure 4-1 shows the TOC, UV_{254} and SUVA removal using P25 and P25-1.29 wt% Ag during adsorption. The TOC removal did not change significantly during dark period and about 9% of UV_{254} removed using P25-1.29 wt% Ag. P25-1.29 wt% Ag high surface area resulted in higher adsorption of UV_{254} in comparison to P25. Studies showed that larger fractions of humic compounds are prone to photocatalysts surface. Thus, these compounds favorably decompose

as they occupy more surface than smaller molecules [136]. Higher UV_{254} removal than TOC in the absence of irradiation indicated that breaking down the aromatic compounds was easier for phototcatalyst than complete degradation.

By starting the irradiation, the reaction between the photocatalysis and NOM happened in the bulk of the solution while nanomaterials had equal access to all NOM size fractions according to their initial concentration [135].

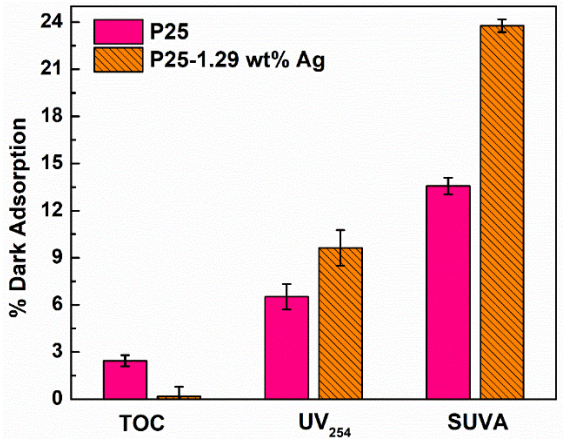

Figure 4-1 TOC, UV_{254} and SUVA adsorption during dark period for P25 and P25-1.29 wt% Ag

4.3.1.2 **Photocatalytic degradation**

4.3.1.2.1 TOC removal

Figure 4-2 shows the TOC removal calculated using Equation 4-1 after 60 minutes irradiation.

$$\boldsymbol{TOC\ Removal}\ \% = \frac{C_0 - C_t}{C_0} \times 100 \qquad \textbf{(Equation 4-1)}$$

Where C_0 is the initial TOC concentration at time zero and C_t is the TOC concentration at time t.

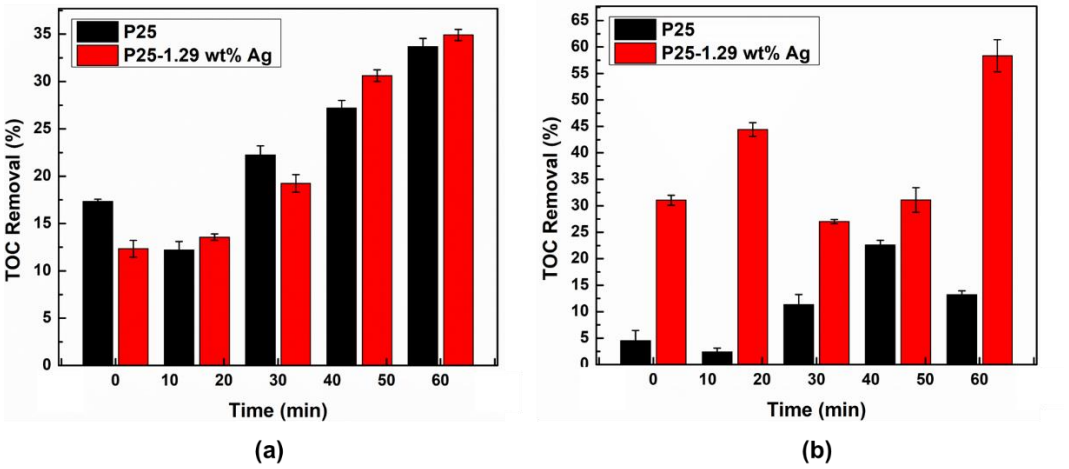

Figure 4-2 (a) TOC removal after 60 minutes under UV irradiation (b) TOC removal after 60 minutes under visible irradiation

According to Figure 4-2, Both P25 and P25- 1.29 wt% Ag removed about 34% TOC under the UV light irradiation. The rate constant of the reaction calculated using Pseudo- first order and it was determined that reaction happen faster when using P25- 1.29 wt% Ag (k_1= 0.0055 min^{-1}) in comparison to P25 (k_1= 0.004 min^{-1}) probably because of producing more ·OH radicals. However, the final TOC removal using both photocatalysts were similar. Considering the mechanism used by P25 and Ag-doped P25 to decompose the NOM makes it understandable since ·OH radicals produced by each nanomaterials can preferably attack the larger fractions of NOM and initial concentration of aromatic NOM compounds was constant in the solution [137].

Under the visible light irradiation, P25 removed TOC up to 15% with the rate constant of 0.0038 min^{-1}. There was no significant difference in TOC removal using P25 and Ag-doped P25 under UV light and P25 under visible light. While P25- 1.29 wt% Ag showed higher TOC removal (about 55%). The rate constant could not be calculated since the regression was not linear using P25- 1.29 wt% Ag (Table C-1 in appendix C).

The reduction and increase in TOC removal at different time points using P25- 1.29 wt% Ag have been reported in previous studies and is attributed to adsorption of NOM, production of intermediate products and desorption of byproducts [138]. Higher TOC removal using P25-1.29 wt% Ag than P25 under the visible light might because of its higher surface area that can

adsorb more NOM compounds. Similar result was reported by Ljubas, who indicated that combining photocatalysis with solar radiation would increase the degradation of NOM even in the presence of other chemicals. He emphasized that TiO_2 photocatalysis was able to degrade higher molecular weight organics compared to lower ones [139].

TOC removal under periodic UV and visible light irradiations was tested using P25-1.29 wt% Ag and P25. According to Figure 4-3 (a) by increasing the UV light duty cycle, the TOC removal would increase which is related to the production of more ·OH radicals. the highest TOC removal is 35% under 80% UV light duty cycle. Figure 4-3 (b) illustrates TOC removal using P25- 1.29 wt% Ag under different UV light duty cycles. Increasing the UV light duty cycle did not change the TOC removal significantly. The highest TOC removal was 25% using 20%, 60% and 80% UV duty cycles.

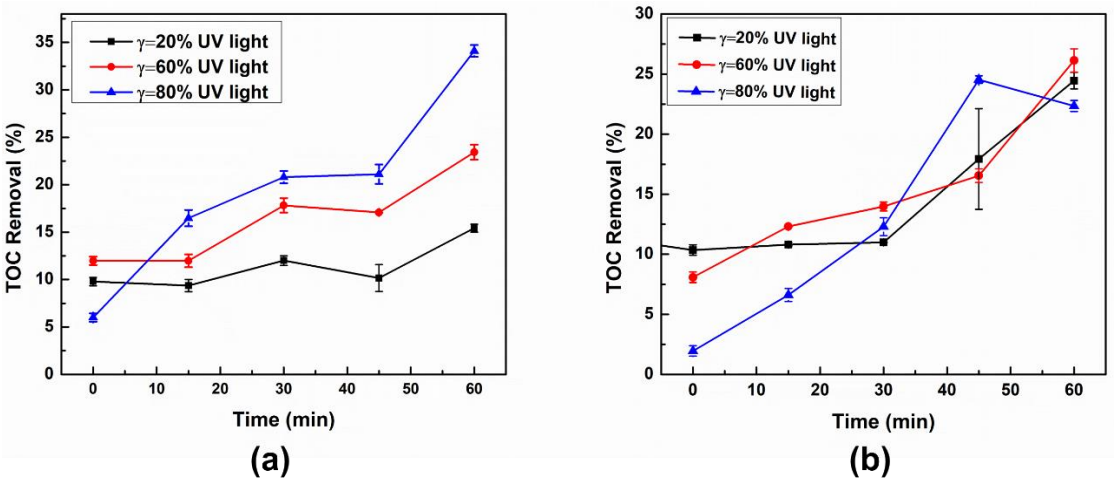

Figure 4-3 TOC removal using (a) P25 and (b) P25- 1.29 wt% Ag under periodic UV and visible light irradiation.

The final amount of TOC at the end of each treatment is approximately 4 mg/L, proving that complete degradation is not achievable. This is in accordance with previous studies on NOM removal using AOPs. The existence of refractory compounds in the synthetic water or formation of by-products as a result of silver oxidation might be the reason of limited TOC removal [109, 116, 140].

4.3.1.2.2 UV_{254}

Fig 4-4 shows UV_{254} removal using P25 and P25-1.29 wt% Ag under constant illumination of UV and visible light. Under the UV light irradiation P25 and P25-1.29 wt% Ag removed the UV_{254} up to 80% indicating that about 80% of aromatic NOM compounds removed from the water matrices and were broke down to smaller compounds (Figure 4-4 a). However, under the visible light, the UV_{254} removal decreased significantly using the same photocatalysts. The highest UV_{254} removal using P25 and P25-1.29 wt% Ag under the visible light were about 20% after 60 minutes irradiation (Figure 4-4 b).

Higher UV_{254} removal under UV irradiation is due to higher energy of UV light in comparison to visible light that resulted in higher ·OH production as was explained in details in pervious chapters.

Comparing the UV_{254} and TOC removal revealed that UV_{254} removal was higher than TOC removal using photocatalysts. This illustrated that breaking down the aromatic NOM was easier than mineralization of NOM in AOPs [141]. Previous studies by Liu et al. showed that hydrophobic NOM fractions were more easily removed using TiO_2. This is predictable based on complex and heterogeneous composition of NOM which can from the large amount of intermediates with different reactivates toward oxidation and intervene degradation process [137].

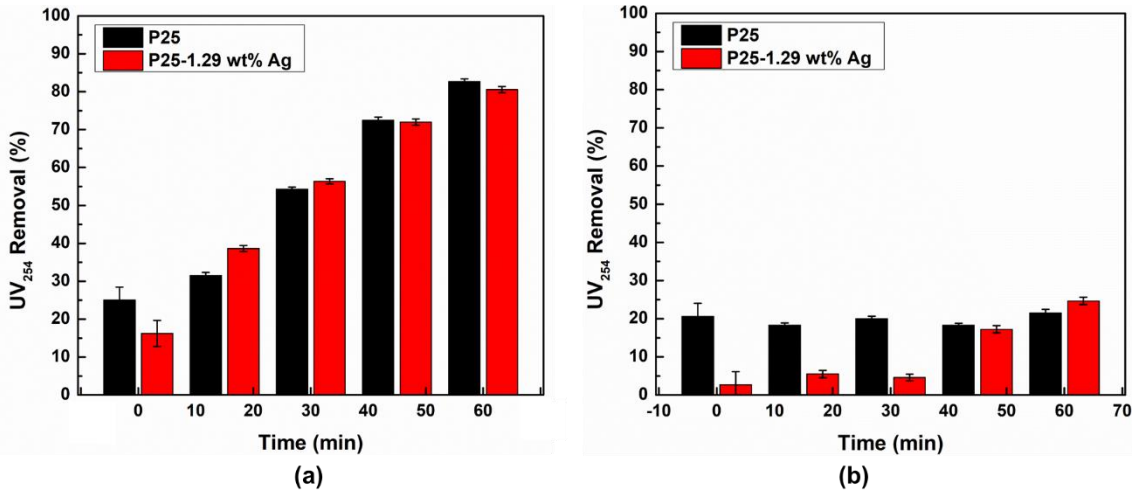

Figure 4-4 UV_{254} removal under using P25 and P25-1.29 wt% Ag under constant illumination of (a) UV light and (b) visible light

Figure 4-5 illustrates UV_{254} removal using P25 and Ag-doped P25 under periodic UV and visible light irradiations. By increasing the UV light duty cycle when using P25 as photocatalysts, more aromatic compounds were broken down to non-aromatic compounds from the synthetic water and the UV_{254} removal increased (Figure 4-5 a).

UV_{254} removal increased by increasing UV light duty cycle using P25-1.29 wt% Ag (Figure 4-5 b). However, the average of UV_{254} removal under each cycle was lower than P25. This result did not correlate with higher surface area and lower band gap of P25-1.29 wt% Ag in comparison to P25, suggested that other factors can effect UV_{254} removal. Formation of intermittent compounds and agglomeration of Ag-doped P25 might be the issues that decreased the effective surface area of the photocatalyst and consequently decreased the UV_{254} degradation.

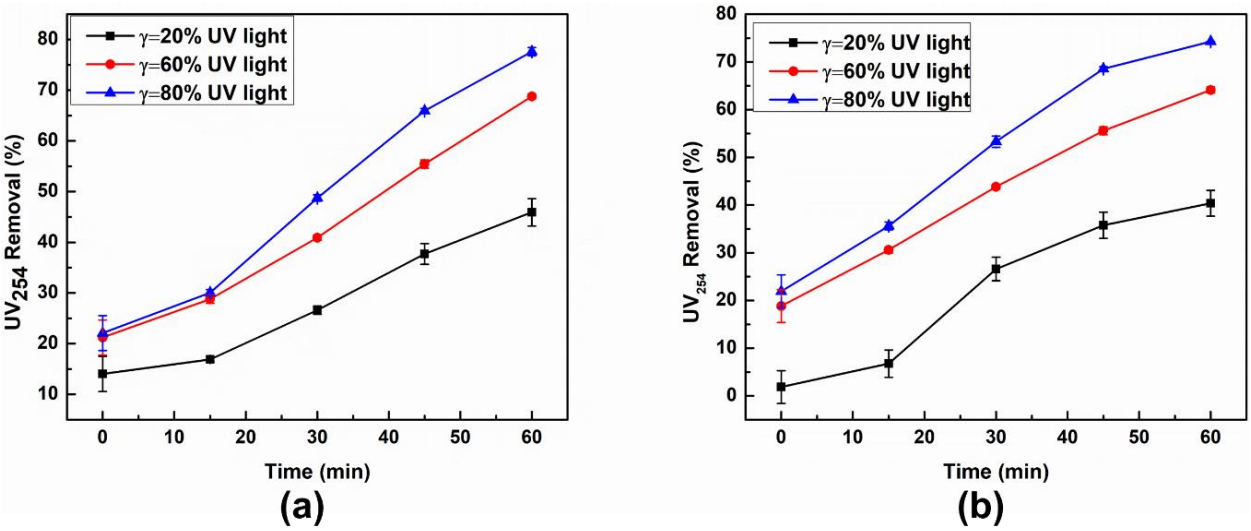

Figure 4-5 UV_{254} removal using (a) P25 (b) P25-1.29 wt% Ag under different UV light fractions

4.3.1.2.3 SUVA

The SUVA value calculates by normalizing UV_{254} absorbance to TOC concentration. It is usually used to indicate the coagulation potential in different water matrices as well as NOM indicator and DBP formation potential predictor [142]. As a rule of thumb, SUVA<2-3 L. mg^{-1}. m^{-1} suggests that the sample mostly contains hydrophilic compounds and low molecule weight NOM (non-humic substances) e. g polysaccharose, amino sugar and micromoleculare organic compounds, while SUVA>4 L. mg^{-1}. m^{-1} indicates that the water matrices is mainly composed of humic compounds [143-145].

The average SUVA value in synthetic water was 2.73 L. mg^{-1}. m^{-1} before starting the treatments, which indicated that the water sample in this study mostly contained hydrophilic, non-humic and low molecular weight fractions. Figure 4-6 (a) illustrates the variation in SUVA when the UV light irradiation started. At the beginning of treatment, the SUVA value was 2.53 and 2.64 L. mg^{-1}. m^{-1} using P25 and Ag-doped P25 as photocatalysts. The SUVA values and the treatment time were negatively corrected, which was resulted from the decomposition of macromolecular organic compounds into smaller compounds. After 60 minues UV light

irradiation, SUVA reduced to 0.73 and 0.83 L. mg^{-1}. m^{-1} using P25 and P25- 1.29 wt% Ag respectively.

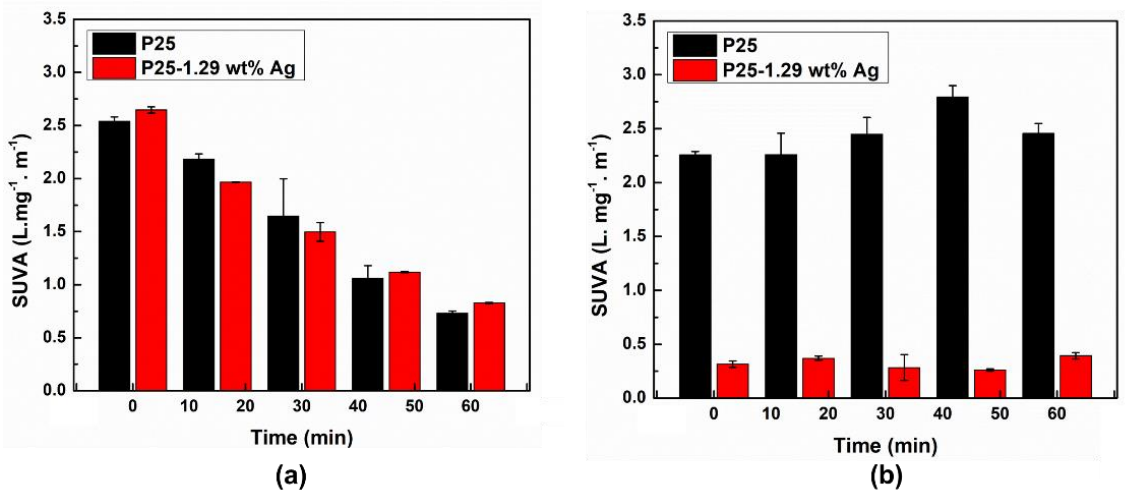

Figure 4-6 SUVA values of P25 and P25-1.29 wt% Ag under constant illumination of (a) UV light and (b) visible light

Under the visible light irradiation the SUVA was constant during the 60 minutes treatment time using P25, indicating that the treatment was not successful in NOM degradation (Figure 4-5 b). However, P25-1.29 wt% Ag reduced SUVA more effectively under visible light than the P25. At the beginning of the visible light irradiation, the SUVA calculated to be 0.029 L. mg^{-1}. m^{-1} and remained constant after 60 minutes of irradiation. As discussed in Chapter 4, P25-1.29 wt% Ag was able to take advantage of the large proportion of the visible light because of its low band gap energy. The band gap energy of this photocatalyst was 2.86 eV, which was lower than P25. This discrepancy was used to explain the P25-1.29 wt% Ag higher ·OH formation and higher SUVA reduction.

Figure 4-7 shows the normalized SUVA values vs. treatment time using P25 and P25-1.29 wt% Ag under periodic illumination of UV and visible light. The normalized SUVA calculated using Equation 4-2:

$$\boldsymbol{Normalized\ SUVA} = \frac{\boldsymbol{SUVA_t}}{\boldsymbol{SUVA_0}} \qquad \textbf{(Equation 4-2)}$$

Where $SUVA_t$ is SUVA at time t and $SUVA_0$ is the SUVA at t=0 min.

Figure 4-7 (a) illustrates that increasing the UV light duty cycle did not change the SUVA reduction using P25. Normalized SUVA value calculated to be 0.40, 0.45 and 0.41 L. mg^{-1}. m^{-1} under 20%, 60% and 80% duty cycle after 60 minutes treatment time. There was coloration between the amount of ·OH produced by increasing the duty cycle and SUVA value using P25.

In the case of P25-1.29 wt% Ag, increasing the UV light duty cycle from 20% to 80%, increased the SUVA reduction (Figure 4-7 (b)). Increasing the duty cycle would increase the production of ·OH in the solution and accordingly the SUVA values decreased. It means that ·OH were able to oxidize large molecules of NOM in the water samples and generated smaller molecules.

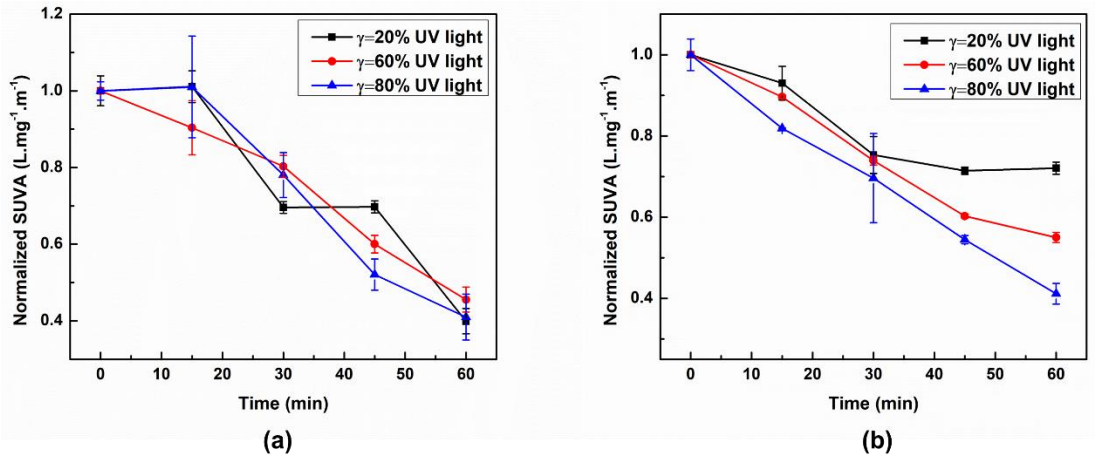

Figure 4-7 SUVA reduction over time using (a) P25 (b) P25-1.29 wt% Ag under different duty cycles

The diagrams illustrating the variation of pH during each duty cycle is represented in Figure C-1 in Appendix C.

4.4 Conclusion

1.29 wt% Ag was compared to bare P25 in terms of its ability to decompose natural organic matter in synthetic water solution. The photocatalysts were tested under constant illumination of UV light and visible light as well as periodic illumination of UV light and visible light in constant frequency of 0.5 Hz.

TOC and UV_{254} removal were selected as NOM surrogate parameters to compare each treatment condition. Under the constant irradiation of UV light, both P25-1.29 wt% Ag and P25 removed about 35% of the TOC in the solution while P25-1.29 wt% Ag did it with faster rate ($k_{1\text{-}P25}$= 0.0055 min^{-1}, $k_{1\text{-}P25\text{-}1.29\ wt\%\ Ag}$= 0.004 min^{-1}). Under the visible light, P25 removed 20% of the TOC. Using two-way anova revealed that there was no significant difference in TOC removal between P25, Ag doped P25 under the UV light and P25 under the visible light. The TOC removal was higher using P25-1.29 wt% Ag under the visible light (about 55%) which might be related to higher surface area of P25-1.29 wt% Ag in compare to P25. Under the periodic illumination of UV and visible light, TOC removal increased by increasing the duty cycle using P25 as photocatalysts, while using Ag-doped P25 did not change the TOC removal in different duty cycles.

UV_{254} removal for both photocatalysts were about 80% under the UV light illumination, Higher UV_{254} removal than TOC removal revealed that breaking down aromatic NOM was easier than mineralization using AOPs. UV_{254} removal under constant irradiation of visible light was lower using P25 and Ag-doped P25. Under the periodic illumination of UV and visible light, UV_{254} removal increased by increasing UV light duty cycle.

The calculated SUVA values indicated that the synthetic water mainly contained hydrophilic NOM and P25-1.29 wt% Ag and P25 reduced the SUVA under UV light irradiation after 60 minutes up to 0.73 and 0.83 L. mg^{-1}. m^{-1}. P25 was not successful to change the NOM compound under the visible light irradiation while P25-1.29 wt% Ag reduced the SUVA up to 0.4 L. mg^{-1}. m^{-1} in the beginning of the irradiation.

Despite the increased in ·OH production using P25-1.29 wt% Ag as photocatalysts, it was difficult to relate the changed in NOM degradation to direct effect of ·OH formation. The agglomeration behavior of the nanomaterials could decrease the required surface area for adsorption and influence the NOM degradation under certain circumstances.

Further research is recommended to clarify the fundamental of the reaction between NOM and photocatalysis.

Chapter 5: **Pharmaceutical removal using Ag-TiO_2 under UV and visible light irradiations**

5.1 Introduction

Pharmaceuticals serve the nations by fighting infectious diseases and improving worldwide public health. However, the consumption of pharmaceuticals, especially antibiotics adversely impact the human health and the environment [121]. These compounds find their way into the surface water simply by excretion and transfer through wastewater systems as well as disposal of manufacturers and hospitals wastes [146, 147]. Pharmacokinetic studies have demonstrated that a considerable proportion of pharmaceuticals excreted through the body and entered the wastewater effluent. Another source for wastewater contamination is disposal of expired medicine via toilet, but it's difficult to estimate the amount since there is no reliable data available [148].

Studies have shown adverse effect of pharmaceutical compounds on aquatic species in the surface water. Examples of this include the phenomena called intersex fish i. e. feminized male fish with oocytes (eggs) developing in their testes when exposed to municipal wastewater [19]. In addition, antidepressants drugs caused lethargic behavior in fish population and changes in their mating habits [18].

Pharmaceuticals not only contaminated the surface water, but also contaminated the ground water by penetration of surface water containing pharmaceutical remains through the drips in landfill sites and sewer drains. Thus, removal of pharmaceuticals from water and wastewater may therefore reduce the risks to both the environment and humans (e.g. drinking water). However, effectively eliminating the pharmaceuticals from the water is still a challenge. Conventional wastewater treatment plants are not able to remove the pharmaceuticals completely. The pharmaceuticals detected in drinking water resources are less than parts per trillion levels. Although no adverse effects have been reported for human health at these levels the uncertainty associated with these complex mixtures continues to create public concern.

Photocatalysis has been widely considered as an effective method to remove emerging contaminants from wastewater and drinking water sources. The reactive oxygen species (ROS) produced using the semiconductors and ultraviolet (UV) light in photocatalysis process are able of degrading or converting pharmaceutical compounds to less harmful substances. Titanium dioxide (TiO_2) is the semiconductor that is commonly used for photocatalytic reactions since they are commercially available and have demonstrated high photocatalytic activity [121]. The photocatalytic efficiency of TiO_2 would be increased by doping metals and non-metals such as silver [126].

Previous studies on pharmaceutical contaminant removal using photocatalysis often used pure water matrices in the experiments. However, actual industrial or municipal applications require considering the natural waters and effluents that contain a complex mixture of chemicals to influence the efficiency of photocatalysts. Although photocatalysts have been used in pharmaceuticals removal in water and wastewater, few studies have been conducted under these actual conditions. In this study Suwannee River natural organic matter (NOM) was used as an actual source of pharmaceuticals in surface water. A cocktail of 24 pharmaceuticals was spiked into the synthetic water containing NOM. The prepared solution was then tested for photocatalytic degradation using P25 and Ag-P25 in photocatalytic testing set up. To compare the photocatalytic degradation under UV and visible light, both photocatalysts were illuminated under constant UV and visible light.

5.2 Materials and Methods

5.2.1 Reagents

P25-1.29 wt% Ag photocatalysis and Suwannee River NOM were prepared using the same procedure as described in Chapter 4. Pharmaceutical compounds contained 24 different chemicals (mostly pharmaceuticals, degradation products or wastewater related contaminants) were purchased from Sigma-Aldrich and dissolved in methanol as 1 g/L stock solutions in glass vials and stored at -20℃. The full list of pharmaceutical compounds, their dissociation constants and applications is tabulated in Table 5-1.

Table 5-1 Chemicals used in this study and some of their properties. All data was collected from TOXNET: Toxicology Data Network.

Pharmaceutical	Abb.	Molecular Formula	Dissociation Constant(s)	Purpose
Ibuprofen	IBU	C13-H18-O2	5.2, 4.91	anti-inflammatory
Naproxen	NPX	C14-H14-O3	4.15	anti- inflammatory
Gemfibrozil	GEM	C15-H22-O3	4.5	lipid lowering
Triclosan	TCS	C12-H7-Cl3-O2	7.9	antimicrobial
Atrazine	ARTZ	C8-H14-Cl-N5	1.6	herbicide
Carbamazepine	CBZ	C15-H12-N2-O	13.9	anti-epileptic
Fluoxetine	FLX	C17-H18-F3-N-O	9.8	SSRI (anti-depressant)
Atorvastatin	ATOR	C33-H35-F-N2-O5	4.3, 14.9	lipid lowering
Venlafaxine	VEN	C17-H27-N-O2	10.09	SSRI (anti-depressant)
Lincomycin	LIN	C18-H34-N2-O6-S	7.6	antibacterial
Monensin	MON	C36-H62-O11	4.2	antibiotic
Sulfanilamide	SULFA	C6-H8-N2-O2-S	10.43	antibacterial
Trimethoprim	TRIM	C14-H18-N4-O3	7.12	antimicrobial
Norfluoxetine	NFLX	C16-H18-F-N3-O3	6.34, 8.75	Fluoxetine degradation product
Atenolol	ATEN	C14-H22-N2-O3	9.6	beta-blocker
Caffeine	CAFF	C8-H10-N4-O2	14	beverage
Carbamazepine-10,11-Epoxide	eCBZ	C15-H12-N2-O	13.9	carbamazepine degradation product
p-Atorvastatin	p-ATOR	C33-H35-F-N2-O5	4.3, 14.9	Atorvastatin degradation product
o-Atorvastatin	O-ATOR	C33-H35-F-N2-O5	4.3, 14.9	Atorvastatin degradation product
Sulfamethoxazole	SMZ	C10-H11-N3-O3-S	1.6, 5.7	antibiotic
Acetaminophen	ACE	C8-H9-N-O2	9.38	analgesic
Desvenlafaxine	DESVEN	C16-H25-N-O2	9.45, 10.66	anti-depressant
Diclofenac	DCF	C14-H11-Cl2-NO2	4.15	anti-inflammatory
Bisphenol A	BPA	C15-H16-O2	9.6	plastic filler

5.2.2 Photocatalytic degradation

A stock solution composed of 24 different pharmaceuticals was spiked to the synthetic water to create a suspension of 2 µg/L of each pharmaceutical compound. The pharmaceuticals in methanol were first evaporated in the fume hood before 300 mL of synthetic water solution was added to the beakers. 30 mg of the photocatalyst was added to the beakers. The same photocatalytic set up was used as in Chapter 4. Sixty minutes dark illumination was used for all the tests and then the lights turned on for constant illumination at time zero. Samples were taken in 4.5 mL aliquots at -60, 0, 5, 10, 20, 40, 60, 90, 120 and 180 minutes. Degradation tests were completed in four conditions outline in Table 5-2. The experiment methodology illustrates in Fig 5-1.

Table 5-2 Treatment conditions

Photocatalysts	Constant UV light irradiation	Constant visible light Irradiation
P25-1.29 wt% Ag	✓	✓
P25	✓	✓

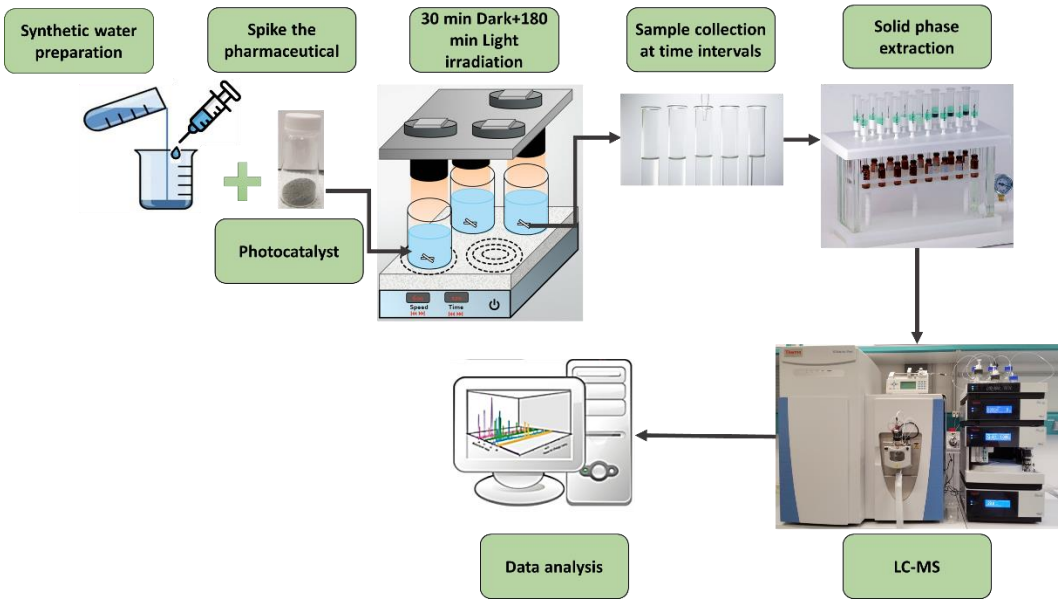

Figure 5-1 Experimental methodology for pharmaceutical tests

5.2.3 Solid phase extraction and LC-MS

After the photodegradation experiments, samples were centrifuged at 3500 rpm to remove the particulate matter. Four mL of the samples transferred to new glass tubes and 32 µL of 100 ug/L deuterated pharmaceutical standards spiked into the new glass tubes. Solid phase extraction (SPE) was completed using Oasis HLB 1cc cartridges with 30 mg sorbent per package and a 30 µm particle size. A detailed SPE procedure can be found in Appendix D Solid Phase Extraction of Pharmaceuticals.

After extraction, the samples were evaporated using the Thermo Scientific™ Rocket Synergy™ Evaporator System. The dried samples were then suspended in 160 µL of reconstitution solution, composed of methanol containing lorazepam and chloramphenicol (75 µg/L). The samples were then stored in a -20℃ freezer until Liquid Chromatography-Mass Spectroscopy analysis.

The liquid chromatography and tandem mass spectrometry (LC-MS/MS) was completed using an Agilent 1200 HPLC coupled to an Applied Biosystems 3200 QTRAP mass spectrometer (ABSciex, Concord, ON, Canada). Selected isotopically labeled standards were used for LC-MS/MS analysis and quantified using lorazepam as the internal standards. These standards were purchased from CDN Isotopes Inc. (Pointe-Claire, QC, Canada), except for atorvastatin-d5, which was purchased from Toronto Research Chemicals (Toronto, ON, Canada).

5.2.4 Data analysis

Data processing was completed using Origin pro. The photocatalytic degradation of pharmaceuticals described using Langmiur-Hinshelwood kinetics model in Equation 5-1:

$$\ln \frac{C_t}{C_0} = -k_{app} t \qquad \textbf{Equation 5-1}$$

Where C_0 and C_t are the initial concentration and the concentration at time t. k_{app} is the apparent first order reaction rate constant [17].

5.3 Results

Successful degradation of pharmaceuticals was achieved using photocatalysis under UV and visible light. The concentration of some of the compounds dropped below the detection limit as quickly as 5 minutes after illumination, while in some cases the compounds degraded in 120 minutes. Figure 5-2 shows the variation of removal of selected compounds under different treatment conditions. Ibuprofen was removed in 90 minutes with the rate constant of 0.046 min^{-1} using P25 under UV irradiation while gemfibrozil and naproxen were removed with faster degradation rate of 0.066 min^{-1} and 0.148 min^{-1} in 40 and 20 minutes respectively (Figure 5-2 a).

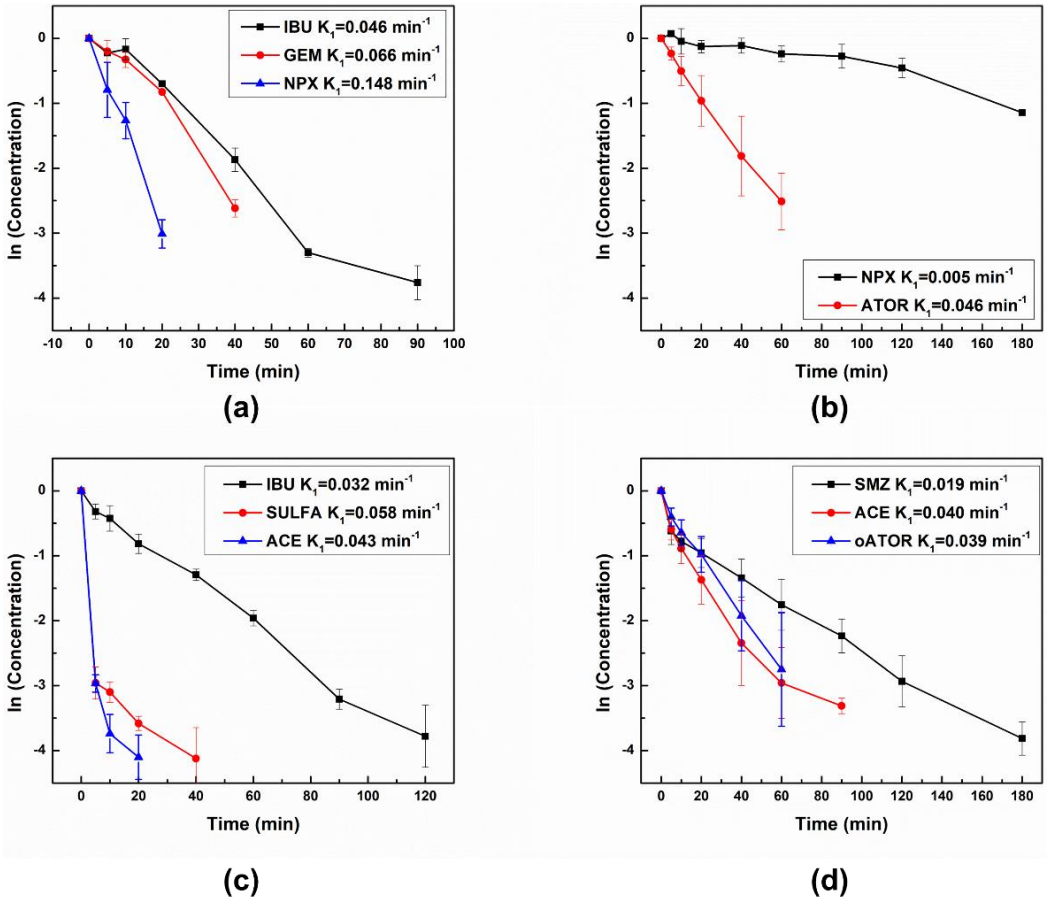

Figure 5-2 ln concentration vs. time for different pharmaceuticals using a) P25 under UV irradiation b) P25 under Visible irradiation c)P25-1.29 wt%Ag under UV irradiation and d) P25-1.29 wt%Ag under Visible irradiation

Under the visible light irradiation, naproxen was removed with lower rate constant of 0.005 min^{-1} using P25. Atorvastatin rate constant was higher in comparison to naproxen in the same condition (0.046 min^{-1}) (Figure 5-2b).

Under the UV light irradiation, P25-1.29 wt% Ag removed ibuprofen with slower rate in comparison to P25 (0.032 min^{-1} vs. 0.046 min^{-1}). Sulfamethoxazole and acetaminophen were removed with rate constant of 0.058 and 0.046 min^{-1}, illustrated in Figure 5-2c. Under the visible light irradiation, P25-1.29 wt% Ag photocatalyst removed Sulfamethoxazole with the rate constant of 0.019 min^{-1} which was lower than acetaminophen and o-atorvastatin with rate constants of 0.040 and 0.039 min^{-1} respectively (Figure 5-2d).

Figure 5-3 compares the rate constants of pharmaceutical compounds using P25 and P25-1.29 wt% Ag under UV and visible light irradiation. Apparently, the rate constants were higher under the UV light irradiation compare to the visible light, that might be related to higher ·OH production [149]. However, by using two-way anova, we found that there is no significant difference between the rate constants of pharmaceuticals using P25 and P25-1.29 wt% Ag under the visible light.

Under the UV light illumination, both P25 and P25-1.29 wt% Ag removed o-atorvastatin completely in 5 minute. Comparing the rate constants using P25 and P25-1.29 wt% Ag under the UV light, indicated that atorvastatin, p-atorvastatin, desvenlafaxine, sulfamethoxazole, acetaminophen, lincomycin and trimethoprim had higher rate constant using P25-1.29 wt% Ag than bare P25.

The difference between the rate constants of the chemicals may be related to the dissociation constants (pK_a) since partitioning to the organic matter made them less available for chemical reactions. Figure 5-4 illustrates the charge of pharmaceutical compounds at pH=8 of the treatment condition based on their pK_a.

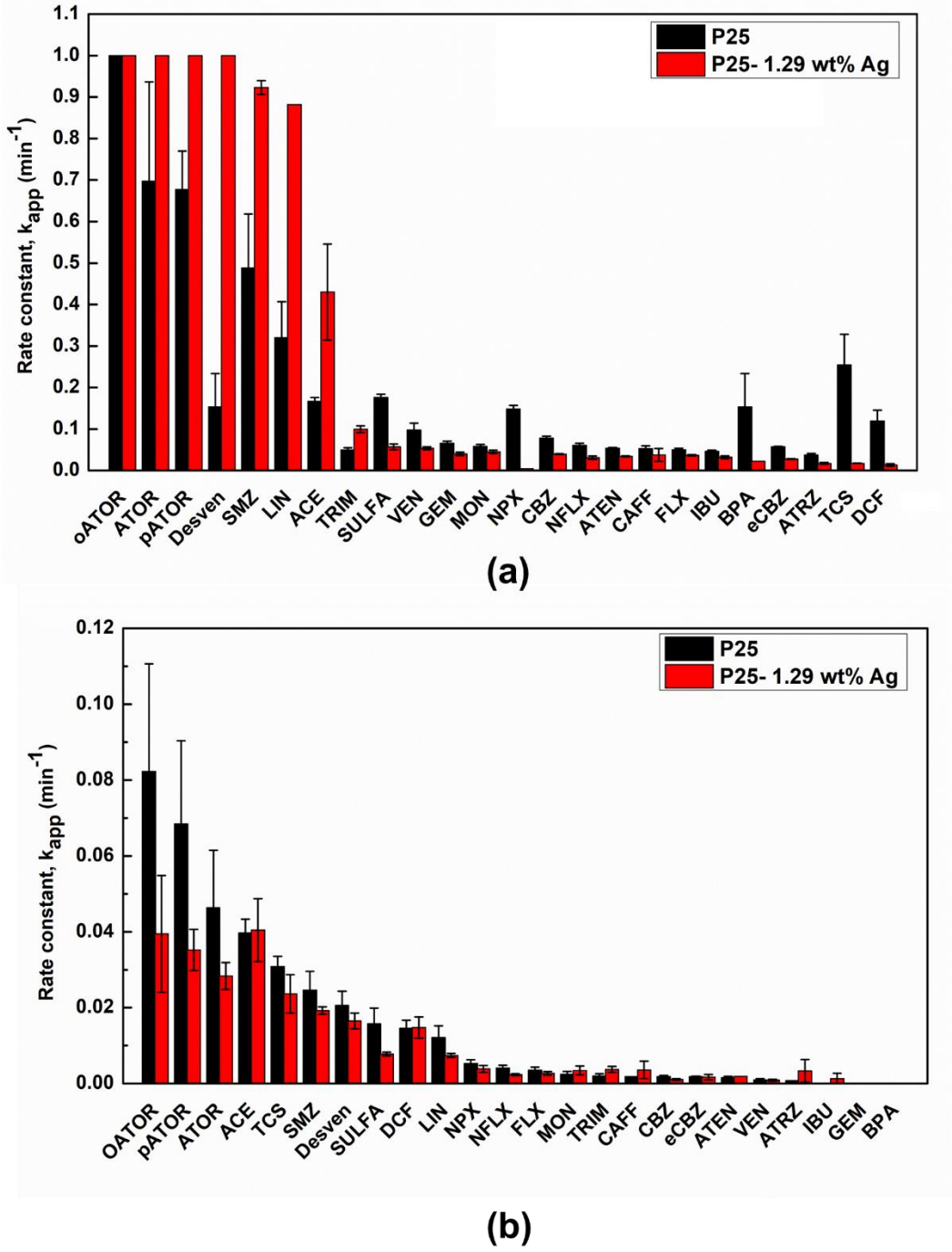

Figure 5-3 rate constant (k_{app}) of different compounds using a) P25 and P25-1.29 wt% Ag under UV light b) P25 and P25-1.29 wt% Ag under visible light

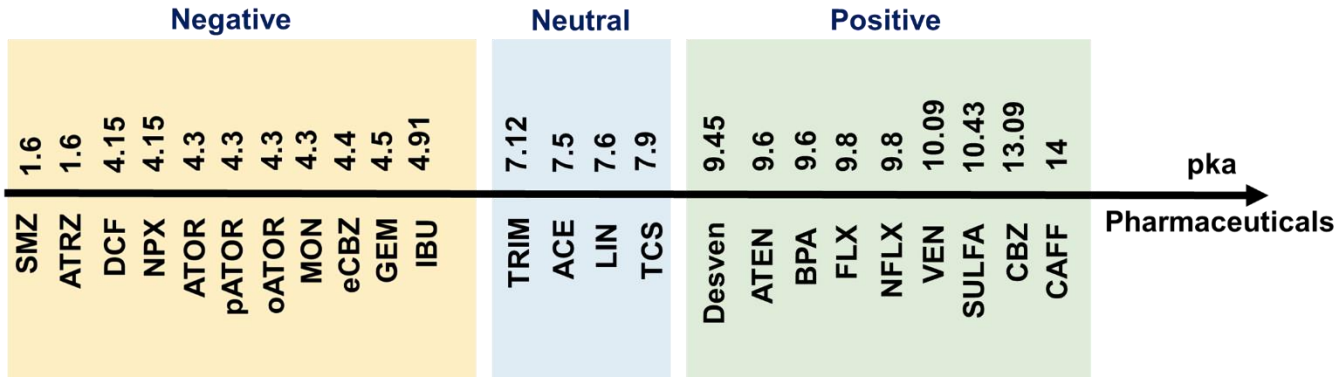

Figure 5-4 Pharmaceutical's charges in pH=8 regarding to their pKa

Generally, oppositely charged particles should have a higher chance of electrostatic interaction [150]. The increase in attraction force would increase the chance of adsorption, which is a crucial step for photocatalysis [104].

The point of zero charge of P25 has been established at a pH of 6-7.5 [151]. The P25 photocatalyst is therefore slightly negative at a pH of 8. It is therefore presumed that pharmaceuticals that exhibit a positive charge in solution will have a higher degradation rate constant due to electrostatic attraction to the photocatalysis [152, 153].

Besides, Ag has the structure of [Kr] $4d^{10}5s^{1}$ while the electron in the $5s^{1}$ orbital is intended to attract H^{+} in the hydroxyl group. In the present solution with pH>8, it is probable that the positively charged hydroxyl groups were dissociated to H^{+} that attracted to Ag and the remained O^{-} stayed on the surface of Ag, introducing negative charge to Ag particles [154].

In the present study o-atorvastatin, p-atorvastatin, and atorvastatin were negatively charged and desvenlafaxine was positively charged. All of these compounds showed highest rate constant (k_{app}=1 min^{-1}) using P25 and P25- 1.29 wt% Ag under the UV light. Sulfamethoxazole with rate constant of 0.92 min^{-1} is negatively charged while lincomycin and acetaminophen with rate constants of 0.88 and 0.43 were neutral in the synthetic water matrices. Therefore, there was no specific relation between pharmaceutical's charges and constant rates. It was probably related to existence of NOM in the solution, which might influence the removal patterns.

5.4 Conclusions

The photocatalytic removal of pharmaceuticals in NOM solution were compared using P25 and P25-1.29 wt% Ag under irradiation of UV and visible light. Overall, photocatalysts were demonstrated to successfully remove o-atorvastatin, p-atorvastatin, and atorvastatin to below the detection limit under irradiation of UV light. P25-1.29 wt% Ag removed desvenlafaxine, sulfamethoxazole, acetaminophen, lincomycin and trimethoprim with higher rate constant compare to P25. Removal of pharmaceuticals using photocatalysts is based on production of ·OH that can degrade the organic compounds. Doping P25 with Ag, can improve the photocataytic efficiency by producing more ·OH. However, this was not general for all the pharmaceuticals. Pharmaceuticals rate constants were lower under visible light and there was no significant difference between the rate constants using P25 and P25- 1.29 wt% Ag under the visible light.

The low rate constants in photocatalytic reactions will remain a challenge in water treatment industry, especial in the presence of high levels of organic matter and where a high throughput of water is required.

Chapter 6

Conclusions and Recommendations

The objectives of this research were to explore the use of photocatalysis in water and wastewater purifications. A large barrier in photocatalyst applications is the low efficiency of TiO_2 under the UV due to e/h recombination. In addition, using TiO_2 is not commercialize yet, since it can't generate photo-induced charges under the irradiation of visible light which represent about 40% of the solar spectrum. Functionalization of TiO_2 nanoparticle with metal and non-metal elements was investigated to determine if the photocatalytic efficiency of TiO_2 for contaminant removal could be improved.

Graphene and silver were used as non-metal and metal elements to dope with TiO_2. Ag-P25 demonstrated higher rate constant and was therefore used in studies for NOM and pharmaceuticals removal under the irradiation of UV and visible light. In addition to antibacterial properties of Ag that makes is suitable for water treatment applications, it can improved electron-hole separation provided by the Schottky barriers and LSPR effect. It was found that increasing silver content resulted in a significant improvement in the photocatalytic efficiency of TiO_2 up an optimum optimal ratio of 1.29 wt.% Ag. The hydrothermal synthesis method was used to form P25 doped Ag nanoparticles. TEM results indicated the uniform dispersion of Ag nanoparticles on the surface of P25 with the size of 1-3 nm. Material characterization demonstrated that P25- 1.29 wt% Ag had the highest surface area (113.65 m^2g^{-1}) and lower band gap energy (2.86 eV) among other samples with different silver concentration. The decreased in band gap energy, increased the adsorption edge to 433.5 nm which demonstrated improvement in photocatalytic reaction under visible light using P25- 1.29 wt% Ag . Increasing the Ag concentration more than 1.29 wt%, caused agglomeration and decreased the surface area of the photocatalysis. HTPA was used as probing molecule to compare the photocatalytic efficiency of Ag-doped P25 under UV and visible light. It was found that 1.29 wt% Ag had highest rate constant under both UV and visible irradiation (k_1=1.65 and 0.012 min^{-1}).

Periodic illumination of UV and visible light was tested to evaluate the photocatalytic efficiency of Ag-doped TiO_2 in different UV light frc=actions. It was found that, in constant frequency of 0.5 Hz, increasing the UV light duty cycle, increased the HTPA formation rate. In constant duty cycle of 50%, increasing the frequency didn't change the HTPA formation rate of the P25- 1.29 wt% Ag, meaning that exposure time variation does not affect the photocatalytic efficiency of this sample.

Chapter 4 compared the photocatalytic removal of NOM in synthetic water using P25 and P25-1.29 wt% Ag. Photocatalysts greatly improved the removal of NOM in the synthetic water matrices under UV and visible irradiation. Periodic illumination of UV and visible light were tested using both photocatalysts with constant frequency of 0.5 Hz. TOC and UV_{254} removal were selected as NOM surrogate parameters to compare the treatment conditions. Under the constant irradiation of UV light, both P25-1.29 wt% Ag and P25 were able to remove about 35% of the TOC in the solution while P25-1.29 wt% Ag could do it at a faster rate. UV_{254} removal for both samples were about 80% under the UV light irradiation, revealing that UV_{254} removal is higher than TOC which illustrated that breaking down of aromatic NOM is easier than mineralization of NOM. TOC and UV_{254} removal was lower under constant irradiation of visible light that might be related to less production of ·OH.

Despite the higher ability of P25-1.29 wt% Ag to produce ·OH in the solution, it was hard to relate the changed in NOM degradation to direct effect of ·OH formation. The agglomeration behavior of the nanomaterials seems to be effective in decreasing the NOM degradation under certain circumstances. Agglomeration can decrease the overall surface area available for adsorption and as such is likely to have an impact on the ability of P25 nanomaterials to absorb NOM. According to the SUVA values, the higher molecular weight organics such as humic acid, aromatic compounds, and polysaccharide degrade to the lower molecular weight organics compounds such as amino sugars. Further work is recommended to more clearly elucidate the process underlying the reaction between NOM and photocatalysis.

Chapter 5 tested the photocatalytic removal of pharmaceuticals from synthetic water using P25 and P25- 1.29 wt% Ag under constant UV and visible light irradiation. Photocatalysts

greatly improved the removal of pharmaceuticals under the UV irradiation in compare to visible light. However, under visible light irradiation, the photocatalysts became less active. This is due to the high intensity of UV light to break the bonds in different organics in compare to visible light. Although, P25- 1.29 wt% Ag was shown to have higher photocatalytic efficiency than P25 in Chapter 3, the removal rate of pharmaceutical compounds were not higher using this photocatalysts than P25. This is probably related to the silver oxidation or scavenging and shielding of UV light by the organic compounds. There was no direct relation between pharmaceuticals charges and rate constants. While both P25 and P25- 1.29 wt% Ag considered as negative compounds in the solution, they tended to attract negative charged pharmaceuticals such as atorvastatin, o-Atorvastatin , p-atorvastatin that demonstrated the highest rate constants in the solution.

Future research in photocatalytic testing should consider the fundamental chemistry concepts of photocatalysis with NOM and pharmaceuticals to improve the removal rate. To commercialize the photocatalysis in water treatment industry, removal of nanomaterials after treatment should considered. Low photocatalytic efficiency, and the long treatment times need modification as well. However, the fast removal of pharmaceuticals reported in this thesis and the environmental pressures imposed by emerging contaminants on the environment provide high motivation to continue research in photocatalytic water treatment.

Removal of the nanomaterials is a big challenge, and future researchers may consider the exploration of core-shell magnetic photocatalysis to create photocatalysis that may be removed by applying magnetic field to the solution, or immobilization and filtering methods that do not result in a considerable loss in efficiency. An ideal photocatalytic setup would consider with a specific contaminant that must be removed, one may group contaminants by physical properties that indicate they may have similar mechanisms for removal. Charge of the contaminant and photocatalysis may be a strong consideration, as demonstrated by the improved degradation rate constants by electrostatic attraction. Alteration in pH may be explored to improve removal or target analyses.

There is also a challenge regarding the degradation byproducts. Some of the intermediates of NOM and pharmaceutical degradation may be more harmful than the initial contaminant. Enhancement of analysis methods by inclusion of additional degradation intermediates may provide insight into whether the contaminant is fully mineralized, rather than just removed. This consideration may be made for pharmaceuticals as well as other emerging contaminants.

While vast improvements have been made in photocatalytic water treatment over the past forty years of research, there still exists ample opportunities to improve water treatment methods to ensure sustainable water sources. The need for novel treatment approaches will continue to grow as the diversity of contaminants and their risks continue to emerge.

References

[1] S. Y. Lee and S. J. Park, "TiO_2 photocatalyst for water treatment applications," *J. Ind. Eng. Chem.*, vol. 19, no. 6, pp. 1761–1769, 2013.

[2] A. Fujishima, X. Zhang, and D. A. Tryk, "TiO_2 photocatalysis and related surface phenomena," *Surf. Sci. Rep.*, vol. 63, no. 12, pp. 515–582, 2008.

[3] K. Hashimoto, H. Irie, and A. Fujishima, "TiO_2 photocatalysis: A historical overview and future prospects," *Japanese J. Appl. Physics, Part 1 Regul. Pap. Short Notes Rev. Pap.*, vol. 44, no. 12, pp. 8269–8285, 2005.

[4] A. Zaleska, "Doped-TiO2: A Review," *Recent Patents Eng.*, vol. 2, no. 3, pp. 157–164, 2008.

[5] S. Zhu and D. Wang, "Photocatalysis: Basic principles, diverse forms of implementations and emerging scientific opportunities," *Adv. Energy Mater.*, vol. 7, no. 23, pp. 1–24, 2017.

[6] L. G. Devi and R. Kavitha, "A review on non metal ion doped titania for the photocatalytic degradation of organic pollutants under UV/solar light: Role of photogenerated charge carrier dynamics in enhancing the activity," *Appl. Catal. B Environ.*, vol. 140–141, pp. 559–587, 2013.

[7] Y. Zhang and C. Pan, "TiO_2/graphene composite from thermal reaction of graphene oxide and its photocatalytic activity in visible light," *J. Mater. Sci.*, vol. 46, no. 8, pp. 2622–2626, 2011.

[8] S. D. Perera, R. G. Mariano, K. Vu, N. Nour, and O. Seitz, "Composites With Enhanced Photocatalytic Activity," pp. 2–5, 2015.

[9] X.-Y. Zhang, H.-P. Li, X.-L. Cui, and Y. Lin, "Graphene/TiO2 nanocomposites: synthesis, characterization and application in hydrogen evolution from water photocatalytic splitting," *J. Mater. Chem.*, vol. 20, no. 14, p. 2801, 2010.

[10] A. Fattahi *et al.*, "Photocatalytic degradation using TiO2-graphene nanocomposite under UV-LED illumination: Optimization using response surface methodology," *J.*

Environ. Chem. Eng., vol. 7, no. 5, p. 103366, 2019.

[11] H. Zhang, X. Lv, Y. Li, Y. Wang, and J. Li, "P25- graphene composite as a high performance photocatalyst," *ACS Nano*, vol. 4, no. 1, pp. 380–386, 2009.

[12] G. Li and K. A. Gray, "The solid-solid interface: Explaining the high and unique photocatalytic reactivity of TiO2-based nanocomposite materials," *Chem. Phys.*, vol. 339, no. 1–3, pp. 173–187, 2007.

[13] N. J. Bell, Y. H. Ng, A. Du, H. Coster, S. C. Smith, and R. Amal, "Understanding the enhancement in photoelectrochemical properties of photocatalytically prepared TiO2-reduced graphene oxide composite," *J. Phys. Chem. C*, vol. 115, no. 13, pp. 6004–6009, 2011.

[14] W. Yang and C. A. Wolden, "Plasma-enhanced chemical vapor deposition of TiO2 thin films for dielectric applications," *Thin Solid Films*, vol. 515, no. 4, pp. 1708–1713, 2006.

[15] D. Gerrity, B. Mayer, H. Ryu, J. Crittenden, and M. Abbaszadegan, "A comparison of pilot-scale photocatalysis and enhanced coagulation for disinfection byproduct mitigation," *Water Res.*, vol. 43, no. 6, pp. 1597–1610, 2009.

[16] J. Schneider *et al.*, "Understanding TiO 2 Photocatalysis : Mechanisms and Materials," 2014.

[17] M. J. Arlos *et al.*, "Influence of methanol when used as a water-miscible carrier of pharmaceuticals in TiO2 photocatalytic degradation experiments," *J. Environ. Chem. Eng.*, vol. 5, no. 5, pp. 4497–4504, 2017.

[18] J. H. Bisesi, W. Bridges, and S. J. Klaine, "Reprint of: Effects of the antidepressant venlafaxine on fish brain serotonin and predation behavior," *Aquat. Toxicol.*, vol. 151, pp. 88–96, 2014.

[19] G. R. Tetreault, C. J. Bennett, K. Shires, B. Knight, M. R. Servos, and M. E. McMaster, "Intersex and reproductive impairment of wild fish exposed to multiple municipal wastewater discharges," *Aquat. Toxicol.*, vol. 104, no. 3–4, pp. 278–290, 2011.

[20] C. Hignite and D. L. Azarnoff, "Drugs and drug metabolites as environmental

contaminants: Chlorophenoxyisobutyrate and salicylic acid in sewage water effluent," *Life Sci.*, vol. 20, no. 2, pp. 337–341, 1977.

[21] D. Ravelli, D. Dondi, M. Fagnoni, and A. Albini, "Photocatalysis. A multi-faceted concept for green chemistry," *Chem. Soc. Rev.*, vol. 38, no. 7, pp. 1999–2011, 2009.

[22] A. Albini and M. Fagnoni, "1908: Giacomo ciamician and the concept of green chemistry," *ChemSusChem*, vol. 1, no. 1–2, pp. 63–66, 2008.

[23] J. M. Herrmann, "Heterogeneous photocatalysis: Fundamentals and applications to the removal of various types of aqueous pollutants," *Catal. Today*, vol. 53, no. 1, pp. 115–129, 1999.

[24] H. L. Tan, F. F. Abdi, and Y. H. Ng, "Heterogeneous photocatalysts: An overview of classic and modern approaches for optical, electronic, and charge dynamics evaluation," *Chem. Soc. Rev.*, vol. 48, no. 5, pp. 1255–1271, 2019.

[25] M. R. Hoffmann, S. T. Martin, W. Choi, and D. W. Bahnemann, "Environmental Applications of Semiconductor Photocatalysis," *Chem. Rev.*, vol. 95, no. 1, pp. 69–96, 1995.

[26] K. Hashimoto, H. Irie, and A. Fujishima, "TiO_2 Photocatalysis: A Historical Overview and Future Prospects," *Jpn. J. Appl. Phys.*, vol. 44, no. 12, pp. 8269–8285, 2005.

[27] O. M. Alfano, M. I. Cabrera, and A. E. Cassano, "Photocatalytic reactions involving hydroxyl radical attack: I. Reaction kinetics formulation with explicit photon absorption effects," *J. Catal.*, vol. 172, no. 2, pp. 370–379, 1997.

[28] S. Gligorovski, R. Strekowski, S. Barbati, and D. Vione, "Environmental Implications of Hydroxyl Radicals (•OH)," *Chem. Rev.*, vol. 115, no. 24, pp. 13051–13092, 2015.

[29] S. G. Kumar and K. S. R. K. Rao, "Comparison of modification strategies towards enhanced charge carrier separation and photocatalytic degradation activity of metal oxide semiconductors (TiO_2 , WO_3 and ZnO)," *Appl. Surf. Sci.*, vol. 391, pp. 124–148, 2017.

[30] Q. Xiang, J. Yu, and P. K. Wong, "Quantitative characterization of hydroxyl radicals produced by various photocatalysts," *J. Colloid Interface Sci.*, vol. 357, no. 1, pp. 163–

167, 2011.

[31] C. Jayaseelan *et al.*, "Biological approach to synthesize TiO2 nanoparticles using Aeromonas hydrophila and its antibacterial activity," *Spectrochim. Acta - Part A Mol. Biomol. Spectrosc.*, vol. 107, pp. 82–89, 2013.

[32] A. Fujishima, T. N. Rao, and D. A. Tryk, "Titanium dioxide photocatalysis," *Journal of Photochemistry and Photobiology C: Photochemistry Reviews*, vol. 1, no. 1. pp. 1–21, 2000.

[33] K. Nakata and A. Fujishima, "TiO_2 photocatalysis: Design and applications," *J. Photochem. Photobiol. C Photochem. Rev.*, vol. 13, no. 3, pp. 169–189, 2012.

[34] M. Cargnello, T. R. Gordon, and C. B. Murray, "Solution-phase synthesis of titanium dioxide nanoparticles and nanocrystals," *Chem. Rev.*, vol. 114, no. 19, pp. 9319–9345, 2014.

[35] D. Reyes-Coronado, G. Rodríguez-Gattorno, M. E. Espinosa-Pesqueira, C. Cab, R. De Coss, and G. Oskam, "Phase-pure TiO2 nanoparticles: Anatase, brookite and rutile," *Nanotechnology*, vol. 19, no. 14, 2008.

[36] J. Zhang, P. Zhou, J. Liu, and J. Yu, "New understanding of the difference of photocatalytic activity among anatase, rutile and brookite TiO2," *Phys. Chem. Chem. Phys.*, vol. 16, no. 38, pp. 20382–20386, 2014.

[37] S. Bakardjieva, J. Šubrt, V. Štengl, M. J. Dianez, and M. J. Sayagues, "Photoactivity of anatase-rutile TiO2 nanocrystalline mixtures obtained by heat treatment of homogeneously precipitated anatase," *Appl. Catal. B Environ.*, vol. 58, no. 3–4, pp. 193–202, 2005.

[38] J. E. G. J. Wijnhoven and W. L. Vos, "Preparation of photonic crystals made of air spheres in titania," *Science (80-.).*, vol. 281, no. 5378, pp. 802–804, 1998.

[39] H. Zhang, R. L. Penn, R. J. Hamers, and J. F. Banfield, "Enhanced adsorption of molecules on surfaces of nanocrystalline particles," *J. Phys. Chem. B*, vol. 103, no. 22, pp. 4656–4662, 1999.

[40] G. Varshney *et al.*, "Nanoscale TiO_2 films and their application in remediation of

organic pollutants," *Coord. Chem. Rev.*, vol. 306, no. P1, pp. 43–64, 2016.

[41] X. Chen and S. S. Mao, "Titanium dioxide nanomaterials: Synthesis, properties, modifications and applications," *Chem. Rev.*, vol. 107, no. 7, pp. 2891–2959, 2007.

[42] J. Ng, X. Wang, and D. D. Sun, "One-pot hydrothermal synthesis of a hierarchical nanofungus-like anatase TiO2 thin film for photocatalytic oxidation of bisphenol A," *Appl. Catal. B Environ.*, vol. 110, pp. 260–272, 2011.

[43] R. S. Sonawane, B. B. Kale, and M. K. Dongare, "Preparation and photo-catalytic activity of Fe-TiO2 thin films prepared by sol-gel dip coating," *Mater. Chem. Phys.*, vol. 85, no. 1, pp. 52–57, 2004.

[44] K. Rajendran, V. Senthil Kumar, and K. Anitha Rani, "Synthesis and characterization of immobilized activated carbon doped TiO_2 thin films," *Optik (Stuttg).*, vol. 125, no. 8, pp. 1993–1996, 2014.

[45] A. Sobczyk-Guzenda, B. Pietrzyk, H. Szymanowski, M. Gazicki-Lipman, and W. Jakubowski, "Photocatalytic activity of thin TiO_2 films deposited using sol-gel and plasma enhanced chemical vapor deposition methods," *Ceram. Int.*, vol. 39, no. 3, pp. 2787–2794, 2013.

[46] A. Gültekin, G. Karanfil, F. Özel, M. Kuş, R. Say, and S. Sönmezoğlu, "Synthesis and characterisations of Au-nanoparticle-doped TiO 2 and CdO thin films," *J. Phys. Chem. Solids*, vol. 75, no. 6, pp. 775–781, 2014.

[47] V. G. Bessergenev *et al.*, "Study of physical and photocatalytic properties of titanium dioxide thin films prepared from complex precursors by chemical vapour deposition," *Thin Solid Films*, vol. 503, no. 1–2, pp. 29–39, 2006.

[48] Y. Zhang, J. Wan, and Y. Ke, "A novel approach of preparing TiO_2 films at low temperature and its application in photocatalytic degradation of methyl orange," *J. Hazard. Mater.*, vol. 177, no. 1–3, pp. 750–754, 2010.

[49] M. Ammam, "Electrophoretic deposition under modulated electric fields: A review," *RSC Adv.*, vol. 2, no. 20, pp. 7633–7646, 2012.

[50] I. Liepina, G. Bajars, A. Lusis, G. Mezinskis, and M. Vanags, "Preparation and

characterization of nanostructured Fe-TiO_2 thin films produced by electrophoretic deposition," *IOP Conf. Ser. Mater. Sci. Eng.*, vol. 49, no. 1, 2013.

[51] F. Chen, F. Cao, H. Li, and Z. Bian, "Exploring the important role of nanocrystals orientation in TiO2 superstructure on photocatalytic performances," *Langmuir*, vol. 31, no. 11, pp. 3494–3499, 2015.

[52] D. Mardare, F. Iacomi, N. Cornei, M. Girtan, and D. Luca, "Undoped and Cr-doped TiO2 thin films obtained by spray pyrolysis," *Thin Solid Films*, vol. 518, no. 16, pp. 4586–4589, 2010.

[53] A. Nakaruk and C. C. Sorrell, "Conceptual model for spray pyrolysis mechanism: Fabrication and annealing of titania thin films," *J. Coatings Technol. Res.*, vol. 7, no. 5, pp. 665–676, 2010.

[54] M. Radecka, M. Rekas, A. Trenczek-Zajac, and K. Zakrzewska, "Importance of the band gap energy and flat band potential for application of modified TiO2 photoanodes in water photolysis," *J. Power Sources*, vol. 181, no. 1, pp. 46–55, 2008.

[55] X. Chen, S. Shen, L. Guo, and S. S. Mao, "Semiconductor-based photocatalytic hydrogen generation," *Chem. Rev.*, vol. 110, no. 11, pp. 6503–6570, 2010.

[56] B. Adeli and F. Taghipour, "A review of synthesis techniques for gallium-zinc oxynitride solar-activated photocatalyst for water splitting," *ECS J. Solid State Sci. Technol.*, vol. 2, no. 7, pp. 118–126, 2013.

[57] D. Dvoranová, V. Brezová, M. Mazúr, and M. A. Malati, "Investigations of metal-doped titanium dioxide photocatalysts," *Appl. Catal. B Environ.*, vol. 37, no. 2, pp. 91–105, 2002.

[58] S. I. Mogal *et al.*, "Single-step synthesis of silver-doped titanium dioxide: Influence of silver on structural, textural, and photocatalytic properties," *Ind. Eng. Chem. Res.*, vol. 53, no. 14, pp. 5749–5758, 2014.

[59] H. Zhang and G. Chen, "potent antibacterial activities of Ag/TiO_2 nanocomposite powders synthesized by a one-pot sol-gel method," *Environ. Sci. Technol.*, vol. 43, no. 8, pp. 2905–2910, 2009.

[60] B. Zhao and Y. W. Chen, "Ag/TiO_2 sol prepared by a solgel method and its photocatalytic activity," *J. Phys. Chem. Solids*, vol. 72, no. 11, pp. 1312–1318, 2011.

[61] J. O. Carneiro, V. Teixeira, A. Portinha, L. Dupák, A. Magalhães, and P. Coutinho, "Study of the deposition parameters and Fe-dopant effect in the photocatalytic activity of TiO2 films prepared by dc reactive magnetron sputtering," *Vacuum*, vol. 78, no. 1, pp. 37–46, 2005.

[62] J. C. S. Wu and C. H. Chen, "A visible-light response vanadium-doped titania nanocatalyst by sol-gel method," *J. Photochem. Photobiol. A Chem.*, vol. 163, no. 3, pp. 509–515, 2004.

[63] X. Z. Li and F. B. Li, "Study of Au/Au3+-TiO2 photocatalysts toward visible photooxidation for water and wastewater treatment," *Environ. Sci. Technol.*, vol. 35, no. 11, pp. 2381–2387, 2001.

[64] F. B. Li and X. Z. Li, "The enhancement of photodegradation efficiency using Pt-TiO2 catalyst," *Chemosphere*, vol. 48, no. 10, pp. 1103–1111, 2002.

[65] Z. Wu, F. Dong, W. Zhao, and S. Guo, "Visible light induced electron transfer process over nitrogen doped TiO2 nanocrystals prepared by oxidation of titanium nitride," *J. Hazard. Mater.*, vol. 157, no. 1, pp. 57–63, 2008.

[66] R. Asahi, T. Morikawa, T. Ohwaki, K. Aoki, and Y. Taga, "Visible-light photocatalysis in nitrogen-doped titanium oxides," *Science (80-.).*, vol. 293, no. 5528, pp. 269–271, 2001.

[67] T. Ohno, T. Mitsui, and M. Matsumura, "Photocatalytic activity of S-doped TiO2 photocatalyst under visible light," *Chem. Lett.*, vol. 32, no. 4, pp. 364–365, 2003.

[68] J. Yu, M. Zhou, B. Cheng, and X. Zhao, "Preparation, characterization and photocatalytic activity of in situ N,S-codoped TiO2 powders," *J. Mol. Catal. A Chem.*, vol. 246, no. 1–2, pp. 176–184, 2006.

[69] S. Y. Treschev, P. W. Chou, Y. H. Tseng, J. Bin Wang, E. V. Perevedentseva, and C. L. Cheng, "Photoactivities of the visible-light-activated mixed-phase carbon-containing titanium dioxide: The effect of carbon incorporation," *Appl. Catal. B Environ.*, vol. 79,

no. 1, pp. 8–16, 2008.

[70] A. Zaleska, J. W. Sobczak, E. Grabowska, and J. Hupka, “Preparation and photocatalytic activity of boron-modified TiO_2 under UV and visible light,” *Appl. Catal. B Environ.*, vol. 78, no. 1–2, pp. 92–100, 2008.

[71] H. Natori, K. Kobayashi, and M. Takahashi, “Preparation and photocatalytic property of phosphorus-doped TiO2 particles,” *J. Oleo Sci.*, vol. 58, no. 7, pp. 389–394, 2009.

[72] J. Choi, H. Park, and M. R. Hoffmann, “Effects of single metal-ion doping on the visible-light photoreactivity of TiO2,” *J. Phys. Chem. C*, vol. 114, no. 2, pp. 783–792, 2010.

[73] Y. Zhu *et al.*, “Graphene and graphene oxide: Synthesis, properties, and applications,” *Adv. Mater.*, vol. 22, no. 35, pp. 3906–3924, 2010.

[74] A. K. Geim, “Graphene : Status and Prospects,” vol. 324, no. 5934, pp. 1530–1534, 2009.

[75] M. D. Stoller, S. Park, Y. Zhu, J. An, and R. S. Ruoff, “Graphene-Based Ultracapacitors,” pp. 6–10, 2008.

[76] M. J. McAllister *et al.*, “Single sheet functionalized graphene by oxidation and thermal expansion of graphite,” *Chem. Mater.*, vol. 19, no. 18, pp. 4396–4404, 2007.

[77] Y. S. Ocak *et al.*, “Current-voltage and capacitance-voltage characteristics of a Sn/Methylene Blue/p-Si Schottky diode,” *Synth. Met.*, vol. 159, no. 3, pp. 1603–1607, 2009.

[78] N. R. Khalid, E. Ahmed, Z. Hong, L. Sana, and M. Ahmed, “Enhanced photocatalytic activity of graphene-TiO2 composite under visible light irradiation,” *Curr. Appl. Phys.*, vol. 13, no. 4, pp. 659–663, 2013.

[79] Z. Mou, Y. Wu, J. Sun, P. Yang, Y. Du, and C. Lu, “TiO2 nanoparticles-functionalized N-doped graphene with superior interfacial contact and enhanced charge separation for photocatalytic hydrogen generation,” *ACS Appl. Mater. Interfaces*, vol. 6, no. 16, pp. 13798–13806, 2014.

[80] S. D. Perera *et al.*, “Hydrothermal synthesis of graphene-TiO_2 nanotube composites

with enhanced photocatalytic activity," *ACS Catal.*, vol. 2, no. 6, pp. 949–956, 2012.

[81] K. Zhou, Y. Zhu, X. Yang, X. Jiang, and C. Li, "Preparation of graphene-TiO2 composites with enhanced photocatalytic activity," *New J. Chem.*, vol. 35, no. 2, pp. 353–359, 2011.

[82] Y. Chen, H. Gao, J. Xiang, X. Dong, and Y. Cao, "Enhanced photocatalytic activities of TiO 2 -reduced graphene oxide nanocomposites controlled by Ti–O–C interfacial chemical bond," *Mater. Res. Bull.*, vol. 99, no. August 2017, pp. 29–36, 2018.

[83] H. Eom *et al.*, "Strong localized surface plasmon resonance effects of Ag/TiO2 core-shell nanowire arrays in UV and visible light for photocatalytic activity," *Nanoscale*, vol. 6, no. 1, pp. 226–234, 2014.

[84] X. Wu *et al.*, "Reports on Progress in Physics Plasmonic photocatalysis Direct photocatalysis of supported metal nanostructures for organic synthesis Photocatalytic composites based on titania nanoparticles and carbon nanomaterials Plasmonic photocatalysis," *Rep. Prog. Phys*, vol. 76, pp. 46401–41, 2013.

[85] P. Wang, B. Huang, Y. Dai, and M. H. Whangbo, "Plasmonic photocatalysts: Harvesting visible light with noble metal nanoparticles," *Phys. Chem. Chem. Phys.*, vol. 14, no. 28, pp. 9813–9825, 2012.

[86] Y. Nishijima, K. Ueno, Y. Yokota, K. Murakoshi, and H. Misawa, "Plasmon-assisted photocurrent generation from visible to near-infrared wavelength using a Au-nanorods/TiO2 electrode," *J. Phys. Chem. Lett.*, vol. 1, no. 13, pp. 2031–2036, 2010.

[87] Z. Liu, W. Hou, P. Pavaskar, M. Aykol, and S. B. Cronin, "Plasmon resonant enhancement of photocatalytic water splitting under visible illumination," *Nano Lett.*, vol. 11, no. 3, pp. 1111–1116, 2011.

[88] M. H. Ahmed, T. E. Keyes, J. A. Byrne, C. W. Blackledge, and J. W. Hamilton, "Adsorption and photocatalytic degradation of human serum albumin on TiO 2 and Ag-TiO 2 films," *J. Photochem. Photobiol. A Chem.*, vol. 222, no. 1, pp. 123–131, 2011.

[89] M. Harikishore, M. Sandhyarani, K. Venkateswarlu, T. A. Nellaippan, and N. Rameshbabu, "Effect of Ag Doping on Antibacterial and Photocatalytic Activity of

Nanocrystalline TiO_2," *Procedia Mater. Sci.*, vol. 6, no. Icmpc, pp. 557–566, 2014.

[90] N. Zhou *et al.*, "TiO_2 coated Au/Ag nanorods with enhanced photocatalytic activity under visible light irradiation," *Nanoscale*, vol. 5, no. 10, pp. 4236–4241, 2013.

[91] B. Cheng, Y. Le, and J. Yu, "Preparation and enhanced photocatalytic activity of Ag@TiO_2 core-shell nanocomposite nanowires," *J. Hazard. Mater.*, vol. 177, no. 1–3, pp. 971–977, 2010.

[92] Z. Zheng, B. Huang, X. Qin, X. Zhang, Y. Dai, and M. H. Whangbo, "Facile in situ synthesis of visible-light plasmonic photocatalysts M@TiO_2 (M = Au, Pt, Ag) and evaluation of their photocatalytic oxidation of benzene to phenol," *J. Mater. Chem.*, vol. 21, no. 25, pp. 9079–9087, 2011.

[93] V. Tomašić, F. Jović, and Z. Gomzi, "Photocatalytic oxidation of toluene in the gas phase: Modelling an annular photocatalytic reactor," *Catal. Today*, vol. 137, no. 2–4, pp. 350–356, 2008.

[94] A. Gora, B. Toepfer, V. Puddu, and G. Li Puma, "Photocatalytic oxidation of herbicides in single-component and multicomponent systems: Reaction kinetics analysis," *Appl. Catal. B Environ.*, vol. 65, no. 1–2, pp. 1–10, 2006.

[95] C. Guzmán, G. Del Ángel, R. Gómez, F. Galindo-Hernández, and C. Ángeles-Chavez, "Degradation of the herbicide 2,4-dichlorophenoxyacetic acid over Au/TiO_2-CeO_2 photocatalysts: Effect of the CeO_2 content on the photoactivity," *Catal. Today*, vol. 166, no. 1, pp. 146–151, 2011.

[96] M. M. Ballari, M. Hunger, G. Hüsken, and H. J. H. Brouwers, "NOx photocatalytic degradation employing concrete pavement containing titanium dioxide," *Appl. Catal. B Environ.*, vol. 95, no. 3–4, pp. 245–254, 2010.

[97] G. Vincent, P. M. Marquaire, and O. Zahraa, "Abatement of volatile organic compounds using an annular photocatalytic reactor: Study of gaseous acetone," *J. Photochem. Photobiol. A Chem.*, vol. 197, no. 2–3, pp. 177–189, 2008.

[98] M. L. Sauer and D. F. Ollis, "Photocatalyzed oxidation of ethanol and acetaldehyde in humidified air," *J. Catal.*, vol. 158, no. 2, pp. 570–582, 1996.

[99] X. Zhu, D. L. Chang, X. S. Li, Z. G. Sun, X. Q. Deng, and A. M. Zhu, “Inherent rate constants and humidity impact factors of anatase TiO<inf>2</inf> film in photocatalytic removal of formaldehyde from air,” *Chem. Eng. J.*, vol. 279, pp. 897–903, 2015.

[100] K. H. Wang, H. H. Tsai, and Y. H. Hsieh, “The kinetics of photocatalytic degradation of trichloroethylene in gas phase over TiO2 supported on glass bead,” *Appl. Catal. B Environ.*, vol. 17, no. 4, pp. 313–320, 1998.

[101] B. Toepfer, A. Gora, and G. Li Puma, “Photocatalytic oxidation of multicomponent solutions of herbicides: Reaction kinetics analysis with explicit photon absorption effects,” *Appl. Catal. B Environ.*, vol. 68, no. 3–4, pp. 171–180, 2006.

[102] G. Camera-Roda *et al.*, “A reaction engineering approach to kinetic analysis of photocatalytic reactions in slurry systems,” *Catal. Today*, vol. 259, pp. 87–96, 2016.

[103] I. K. Konstantinou and T. A. Albanis, “TiO2-assisted photocatalytic degradation of azo dyes in aqueous solution: Kinetic and mechanistic investigations: A review,” *Appl. Catal. B Environ.*, vol. 49, no. 1, pp. 1–14, 2004.

[104] C. S. Turchi and D. F. Ollis, “Photocatalytic degradation of organic water contaminants: Mechanisms involving hydroxyl radical attack,” *J. Catal.*, vol. 122, no. 1, pp. 178–192, 1990.

[105] U. Černigoj, M. Kete, and U. L. Štangar, “Development of a fluorescence-based method for evaluation of self-cleaning properties of photocatalytic layers,” *Catal. Today*, vol. 151, no. 1–2, pp. 46–52, 2010.

[106] R. Thiruvenkatachari, T. O. Kwon, J. C. Jun, S. Balaji, M. Matheswaran, and I. S. Moon, “Application of several advanced oxidation processes for the destruction of terephthalic acid (TPA),” *J. Hazard. Mater.*, vol. 142, no. 1–2, pp. 308–314, 2007.

[107] B. J. R. Thio, D. Zhou, and A. A. Keller, “Influence of natural organic matter on the aggregation and deposition of titanium dioxide nanoparticles,” *J. Hazard. Mater.*, vol. 189, no. 1–2, pp. 556–563, 2011.

[108] S. L. Gora, R. Liang, Y. N. Zhou, and S. A. Andrews, “Photocatalysis with easily

recoverable linear engineered TiO_2 nanomaterials to prevent the formation of disinfection byproducts in drinking water," *J. Environ. Chem. Eng.*, vol. 6, no. 1, pp. 197–207, 2018.

[109] S. Liu *et al.*, "Removal of humic acid using TiO2 photocatalytic process - Fractionation and molecular weight characterisation studies," *Chemosphere*, vol. 72, no. 2, pp. 263–271, 2008.

[110] S. L. Gora and S. A. Andrews, "Removal of natural organic matter and disinfection byproduct precursors from drinking water using photocatalytically regenerable nanoscale adsorbents," *Chemosphere*, vol. 218, pp. 52–63, 2019.

[111] A. Matilainen, M. Vepsäläinen, and M. Sillanpää, "Natural organic matter removal by coagulation during drinking water treatment: A review," *Adv. Colloid Interface Sci.*, vol. 159, no. 2, pp. 189–197, 2010.

[112] A. Matilainen, E. T. Gjessing, T. Lahtinen, L. Hed, A. Bhatnagar, and M. Sillanpää, "An overview of the methods used in the characterisation of natural organic matter (NOM) in relation to drinking water treatment," *Chemosphere*, vol. 83, no. 11, pp. 1431–1442, 2011.

[113] B. K. Mayer, C. Johnson, Y. Yang, N. Wellenstein, E. Maher, and P. J. McNamara, "From micro to macro-contaminants: The impact of low-energy titanium dioxide photocatalysis followed by filtration on the mitigation of drinking water organics," *Chemosphere*, vol. 217, pp. 111–121, 2019.

[114] E. J. Rosenfeldt and K. G. Linden, "Degradation of endocrine disrupting chemicals bisphenol A, ethinyl estradiol, and estradiol during UV photolysis and advanced oxidation processes," *Environ. Sci. Technol.*, vol. 38, no. 20, pp. 5476–5483, 2004.

[115] H. Dong, G. Zeng, L. Tang, and C. Fan, "ScienceDirect An overview on limitations of TiO 2 -based particles for photocatalytic degradation of organic pollutants and the corresponding countermeasures," *Water Res.*, vol. 79, pp. 128–146, 2015.

[116] A. Matilainen and M. Sillanpää, "Removal of natural organic matter from drinking water by advanced oxidation processes," *Chemosphere*, vol. 80, no. 4, pp. 351–365,

2010.

[117] S. L. Gora and S. A. Andrews, “Adsorption of natural organic matter and disinfection byproduct precursors from surface water on TiO_2 Nanoparticles: pH effects, isotherm modelling and implications for using TiO_2 for drinking water treatment,” *Chemosphere*, vol. 174, pp. 363–370, 2017.

[118] T. aus der Beek *et al.*, “Pharmaceuticals in the environment-Global occurrences and perspectives,” *Environ. Toxicol. Chem.*, vol. 35, no. 4, pp. 823–835, 2016.

[119] T. P. Thanh, “Occurrence of pharmaceutical residues in water and treatment solutions,” no. April, 2018.

[120] A. M. P. T. Pereira, L. J. G. Silva, L. M. Meisel, C. M. Lino, and A. Pena, “Environmental impact of pharmaceuticals from Portuguese wastewaters: Geographical and seasonal occurrence, removal and risk assessment,” *Environ. Res.*, vol. 136, pp. 108–119, 2015.

[121] G. Li, X. Nie, Y. Gao, and T. An, “Can environmental pharmaceuticals be photocatalytically degraded and completely mineralized in water using g-C_3/ N_4/TiO_2 under visible light irradiation?-Implications of persistent toxic intermediates,” *Appl. Catal. B Environ.*, vol. 180, pp. 726–732, 2016.

[122] D. Wodka *et al.*, “Photocatalytic activity of titanium dioxide modified by silver nanoparticles,” *ACS Appl. Mater. Interfaces*, vol. 2, no. 7, pp. 1945–1953, 2010.

[123] Y. Horiguchi, T. Kanda, K. Torigoe, H. Sakai, and M. Abe, “Preparation of gold/silver/titania trilayered nanorods and their photocatalytic activities,” *Langmuir*, vol. 30, no. 3, pp. 922–928, 2014.

[124] E. Grabowska *et al.*, “Modification of titanium(IV) dioxide with small silver nanoparticles: Application in photocatalysis,” *J. Phys. Chem. C*, vol. 117, no. 4, pp. 1955–1962, 2013.

[125] S. G. Shelar, V. K. Mahajan, S. P. Patil, and G. H. Sonawane, “Enhancement of visible light induced photocatalytic degradation of Eosin-Y by using TiO_2 and Ag doped TiO_2 nano catalyst,” vol. 10, no. 5, pp. 431–441, 2019.

[126] Y. Zhang, T. Wang, M. Zhou, Y. Wang, and Z. Zhang, “Hydrothermal preparation of Ag-TiO2 nanostructures with exposed {001}/{101} facets for enhancing visible light photocatalytic activity,” *Ceram. Int.*, vol. 43, no. 3, pp. 3118–3126, 2017.

[127] L. Gomathi Devi and K. Mohan Reddy, “Photocatalytic performance of silver TiO_2 : Role of electronic energy levels,” *Appl. Surf. Sci.*, vol. 257, no. 15, pp. 6821–6828, 2011.

[128] W. Wang, B. Cheng, J. Yu, G. Liu, and W. Fan, “Visible-light photocatalytic activity and deactivation mechanism of Ag 3PO 4 spherical particles,” *Chem. - An Asian J.*, vol. 7, no. 8, pp. 1902–1908, 2012.

[129] J. Catherine, G. Cornu, A. J. Colussi, and M. R. Hoffmann, “Quantum yields of the photocatalytic oxidation of formate in aqueous TiO_2 suspensions under continuous and periodic illumination,” *J. Phys. Chem. B*, vol. 105, no. 7, pp. 1351–1354, 2001.

[130] E. Vasilaki, I. Georgaki, D. Vernardou, M. Vamvakaki, and N. Katsarakis, “Ag-loaded TiO_2 /reduced graphene oxide nanocomposites for enhanced visible-light photocatalytic activity,” *Appl. Surf. Sci.*, vol. 353, pp. 865–872, 2015.

[131] M. Lindner, J. Theurich, and D. W. Bahnemann, “Photocatalytic degradation of organic compounds: Accelerating the process efficiency,” *Water Sci. Technol.*, vol. 35, no. 4, pp. 79–86, 1997.

[132] M. Sillanpää, M. C. Ncibi, A. Matilainen, and M. Vepsäläinen, “Removal of natural organic matter in drinking water treatment by coagulation: A comprehensive review,” *Chemosphere*, vol. 190, pp. 54–71, 2018.

[133] D. Barceló, A. G. Kostianoy, and (ed.), *The Handbook of Environmental Chemistry: Emerging Organic Contaminants and Human Health*, vol. 20. 2012.

[134] J. Herrmann, “Applied Catalysis B : Environmental Photocatalysis fundamentals revisited to avoid several misconceptions,” *"Applied Catal. B, Environ.*, vol. 99, no. 3–4, pp. 461–468, 2010.

[135] S. Gora, A. Sokolowski, M. Hatat-Fraile, R. Liang, Y. N. Zhou, and S. Andrews, “Solar photocatalysis with modified TiO2 photocatalysts: Effects on NOM and disinfection

byproduct formation potential," *Environ. Sci. Water Res. Technol.*, vol. 4, no. 9, pp. 1361–1376, 2018.

[136] A. L. Linsebigler, G. Lu, and J. T. Yates, "Photocatalysis on TiO2 Surfaces: Principles, Mechanisms, and Selected Results," *Chem. Rev.*, vol. 95, no. 3, pp. 735–758, 1995.

[137] S. Liu, M. Lim, R. Fabris, C. Chow, M. Drikas, and R. Amal, "TiO2 photocatalysis of natural organic matter in surface water: Impact on trihalomethane and haloacetic acid formation potential," *Environ. Sci. Technol.*, vol. 42, no. 16, pp. 6218–6223, 2008.

[138] K. H. Choo, R. Tao, and M. J. Kim, "Use of a photocatalytic membrane reactor for the removal of natural organic matter in water: Effect of photoinduced desorption and ferrihydrite adsorption," *J. Memb. Sci.*, vol. 322, no. 2, pp. 368–374, 2008.

[139] D. Ljubas, "Solar photocatalysis - A possible step in drinking water treatment," *Energy*, vol. 30, no. 10, pp. 1699–1710, 2005.

[140] R. Andreozzi, V. Caprio, A. Insola, and R. Marotta, "Advanced oxidation processes (AOP) for water purification and recovery," vol. 53, pp. 51–59, 1999.

[141] W. Sun, H. Chu, B. Dong, D. Cao, and S. Zheng, "The Degradation of natural organic matter in surface water by a nano-TiO2/diatomite photocatalytic reactor," *Clean - Soil, Air, Water*, vol. 42, no. 9, pp. 1190–1198, 2014.

[142] J. K. Edzwald and J. E. Tobiason, "Enhanced coagulation: US requirements and a broader view," *Water Sci. Technol.*, vol. 40, no. 9, pp. 63–70, 1999.

[143] N. Ates, M. Kitis, and U. Yetis, "Formation of chlorination by-products in waters with low SUVA-correlations with SUVA and differential UV spectroscopy," *Water Res.*, vol. 41, no. 18, pp. 4139–4148, 2007.

[144] C. W. Jung and H. J. Son, "The relationship between disinfection by-products formation and characteristics of natural organic matter in raw water," *Korean J. Chem. Eng.*, vol. 25, no. 4, pp. 714–720, 2008.

[145] T. I. Nkambule, A. T. Kuvarega, R. W. M. Krause, J. Haarhoff, and B. B. Mamba, "Synthesis and characterisation of Pd-modified N-doped TiO_2 for photocatalytic degradation of natural organic matter (NOM) fractions," *Environ. Sci. Pollut. Res.*, vol.

19, no. 9, pp. 4120–4132, 2012.

[146] H. W. Leung *et al.*, "Pharmaceuticals in tap water: Human health risk assessment and proposed monitoring framework in China," *Environ. Health Perspect.*, vol. 121, no. 7, pp. 839–846, 2013.

[147] K. S. Le Corre, C. Ort, D. Kateley, B. Allen, B. I. Escher, and J. Keller, "Consumption-based approach for assessing the contribution of hospitals towards the load of pharmaceutical residues in municipal wastewater," *Environ. Int.*, vol. 45, no. 1, pp. 99–111, 2012.

[148] T. A. Ternes *et al.*, "Removal of pharmaceuticals during drinking water treatment," *Environ. Sci. Technol.*, vol. 36, no. 17, pp. 3855–3863, 2002.

[149] H. Bielak, A. Boergers, J. Raab, J. Tuerk, and E. Dopp, "Efficiency of UV-Oxidation in removal of pharmaceuticals from waste water samples and toxicological evaluation before and after the oxidative treatment," in *Disinfection By-products in Drinking Water*, no. July 2016, C. Thompson, S. Gillespie, and E. Goslan, Eds. Cambridge: Royal Society of Chemistry, 2016, pp. 180–188.

[150] A. Kumar, "A Review on the Factors Affecting the Photocatalytic Degradation of Hazardous Materials," *Mater. Sci. Eng. Int. J.*, vol. 1, no. 3, pp. 1–10, 2017.

[151] A. Fernández-Nieves, F. J. de las Nieves, and C. Richter, "Point of zero charge estimation for a TiO2/water interface," in *Trends in Colloid and Interface Science XII*, G. J. M. Koper, B. D., C. Cavaco, and W. F. C. Sager, Eds. Heidelberg: Steinkopff, 1998, pp. 21–24.

[152] M. J. Arlos *et al.*, "Photocatalytic decomposition of organic micropollutants using immobilized TiO_2 having different isoelectric points," *Water Res.*, vol. 101, pp. 351–361, 2016.

[153] M. J. Arlos *et al.*, "Photocatalytic decomposition of selected estrogens and their estrogenic activity by UV-LED irradiated TiO2immobilized on porous titanium sheets via thermal-chemical oxidation," *J. Hazard. Mater.*, vol. 318, pp. 541–550, 2016.

[154] Y. C. Lin, H. Bai, C. H. Lin, and J. F. Wu, "Applying surface charge attraction to

synthesizing TiO2/Ag composition for VOCs photodegradation," *Aerosol Air Qual. Res.*, vol. 13, no. 5, pp. 1512–1520, 2013.

Appendix A

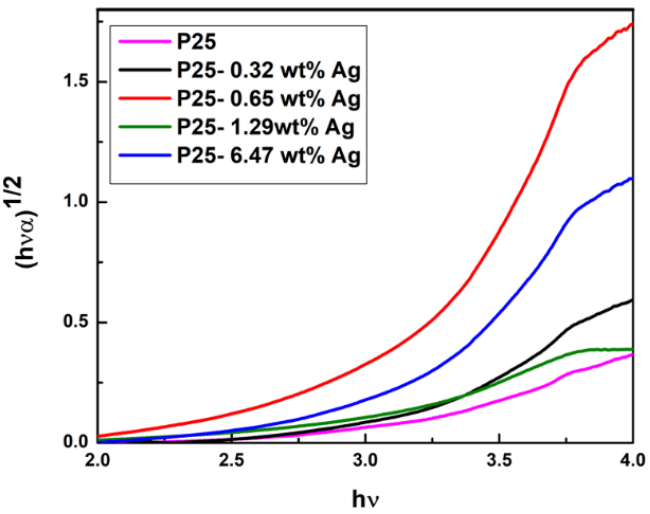

Figure A-0-1 Ag-TiO_2 samples band gap

Appendix B

Table B-1 Actual HTPA formation data in constant frequency

UV Duty Cycle (γ)	P25	STDEV	P25-0.32 wt% Ag	STDEV	P25-0.65 wt% Ag	STDEV	P25-1.29 wt% Ag	STDEV	P25-6.47 wt% Ag	STDEV
0%	0	0	0.00277	7E-4	0.00754	0.00144	0.01188	0.00226	0.00358	9E-4
20%	0.24052	0.0187	0.24259	0.01223	0.18394	0.02237	0.33935	0.0237	0.15772	0.0015
40%	0.5256	0.06037	0.30231	0.05835	0.3401	0.04379	0.81402	0.04546	0.30735	--
50%	0.60945	0.06605	0.5112	0.05996	0.55919	0.03415	0.84977	0.04665	0.47002	0.07331
60%	0.69412	0.02897	0.53866	0.14357	0.55039	0.1027	1.2833	0.11237	0.51519	0.00474
80%	0.77282	0.01641	0.74033	0.05618	0.82306	0.20212	1.45788	0.00158	0.40042	0.06858
90%	0.86003	0.00643	0.66656	0.15092	1.0936	0.06861	1.6224	0.03358	0.54665	0.12359
100%	0.89378	0.04728	1.02779	0.0159	0.82908	0.07378	1.6683	0.07695	0.54038	0.02198

Duty Cycles:

Two Way Analysis of Variance Friday, November 22, 2019, 2:19:36 PM

Data source: Data 2 in Notebook1

General Linear Model

Dependent Variable: K value

Normality Test (Shapiro-Wilk): Failed (P < 0.050)

Equal Variance Test (Brown-Forsythe): Failed (P < 0.050)

Source of Variation	DF	SS	MS	F	P
Duty Cycle	6	13.886	2.314	674.968	<0.001
Treatment	4	5.300	1.325	386.454	<0.001
Duty Cycle x Treatment	24	2.762	0.115	33.563	<0.001
Residual	107	0.367	0.00343		
Total	141	22.336	0.158		

Main effects cannot be properly interpreted if significant interaction is determined. This is because the size of a factor's effect depends upon the level of the other factor.

The effect of different levels of Duty Cycle depends on what level of Treatment is present. There is a statistically significant interaction between Duty Cycle and Treatment. (P = <0.001)

Power of performed test with alpha = 0.0500: for Duty Cycle : 1.000
Power of performed test with alpha = 0.0500: for Treatment : 1.000
Power of performed test with alpha = 0.0500: for Duty Cycle x Treatment : 1.000

Least square means for Duty Cycle :

Group	Mean	SEM
0.000	0.00510	0.0131
20.000	0.232	0.0131
40.000	0.458	0.0128
50.000	0.600	0.0128
60.000	0.713	0.0131
80.000	0.830	0.0131
100.000	0.974	0.0131

Least square means for Treatment :

Group	Mean	SEM
P25	0.532	0.0111
P25-0.32	0.472	0.0111
P25-0.65	0.470	0.0107
P25-1.29	0.912	0.0111

P25-6.47 0.337 0.0111

Least square means for Duty Cycle x Treatment :

Group	Mean	SEM
0.000 x P25	1.041E-016	0.0293
0.000 x P25-0.32	0.00279	0.0293
0.000 x P25-0.65	0.00754	0.0293
0.000 x P25-1.29	0.0116	0.0293
0.000 x P25-6.47	0.00360	0.0293
20.000 x P25	0.240	0.0293
20.000 x P25-0.32	0.241	0.0293
20.000 x P25-0.65	0.184	0.0293
20.000 x P25-1.29	0.339	0.0293
20.000 x P25-6.47	0.156	0.0293
40.000 x P25	0.525	0.0293
40.000 x P25-0.32	0.303	0.0293
40.000 x P25-0.65	0.340	0.0262
40.000 x P25-1.29	0.808	0.0293
40.000 x P25-6.47	0.315	0.0293
50.000 x P25	0.615	0.0293
50.000 x P25-0.32	0.504	0.0293
50.000 x P25-0.65	0.559	0.0262
50.000 x P25-1.29	0.850	0.0293
50.000 x P25-6.47	0.470	0.0293
60.000 x P25	0.684	0.0293
60.000 x P25-0.32	0.529	0.0293
60.000 x P25-0.65	0.550	0.0293
60.000 x P25-1.29	1.289	0.0293
60.000 x P25-6.47	0.514	0.0293
80.000 x P25	0.782	0.0293
80.000 x P25-0.32	0.703	0.0293
80.000 x P25-0.65	0.823	0.0293
80.000 x P25-1.29	1.441	0.0293
80.000 x P25-6.47	0.400	0.0293
100.000 x P25	0.877	0.0293
100.000 x P25-0.32	1.021	0.0293
100.000 x P25-0.65	0.829	0.0293
100.000 x P25-1.29	1.645	0.0293
100.000 x P25-6.47	0.500	0.0293

All Pairwise Multiple Comparison Procedures (Holm-Sidak method):
Overall significance level = 0.05

Comparisons for factor: **Duty Cycle**

Comparison	Diff of Means	t	P	P<0.050
100.000 vs. 0.000	0.969	52.350	<0.001	Yes
80.000 vs. 0.000	0.825	44.544	<0.001	Yes

100.000 vs. 20.000	0.742	40.090	<0.001	Yes
60.000 vs. 0.000	0.708	38.247	<0.001	Yes
50.000 vs. 0.000	0.594	32.430	<0.001	Yes
80.000 vs. 20.000	0.598	32.285	<0.001	Yes
100.000 vs. 40.000	0.516	28.165	<0.001	Yes
60.000 vs. 20.000	0.481	25.987	<0.001	Yes
40.000 vs. 0.000	0.453	24.716	<0.001	Yes
100.000 vs. 50.000	0.375	20.451	<0.001	Yes
80.000 vs. 40.000	0.372	20.280	<0.001	Yes
50.000 vs. 20.000	0.367	20.046	<0.001	Yes
100.000 vs. 60.000	0.261	14.103	<0.001	Yes
60.000 vs. 40.000	0.255	13.919	<0.001	Yes
80.000 vs. 50.000	0.230	12.566	<0.001	Yes
40.000 vs. 20.000	0.226	12.332	<0.001	Yes
20.000 vs. 0.000	0.227	12.260	<0.001	Yes
100.000 vs. 80.000	0.145	7.805	<0.001	Yes
50.000 vs. 40.000	0.141	7.794	<0.001	Yes
80.000 vs. 60.000	0.117	6.297	<0.001	Yes
60.000 vs. 50.000	0.114	6.205	<0.001	Yes

Comparisons for factor: **Treatment**

Comparison	**Diff of Means**	**t**	**P**	**P<0.050**
P25-1.29 vs. P25-6.47	0.575	36.742	<0.001	Yes
P25-1.29 vs. P25-0.65	0.441	28.621	<0.001	Yes
P25-1.29 vs. P25-0.32	0.440	28.101	<0.001	Yes
P25-1.29 vs. P25	0.380	24.286	<0.001	Yes
P25 vs. P25-6.47	0.195	12.456	<0.001	Yes
P25-0.65 vs. P25-6.47	0.134	8.657	<0.001	Yes
P25-0.32 vs. P25-6.47	0.135	8.641	<0.001	Yes
P25 vs. P25-0.65	0.0614	3.981	<0.001	Yes
P25 vs. P25-0.32	0.0597	3.816	<0.001	Yes
P25-0.32 vs. P25-0.65	0.00169	0.110	0.913	No

Comparisons for factor: **Treatment within 0**

Comparison	**Diff of Means**	**t**	**P**	**P<0.050**
P25-1.29 vs. P25	0.0116	0.280	1.000	No
P25-1.29 vs. P25-0.32	0.00881	0.213	1.000	No
P25-1.29 vs. P25-6.47	0.00800	0.193	1.000	No
P25-0.65 vs. P25	0.00754	0.182	1.000	No
P25-0.65 vs. P25-0.32	0.00476	0.115	1.000	No
P25-1.29 vs. P25-0.65	0.00405	0.0979	1.000	No
P25-0.65 vs. P25-6.47	0.00394	0.0952	1.000	No
P25-6.47 vs. P25	0.00360	0.0869	1.000	No
P25-0.32 vs. P25	0.00279	0.0673	0.997	No
P25-6.47 vs. P25-0.32	0.000813	0.0196	0.984	No

Comparisons for factor: **Treatment within 20**

Comparison	Diff of Means	t	P	P<0.050
P25-1.29 vs. P25-6.47	0.183	4.424	<0.001	Yes
P25-1.29 vs. P25-0.65	0.155	3.745	0.003	Yes
P25-1.29 vs. P25	0.0986	2.382	0.142	No
P25-1.29 vs. P25-0.32	0.0975	2.355	0.134	No
P25-0.32 vs. P25-6.47	0.0856	2.068	0.222	No
P25 vs. P25-6.47	0.0845	2.042	0.200	No
P25-0.32 vs. P25-0.65	0.0575	1.389	0.520	No
P25 vs. P25-0.65	0.0564	1.362	0.440	No
P25-0.65 vs. P25-6.47	0.0281	0.679	0.749	No
P25-0.32 vs. P25	0.00112	0.0270	0.979	No

Comparisons for factor: **Treatment within 40**

Comparison	Diff of Means	t	P	P<0.050
P25-1.29 vs. P25-0.32	0.505	12.198	<0.001	Yes
P25-1.29 vs. P25-0.65	0.468	11.907	<0.001	Yes
P25-1.29 vs. P25-6.47	0.493	11.905	<0.001	Yes
P25-1.29 vs. P25	0.282	6.819	<0.001	Yes
P25 vs. P25-0.32	0.223	5.378	<0.001	Yes
P25 vs. P25-6.47	0.211	5.086	<0.001	Yes
P25 vs. P25-0.65	0.185	4.718	<0.001	Yes
P25-0.65 vs. P25-0.32	0.0374	0.951	0.717	No
P25-0.65 vs. P25-6.47	0.0252	0.643	0.771	No
P25-6.47 vs. P25-0.32	0.0121	0.293	0.770	No

Comparisons for factor: **Treatment within 50**

Comparison	Diff of Means	t	P	P<0.050
P25-1.29 vs. P25-6.47	0.380	9.172	<0.001	Yes
P25-1.29 vs. P25-0.32	0.346	8.344	<0.001	Yes
P25-1.29 vs. P25-0.65	0.291	7.398	<0.001	Yes
P25-1.29 vs. P25	0.235	5.678	<0.001	Yes
P25 vs. P25-6.47	0.145	3.494	0.004	Yes
P25 vs. P25-0.32	0.110	2.666	0.044	Yes
P25-0.65 vs. P25-6.47	0.0892	2.270	0.097	No
P25 vs. P25-0.65	0.0555	1.413	0.409	No
P25-0.65 vs. P25-0.32	0.0549	1.398	0.303	No
P25-0.32 vs. P25-6.47	0.0343	0.828	0.410	No

Comparisons for factor: **Treatment within 60**

Comparison	Diff of Means	t	P	P<0.050
P25-1.29 vs. P25-6.47	0.775	18.713	<0.001	Yes
P25-1.29 vs. P25-0.32	0.760	18.347	<0.001	Yes
P25-1.29 vs. P25-0.65	0.738	17.835	<0.001	Yes
P25-1.29 vs. P25	0.605	14.603	<0.001	Yes
P25 vs. P25-6.47	0.170	4.110	<0.001	Yes
P25 vs. P25-0.32	0.155	3.744	0.001	Yes
P25 vs. P25-0.65	0.134	3.232	0.007	Yes

P25-0.65 vs. P25-6.47	0.0364	0.878	0.764	No
P25-0.65 vs. P25-0.32	0.0212	0.512	0.848	No
P25-0.32 vs. P25-6.47	0.0152	0.366	0.715	No

Comparisons for factor: **Treatment within 80**

Comparison	**Diff of Means**	**t**	**P**	**P<0.050**
P25-1.29 vs. P25-6.47	1.041	25.137	<0.001	Yes
P25-1.29 vs. P25-0.32	0.738	17.818	<0.001	Yes
P25-1.29 vs. P25	0.660	15.932	<0.001	Yes
P25-1.29 vs. P25-0.65	0.618	14.929	<0.001	Yes
P25-0.65 vs. P25-6.47	0.423	10.207	<0.001	Yes
P25 vs. P25-6.47	0.381	9.205	<0.001	Yes
P25-0.32 vs. P25-6.47	0.303	7.318	<0.001	Yes
P25-0.65 vs. P25-0.32	0.120	2.889	0.014	Yes
P25 vs. P25-0.32	0.0781	1.887	0.120	No
P25-0.65 vs. P25	0.0415	1.002	0.319	No

Comparisons for factor: **Treatment within 100**

Comparison	**Diff of Means**	**t**	**P**	**P<0.050**
P25-1.29 vs. P25-6.47	1.146	27.666	<0.001	Yes
P25-1.29 vs. P25-0.65	0.816	19.714	<0.001	Yes
P25-1.29 vs. P25	0.768	18.559	<0.001	Yes
P25-1.29 vs. P25-0.32	0.624	15.074	<0.001	Yes
P25-0.32 vs. P25-6.47	0.521	12.592	<0.001	Yes
P25 vs. P25-6.47	0.377	9.107	<0.001	Yes
P25-0.65 vs. P25-6.47	0.329	7.952	<0.001	Yes
P25-0.32 vs. P25-0.65	0.192	4.640	<0.001	Yes
P25-0.32 vs. P25	0.144	3.485	0.001	Yes
P25 vs. P25-0.65	0.0478	1.155	0.251	No

Comparisons for factor: **Duty Cycle within P25**

Comparison	**Diff of Means**	**t**	**P**	**P<0.050**
100.000 vs. 0.000	0.877	21.178	<0.001	Yes
80.000 vs. 0.000	0.782	18.876	<0.001	Yes
60.000 vs. 0.000	0.684	16.524	<0.001	Yes
100.000 vs. 20.000	0.637	15.373	<0.001	Yes
50.000 vs. 0.000	0.615	14.845	<0.001	Yes
80.000 vs. 20.000	0.541	13.071	<0.001	Yes
40.000 vs. 0.000	0.525	12.690	<0.001	Yes
60.000 vs. 20.000	0.444	10.719	<0.001	Yes
50.000 vs. 20.000	0.374	9.040	<0.001	Yes
100.000 vs. 40.000	0.351	8.488	<0.001	Yes
40.000 vs. 20.000	0.285	6.885	<0.001	Yes
100.000 vs. 50.000	0.262	6.333	<0.001	Yes
80.000 vs. 40.000	0.256	6.186	<0.001	Yes
20.000 vs. 0.000	0.240	5.805	<0.001	Yes
100.000 vs. 60.000	0.193	4.654	<0.001	Yes

80.000 vs. 50.000	0.167	4.031	<0.001	Yes
60.000 vs. 40.000	0.159	3.834	0.001	Yes
80.000 vs. 60.000	0.0974	2.352	0.080	No
100.000 vs. 80.000	0.0953	2.303	0.068	No
50.000 vs. 40.000	0.0892	2.155	0.066	No
60.000 vs. 50.000	0.0695	1.679	0.096	No

Comparisons for factor: **Duty Cycle within P25-0.32**

Comparison	**Diff of Means**	**t**	**P**	**P<0.050**
100.000 vs. 0.000	1.018	24.596	<0.001	Yes
100.000 vs. 20.000	0.780	18.832	<0.001	Yes
100.000 vs. 40.000	0.718	17.352	<0.001	Yes
80.000 vs. 0.000	0.701	16.922	<0.001	Yes
60.000 vs. 0.000	0.526	12.713	<0.001	Yes
100.000 vs. 50.000	0.517	12.485	<0.001	Yes
50.000 vs. 0.000	0.501	12.112	<0.001	Yes
100.000 vs. 60.000	0.492	11.883	<0.001	Yes
80.000 vs. 20.000	0.462	11.157	<0.001	Yes
80.000 vs. 40.000	0.401	9.678	<0.001	Yes
100.000 vs. 80.000	0.318	7.675	<0.001	Yes
40.000 vs. 0.000	0.300	7.244	<0.001	Yes
60.000 vs. 20.000	0.288	6.949	<0.001	Yes
50.000 vs. 20.000	0.263	6.347	<0.001	Yes
20.000 vs. 0.000	0.239	5.765	<0.001	Yes
60.000 vs. 40.000	0.226	5.469	<0.001	Yes
50.000 vs. 40.000	0.202	4.868	<0.001	Yes
80.000 vs. 50.000	0.199	4.810	<0.001	Yes
80.000 vs. 60.000	0.174	4.208	<0.001	Yes
40.000 vs. 20.000	0.0613	1.480	0.264	No
60.000 vs. 50.000	0.0249	0.602	0.549	No

Comparisons for factor: **Duty Cycle within P25-0.65**

Comparison	**Diff of Means**	**t**	**P**	**P<0.050**
100.000 vs. 0.000	0.822	19.841	<0.001	Yes
80.000 vs. 0.000	0.816	19.696	<0.001	Yes
100.000 vs. 20.000	0.645	15.581	<0.001	Yes
80.000 vs. 20.000	0.639	15.436	<0.001	Yes
50.000 vs. 0.000	0.552	14.044	<0.001	Yes
60.000 vs. 0.000	0.543	13.111	<0.001	Yes
100.000 vs. 40.000	0.489	12.448	<0.001	Yes
80.000 vs. 40.000	0.483	12.295	<0.001	Yes
50.000 vs. 20.000	0.375	9.553	<0.001	Yes
60.000 vs. 20.000	0.366	8.850	<0.001	Yes
40.000 vs. 0.000	0.333	8.466	<0.001	Yes
100.000 vs. 50.000	0.270	6.871	<0.001	Yes
100.000 vs. 60.000	0.279	6.731	<0.001	Yes
80.000 vs. 50.000	0.264	6.718	<0.001	Yes
80.000 vs. 60.000	0.273	6.585	<0.001	Yes

50.000 vs. 40.000	0.219	5.916	<0.001	Yes
60.000 vs. 40.000	0.210	5.354	<0.001	Yes
20.000 vs. 0.000	0.176	4.260	<0.001	Yes
40.000 vs. 20.000	0.156	3.975	<0.001	Yes
50.000 vs. 60.000	0.00880	0.224	0.969	No
100.000 vs. 80.000	0.00601	0.145	0.885	No

Comparisons for factor: **Duty Cycle within P25-1.29**

Comparison	**Diff of Means**	**t**	**P**	**P<0.050**
100.000 vs. 0.000	1.634	39.457	<0.001	Yes
80.000 vs. 0.000	1.430	34.527	<0.001	Yes
100.000 vs. 20.000	1.306	31.550	<0.001	Yes
60.000 vs. 0.000	1.277	30.847	<0.001	Yes
80.000 vs. 20.000	1.102	26.620	<0.001	Yes
60.000 vs. 20.000	0.950	22.940	<0.001	Yes
50.000 vs. 0.000	0.838	20.243	<0.001	Yes
100.000 vs. 40.000	0.838	20.228	<0.001	Yes
40.000 vs. 0.000	0.796	19.229	<0.001	Yes
100.000 vs. 50.000	0.796	19.214	<0.001	Yes
80.000 vs. 40.000	0.633	15.298	<0.001	Yes
80.000 vs. 50.000	0.591	14.284	<0.001	Yes
50.000 vs. 20.000	0.511	12.336	<0.001	Yes
60.000 vs. 40.000	0.481	11.618	<0.001	Yes
40.000 vs. 20.000	0.469	11.322	<0.001	Yes
60.000 vs. 50.000	0.439	10.604	<0.001	Yes
100.000 vs. 60.000	0.356	8.610	<0.001	Yes
20.000 vs. 0.000	0.327	7.907	<0.001	Yes
100.000 vs. 80.000	0.204	4.930	<0.001	Yes
80.000 vs. 60.000	0.152	3.680	<0.001	Yes
50.000 vs. 40.000	0.0420	1.014	0.313	No

Comparisons for factor: **Duty Cycle within P25-6.47**

Comparison	**Diff of Means**	**t**	**P**	**P<0.050**
60.000 vs. 0.000	0.510	12.327	<0.001	Yes
100.000 vs. 0.000	0.496	11.984	<0.001	Yes
50.000 vs. 0.000	0.466	11.265	<0.001	Yes
80.000 vs. 0.000	0.397	9.584	<0.001	Yes
60.000 vs. 20.000	0.358	8.651	<0.001	Yes
100.000 vs. 20.000	0.344	8.308	<0.001	Yes
50.000 vs. 20.000	0.314	7.588	<0.001	Yes
40.000 vs. 0.000	0.311	7.517	<0.001	Yes
80.000 vs. 20.000	0.245	5.907	<0.001	Yes
60.000 vs. 40.000	0.199	4.810	<0.001	Yes
100.000 vs. 40.000	0.185	4.467	<0.001	Yes
40.000 vs. 20.000	0.159	3.841	0.002	Yes
50.000 vs. 40.000	0.155	3.747	0.003	Yes
20.000 vs. 0.000	0.152	3.676	0.003	Yes
60.000 vs. 80.000	0.114	2.744	0.049	Yes

100.000 vs. 80.000	0.0994	2.401	0.104	No
80.000 vs. 40.000	0.0856	2.067	0.190	No
50.000 vs. 80.000	0.0696	1.681	0.331	No
60.000 vs. 50.000	0.0440	1.063	0.643	No
100.000 vs. 50.000	0.0298	0.720	0.722	No
60.000 vs. 100.000	0.0142	0.343	0.732	No

Frequencies:

Two Way Analysis of Variance Friday, November 22, 2019, 2:50:27 PM

Data source: Data 1 in Notebook1

Balanced Design

Dependent Variable: K

Normality Test (Shapiro-Wilk): Failed (P < 0.050)

Equal Variance Test (Brown-Forsythe): Failed (P < 0.050)

Source of Variation	DF	SS	MS	F	P
Treatment	4	2.965	0.741	133.676	<0.001
HZ	3	0.221	0.0737	13.288	<0.001
Treatment x HZ	12	0.300	0.0250	4.513	<0.001
Residual	60	0.333	0.00555		
Total	79	3.820	0.0483		

Main effects cannot be properly interpreted if significant interaction is determined. This is because the size of a factor's effect depends upon the level of the other factor.

The effect of different levels of Treatment depends on what level of HZ is present. There is a statistically significant interaction between Treatment and HZ. (P = <0.001)

Power of performed test with alpha = 0.0500: for Treatment : 1.000
Power of performed test with alpha = 0.0500: for HZ : 1.000
Power of performed test with alpha = 0.0500: for Treatment x HZ : 0.993

Least square means for Treatment :

Group	Mean
P25	0.582
P25-0.32	0.433
P25-0.65	0.476
P25-1.29	0.827

P25-6.47 0.240
Std Err of LS Mean = 0.0186

Least square means for HZ :

Group	Mean
0.0500	0.493
0.500	0.602
1.000	0.483
5.000	0.469

Std Err of LS Mean = 0.0167

Least square means for Treatment x HZ :

Group	Mean
P25 x 0.050	0.509
P25 x 0.500	0.615
P25 x 1.000	0.540
P25 x 5.000	0.664
P25-0.32 x 0.050	0.404
P25-0.32 x 0.500	0.504
P25-0.32 x 1.000	0.385
P25-0.32 x 5.000	0.438
P25-0.65 x 0.050	0.479
P25-0.65 x 0.500	0.569
P25-0.65 x 1.000	0.465
P25-0.65 x 5.000	0.391
P25-1.29 x 0.050	0.826
P25-1.29 x 0.500	0.850
P25-1.29 x 1.000	0.833
P25-1.29 x 5.000	0.799
P25-6.47 x 0.050	0.245
P25-6.47 x 0.500	0.470
P25-6.47 x 1.000	0.193
P25-6.47 x 5.000	0.0534

Std Err of LS Mean = 0.0372

All Pairwise Multiple Comparison Procedures (Holm-Sidak method):
Overall significance level = 0.05

Comparisons for factor: **Treatment**

Comparison	Diff of Means	t	P	P<0.050
P25-1.29 vs. P25-6.47	0.586	22.274	<0.001	Yes
P25-1.29 vs. P25-0.32	0.394	14.958	<0.001	Yes
P25-1.29 vs. P25-0.65	0.351	13.322	<0.001	Yes
P25 vs. P25-6.47	0.342	12.977	<0.001	Yes
P25-1.29 vs. P25	0.245	9.297	<0.001	Yes
P25-0.65 vs. P25-6.47	0.236	8.952	<0.001	Yes
P25-0.32 vs. P25-6.47	0.193	7.316	<0.001	Yes
P25 vs. P25-0.32	0.149	5.662	<0.001	Yes
P25 vs. P25-0.65	0.106	4.025	<0.001	Yes

P25-0.65 vs. P25-0.32	0.0431	1.637	0.107	No

Comparisons for factor: **HZ**

Comparison	**Diff of Means**	**t**	**P**	**P<0.050**
0.500 vs. 5.000	0.132	5.621	<0.001	Yes
0.500 vs. 1.000	0.118	5.024	<0.001	Yes
0.500 vs. 0.050	0.109	4.623	<0.001	Yes
0.050 vs. 5.000	0.0235	0.998	0.689	No
1.000 vs. 5.000	0.0141	0.598	0.800	No
0.050 vs. 1.000	0.00944	0.401	0.690	No

Comparisons for factor: **HZ within P25**

Comparison	**Diff of Means**	**t**	**P**	**P<0.050**
5.000 vs. 0.050	0.155	2.939	0.028	Yes
5.000 vs. 1.000	0.124	2.362	0.103	No
0.500 vs. 0.050	0.105	1.998	0.187	No
0.500 vs. 1.000	0.0748	1.421	0.408	No
5.000 vs. 0.500	0.0495	0.941	0.578	No
1.000 vs. 0.050	0.0304	0.576	0.566	No

Comparisons for factor: **HZ within P25-0.32**

Comparison	**Diff of Means**	**t**	**P**	**P<0.050**
0.500 vs. 1.000	0.119	2.258	0.155	No
0.500 vs. 0.050	0.100	1.903	0.273	No
0.500 vs. 5.000	0.0661	1.254	0.619	No
5.000 vs. 1.000	0.0529	1.004	0.685	No
5.000 vs. 0.050	0.0341	0.648	0.769	No
0.050 vs. 1.000	0.0187	0.355	0.724	No

Comparisons for factor: **HZ within P25-0.65**

Comparison	**Diff of Means**	**t**	**P**	**P<0.050**
0.500 vs. 5.000	0.178	3.372	0.008	Yes
0.500 vs. 1.000	0.104	1.970	0.240	No
0.500 vs. 0.050	0.0905	1.719	0.317	No
0.050 vs. 5.000	0.0870	1.653	0.280	No
1.000 vs. 5.000	0.0738	1.402	0.305	No
0.050 vs. 1.000	0.0132	0.251	0.802	No

Comparisons for factor: **HZ within P25-1.29**

Comparison	**Diff of Means**	**t**	**P**	**P<0.050**
0.500 vs. 5.000	0.0512	0.972	0.913	No
1.000 vs. 5.000	0.0344	0.653	0.973	No
0.050 vs. 5.000	0.0274	0.520	0.976	No
0.500 vs. 0.050	0.0238	0.452	0.958	No
0.500 vs. 1.000	0.0168	0.319	0.938	No

1.000 vs. 0.050	0.00701	0.133	0.895	No

Comparisons for factor: **HZ within P25-6.47**

Comparison	**Diff of Means**	**t**	**P**	**P<0.050**
0.500 vs. 5.000	0.417	7.912	<0.001	Yes
0.500 vs. 1.000	0.277	5.265	<0.001	Yes
0.500 vs. 0.050	0.225	4.266	<0.001	Yes
0.050 vs. 5.000	0.192	3.646	0.002	Yes
1.000 vs. 5.000	0.139	2.647	0.021	Yes
0.050 vs. 1.000	0.0526	0.999	0.322	No

Comparisons for factor: **Treatment within 0.05**

Comparison	**Diff of Means**	**t**	**P**	**P<0.050**
P25-1.29 vs. P25-6.47	0.581	11.026	<0.001	Yes
P25-1.29 vs. P25-0.32	0.422	8.012	<0.001	Yes
P25-1.29 vs. P25-0.65	0.347	6.598	<0.001	Yes
P25-1.29 vs. P25	0.316	6.010	<0.001	Yes
P25 vs. P25-6.47	0.264	5.016	<0.001	Yes
P25-0.65 vs. P25-6.47	0.233	4.428	<0.001	Yes
P25-0.32 vs. P25-6.47	0.159	3.014	0.015	Yes
P25 vs. P25-0.32	0.105	2.002	0.142	No
P25-0.65 vs. P25-0.32	0.0744	1.414	0.299	No
P25 vs. P25-0.65	0.0310	0.588	0.559	No

Comparisons for factor: **Treatment within 0.5**

Comparison	**Diff of Means**	**t**	**P**	**P<0.050**
P25-1.29 vs. P25-6.47	0.380	7.212	<0.001	Yes
P25-1.29 vs. P25-0.32	0.346	6.561	<0.001	Yes
P25-1.29 vs. P25-0.65	0.281	5.331	<0.001	Yes
P25-1.29 vs. P25	0.235	4.465	<0.001	Yes
P25 vs. P25-6.47	0.145	2.747	0.047	Yes
P25 vs. P25-0.32	0.110	2.096	0.186	No
P25-0.65 vs. P25-6.47	0.0990	1.880	0.235	No
P25-0.65 vs. P25-0.32	0.0648	1.230	0.532	No
P25 vs. P25-0.65	0.0456	0.867	0.627	No
P25-0.32 vs. P25-6.47	0.0343	0.651	0.518	No

Comparisons for factor: **Treatment within 1**

Comparison	**Diff of Means**	**t**	**P**	**P<0.050**
P25-1.29 vs. P25-6.47	0.640	12.158	<0.001	Yes
P25-1.29 vs. P25-0.32	0.448	8.500	<0.001	Yes
P25-1.29 vs. P25-0.65	0.368	6.983	<0.001	Yes
P25 vs. P25-6.47	0.347	6.591	<0.001	Yes
P25-1.29 vs. P25	0.293	5.567	<0.001	Yes
P25-0.65 vs. P25-6.47	0.273	5.175	<0.001	Yes
P25-0.32 vs. P25-6.47	0.193	3.658	0.002	Yes

P25 vs. P25-0.32	0.154	2.933	0.014	Yes
P25-0.65 vs. P25-0.32	0.0799	1.517	0.251	No
P25 vs. P25-0.65	0.0746	1.416	0.162	No

Comparisons for factor: **Treatment within 5**

Comparison	**Diff of Means**	**t**	**P**	**P<0.050**
P25-1.29 vs. P25-6.47	0.745	14.152	<0.001	Yes
P25 vs. P25-6.47	0.611	11.600	<0.001	Yes
P25-1.29 vs. P25-0.65	0.407	7.731	<0.001	Yes
P25-0.32 vs. P25-6.47	0.385	7.309	<0.001	Yes
P25-1.29 vs. P25-0.32	0.360	6.843	<0.001	Yes
P25-0.65 vs. P25-6.47	0.338	6.421	<0.001	Yes
P25 vs. P25-0.65	0.273	5.180	<0.001	Yes
P25 vs. P25-0.32	0.226	4.292	<0.001	Yes
P25-1.29 vs. P25	0.134	2.552	0.026	Yes
P25-0.32 vs. P25-0.65	0.0467	0.888	0.378	No

Appendix C

Constant UV and Visible light

Two Way Analysis of Variance Monday, November 25, 2019, 7:39:32 PM

Data source: Data 4 in Azar stats

Balanced Design

Dependent Variable: UV removal

Normality Test (Shapiro-Wilk): Failed (P < 0.050)

Equal Variance Test (Brown-Forsythe): Passed (P = 0.051)

Source of Variation	DF	SS	MS	F	P
Time	4	3402.941	850.735	13.499	<0.001
Treatment	3	5241.280	1747.093	27.723	<0.001
Time x Treatment	12	2276.026	189.669	3.010	0.004
Residual	40	2520.813	63.020		
Total	59	13441.060	227.815		

Main effects cannot be properly interpreted if significant interaction is determined. This is because the size of a factor's effect depends upon the level of the other factor.

The effect of different levels of Time depends on what level of Treatment is present. There is a statistically significant interaction between Time and Treatment. (P = 0.004)

Power of performed test with alpha = 0.0500: for Time : 1.000
Power of performed test with alpha = 0.0500: for Treatment : 1.000
Power of performed test with alpha = 0.0500: for Time x Treatment : 0.841

Least square means for Time :

Group	Mean
0.000	17.481
15.000	17.085
30.000	21.007
45.000	27.637
60.000	37.080

Std Err of LS Mean = 2.292

Least square means for Treatment :

Group	Mean
P25-UV	21.261
Ag-P25 UV	22.371

P25-Vis 13.480
Ag-P25-Vis 39.120
Std Err of LS Mean = 2.050

Least square means for Time x Treatment :

Group	**Mean**
0.000 x P25-UV	11.477
0.000 x Ag-P25 UV	13.488
0.000 x P25-Vis	11.256
0.000 x Ag-P25-Vis	33.704
15.000 x P25-UV	11.403
15.000 x Ag-P25 UV	13.170
15.000 x P25-Vis	2.891
15.000 x Ag-P25-Vis	40.875
30.000 x P25-UV	22.811
30.000 x Ag-P25 UV	19.728
30.000 x P25-Vis	15.158
30.000 x Ag-P25-Vis	26.330
45.000 x P25-UV	27.105
45.000 x Ag-P25 UV	30.419
45.000 x P25-Vis	22.678
45.000 x Ag-P25-Vis	30.346
60.000 x P25-UV	33.508
60.000 x Ag-P25 UV	35.049
60.000 x P25-Vis	15.419
60.000 x Ag-P25-Vis	64.344

Std Err of LS Mean = 4.583

All Pairwise Multiple Comparison Procedures (Holm-Sidak method):
Overall significance level = 0.05

Comparisons for factor: **Time**

Comparison	**Diff of Means**	**t**	**P**	**P<0.050**
60.000 vs. 15.000	19.995	6.170	<0.001	Yes
60.000 vs. 0.000	19.599	6.047	<0.001	Yes
60.000 vs. 30.000	16.073	4.960	<0.001	Yes
45.000 vs. 15.000	10.552	3.256	0.016	Yes
45.000 vs. 0.000	10.156	3.134	0.019	Yes
60.000 vs. 45.000	9.443	2.914	0.029	Yes
45.000 vs. 30.000	6.630	2.046	0.176	No
30.000 vs. 15.000	3.922	1.210	0.549	No
30.000 vs. 0.000	3.526	1.088	0.486	No
0.000 vs. 15.000	0.396	0.122	0.903	No

Comparisons for factor: **Treatment**

Comparison	**Diff of Means**	**t**	**P**	**P<0.050**
Ag-P25-Vis vs. P25-Vis	25.640	8.845	<0.001	Yes
Ag-P25-Vis vs. P25-UV	17.859	6.161	<0.001	Yes

Ag-P25-Vis vs. Ag-P25 UV	16.749	5.778	<0.001	Yes
Ag-P25 UV vs. P25-Vis	8.890	3.067	0.012	Yes
P25-UV vs. P25-Vis	7.780	2.684	0.021	Yes
Ag-P25 UV vs. P25-UV	1.110	0.383	0.704	No

Comparisons for factor: **Treatment within 0**

Comparison	**Diff of Means**	**t**	**P**	**P<0.050**
Ag-P25-Vis vs. P25-Vis	22.448	3.463	0.008	Yes
Ag-P25-Vis vs. P25-UV	22.227	3.429	0.007	Yes
Ag-P25-Vis vs. Ag-P25 UV	20.216	3.119	0.013	Yes
Ag-P25 UV vs. P25-Vis	2.232	0.344	0.981	No
Ag-P25 UV vs. P25-UV	2.011	0.310	0.941	No
P25-UV vs. P25-Vis	0.221	0.0341	0.973	No

Comparisons for factor: **Treatment within 15**

Comparison	**Diff of Means**	**t**	**P**	**P<0.050**
Ag-P25-Vis vs. P25-Vis	37.984	5.860	<0.001	Yes
Ag-P25-Vis vs. P25-UV	29.472	4.547	<0.001	Yes
Ag-P25-Vis vs. Ag-P25 UV	27.705	4.274	<0.001	Yes
Ag-P25 UV vs. P25-Vis	10.279	1.586	0.320	No
P25-UV vs. P25-Vis	8.512	1.313	0.355	No
Ag-P25 UV vs. P25-UV	1.767	0.273	0.787	No

Comparisons for factor: **Treatment within 30**

Comparison	**Diff of Means**	**t**	**P**	**P<0.050**
Ag-P25-Vis vs. P25-Vis	11.173	1.724	0.441	No
P25-UV vs. P25-Vis	7.653	1.181	0.754	No
Ag-P25-Vis vs. Ag-P25 UV	6.603	1.019	0.779	No
Ag-P25 UV vs. P25-Vis	4.570	0.705	0.863	No
Ag-P25-Vis vs. P25-UV	3.520	0.543	0.832	No
P25-UV vs. Ag-P25 UV	3.083	0.476	0.637	No

Comparisons for factor: **Treatment within 45**

Comparison	**Diff of Means**	**t**	**P**	**P<0.050**
Ag-P25 UV vs. P25-Vis	7.742	1.194	0.806	No
Ag-P25-Vis vs. P25-Vis	7.668	1.183	0.753	No
P25-UV vs. P25-Vis	4.427	0.683	0.937	No
Ag-P25 UV vs. P25-UV	3.315	0.511	0.942	No
Ag-P25-Vis vs. P25-UV	3.242	0.500	0.855	No
Ag-P25 UV vs. Ag-P25-Vis	0.0733	0.0113	0.991	No

Comparisons for factor: **Treatment within 60**

Comparison	**Diff of Means**	**t**	**P**	**P<0.050**
Ag-P25-Vis vs. P25-Vis	48.925	7.548	<0.001	Yes
Ag-P25-Vis vs. P25-UV	30.836	4.757	<0.001	Yes

Ag-P25-Vis vs. Ag-P25 UV	29.295	4.520	<0.001	Yes
Ag-P25 UV vs. P25-Vis	19.630	3.028	0.013	Yes
P25-UV vs. P25-Vis	18.089	2.791	0.016	Yes
Ag-P25 UV vs. P25-UV	1.541	0.238	0.813	No

Comparisons for factor: **Time within P25-UV**

Comparison	**Diff of Means**	**t**	**P**	**P<0.050**
60.000 vs. 15.000	22.106	3.410	0.015	Yes
60.000 vs. 0.000	22.031	3.399	0.014	Yes
45.000 vs. 15.000	15.702	2.422	0.150	No
45.000 vs. 0.000	15.628	2.411	0.136	No
30.000 vs. 15.000	11.408	1.760	0.417	No
30.000 vs. 0.000	11.334	1.749	0.369	No
60.000 vs. 30.000	10.698	1.650	0.363	No
60.000 vs. 45.000	6.404	0.988	0.698	No
45.000 vs. 30.000	4.294	0.662	0.761	No
0.000 vs. 15.000	0.0742	0.0114	0.991	No

Comparisons for factor: **Time within Ag-P25 UV**

Comparison	**Diff of Means**	**t**	**P**	**P<0.050**
60.000 vs. 15.000	21.879	3.375	0.016	Yes
60.000 vs. 0.000	21.561	3.326	0.017	Yes
45.000 vs. 15.000	17.249	2.661	0.086	No
45.000 vs. 0.000	16.932	2.612	0.085	No
60.000 vs. 30.000	15.321	2.364	0.130	No
45.000 vs. 30.000	10.692	1.650	0.432	No
30.000 vs. 15.000	6.558	1.012	0.783	No
30.000 vs. 0.000	6.240	0.963	0.714	No
60.000 vs. 45.000	4.630	0.714	0.729	No
0.000 vs. 15.000	0.318	0.0490	0.961	No

Comparisons for factor: **Time within P25-Vis**

Comparison	**Diff of Means**	**t**	**P**	**P<0.050**
45.000 vs. 15.000	19.787	3.053	0.039	Yes
60.000 vs. 15.000	12.528	1.933	0.429	No
30.000 vs. 15.000	12.267	1.892	0.419	No
45.000 vs. 0.000	11.422	1.762	0.466	No
0.000 vs. 15.000	8.365	1.291	0.746	No
45.000 vs. 30.000	7.520	1.160	0.767	No
45.000 vs. 60.000	7.259	1.120	0.715	No
60.000 vs. 0.000	4.163	0.642	0.892	No
30.000 vs. 0.000	3.902	0.602	0.798	No
60.000 vs. 30.000	0.262	0.0404	0.968	No

Comparisons for factor: **Time within Ag-P25-Vis**

Comparison	**Diff of Means**	**t**	**P**	**P<0.050**

60.000 vs. 30.000	38.013	5.865	<0.001	Yes
60.000 vs. 45.000	33.998	5.245	<0.001	Yes
60.000 vs. 0.000	30.640	4.727	<0.001	Yes
60.000 vs. 15.000	23.469	3.621	0.006	Yes
15.000 vs. 30.000	14.545	2.244	0.169	No
15.000 vs. 45.000	10.529	1.624	0.448	No
0.000 vs. 30.000	7.373	1.138	0.703	No
15.000 vs. 0.000	7.171	1.106	0.619	No
45.000 vs. 30.000	4.016	0.620	0.788	No
0.000 vs. 45.000	3.358	0.518	0.607	No

Table C-1 Anova Analysis for constant rates of NOM removal using P25 and P25-1.29 wt% Ag

		K_1 (min^{-1})	**Sum of Squares**	**Standard Error**	**Adj. R-Square**	**Prob>F**
UV light	**P25**	0.00418	0.0477	0.0011	0.766	0.0329
	P25-1.29 wt%	0.0054	0.07153	08.61752E-4	0.91	0.00805
Visible light	**P25**	0.0036	0.04007	0.00119	0.68419	0.0529
	P25-1.29 wt%	0.007	0.2279	0.00414	0.322	0.1871

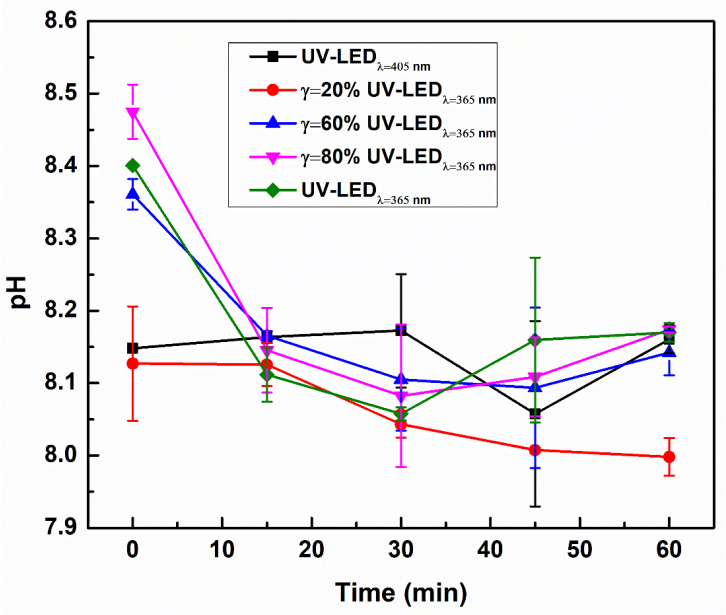

Figure C-1 pH variation in NOM solution using P25-1.29 wt% Ag

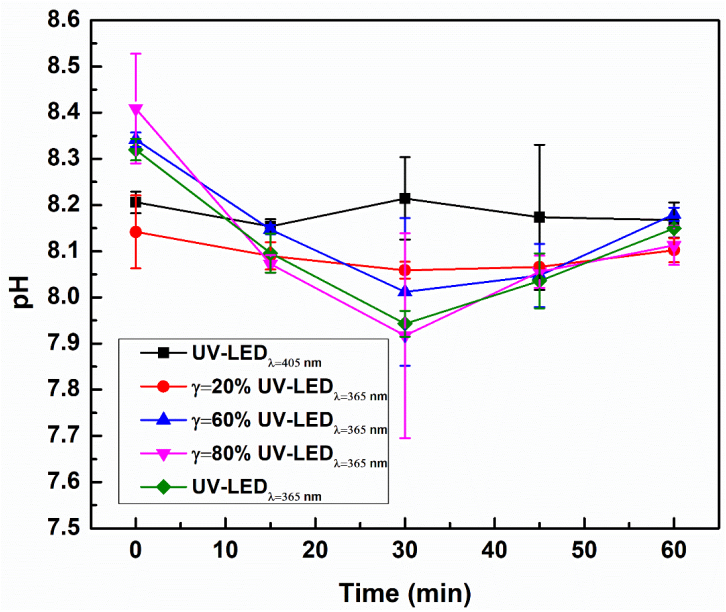

Figure C-2 pH variation for NOM solution using P25

Appendix D

Ven:

One Way Analysis of Variance Monday, November 25, 2019, 7:50:40 PM

Data source: Ven in Pharma

Normality Test (Shapiro-Wilk): Failed (P < 0.050)

Equal Variance Test (Brown-Forsythe): Passed (P = 0.202)

Group Name	N	Missing	Mean	Std Dev	SEM
P25-UV	4	0	0.0974	0.0165	0.00827
P25-Vis	2	0	0.000976	0.000275	0.000194
Ag-UV	4	0	0.0535	0.00344	0.00172
Ag-Vis	4	0	0.00124	0.000704	0.000352

Source of Variation	DF	SS	MS	F	P
Between Groups	3	0.0228	0.00759	88.499	<0.001
Residual	10	0.000857	0.0000857		
Total	13	0.0236			

The differences in the mean values among the treatment groups are greater than would be expected by chance; there is a statistically significant difference (P = <0.001).

Power of performed test with alpha = 0.050: 1.000

All Pairwise Multiple Comparison Procedures (Holm-Sidak method):
Overall significance level = 0.05

Comparisons for factor:

Comparison	Diff of Means	t	P	P<0.050
P25-UV vs. Ag-Vis	0.0961	14.681	<0.001	Yes
P25-UV vs. P25-Vis	0.0964	12.020	<0.001	Yes
Ag-UV vs. Ag-Vis	0.0522	7.979	<0.001	Yes
P25-UV vs. Ag-UV	0.0439	6.702	<0.001	Yes
Ag-UV vs. P25-Vis	0.0525	6.548	<0.001	Yes
Ag-Vis vs. P25-Vis	0.000269	0.0335	0.974	No

One Way Analysis of Variance Monday, November 25, 2019, 7:52:12 PM

Data source: CBZ in Pharma

Normality Test (Shapiro-Wilk): Failed (P < 0.050)

Equal Variance Test (Brown-Forsythe): Passed (P = 0.254)

Group Name	N	Missing	Mean	Std Dev	SEM
P25-UV	4	0	0.0783	0.00452	0.00226
P25-Vis	3	0	0.00185	0.000271	0.000156
Ag-UV	4	0	0.0394	0.00128	0.000641
Ag-Vis	4	1	0.00107	0.000213	0.000123

Source of Variation	DF	SS	MS	F	P
Between Groups	3	0.0143	0.00478	720.075	<0.001
Residual	10	0.0000663	0.00000663		
Total	13	0.0144			

The differences in the mean values among the treatment groups are greater than would be expected by chance; there is a statistically significant difference (P = <0.001).

Power of performed test with alpha = 0.050: 1.000

All Pairwise Multiple Comparison Procedures (Holm-Sidak method):
Overall significance level = 0.05

Comparisons for factor:

Comparison	Diff of Means	t	P	P<0.050
P25-UV vs. Ag-Vis	0.0773	39.276	<0.001	Yes
P25-UV vs. P25-Vis	0.0765	38.879	<0.001	Yes
P25-UV vs. Ag-UV	0.0389	21.383	<0.001	Yes
Ag-UV vs. Ag-Vis	0.0383	19.479	<0.001	Yes
Ag-UV vs. P25-Vis	0.0375	19.082	<0.001	Yes
P25-Vis vs. Ag-Vis	0.000782	0.372	0.718	No

One Way Analysis of Variance Monday, November 25, 2019, 7:53:01 PM

Data source: FLX in Pharma

Normality Test (Shapiro-Wilk): Passed (P = 0.054)

Equal Variance Test (Brown-Forsythe): Passed (P = 0.458)

Group Name	N	Missing	Mean	Std Dev	SEM
P25-UV	4	0	0.0501	0.00339	0.00170
P25-Vis	3	0	0.00354	0.000800	0.000462
Ag-UV	4	0	0.0368	0.00173	0.000864
Ag-Vis	4	0	0.00242	0.000669	0.000335

Source of Variation	DF	SS	MS	F	P

Between Groups	3	0.00650	0.00217	517.395	<0.001
Residual	11	0.0000461	0.00000419		
Total	14	0.00655			

The differences in the mean values among the treatment groups are greater than would be expected by chance; there is a statistically significant difference (P = <0.001).

Power of performed test with alpha = 0.050: 1.000

All Pairwise Multiple Comparison Procedures (Holm-Sidak method):
Overall significance level = 0.05

Comparisons for factor:

Comparison	**Diff of Means**	**t**	**P**	**P<0.050**
P25-UV vs. Ag-Vis	0.0477	32.978	<0.001	Yes
P25-UV vs. P25-Vis	0.0466	29.814	<0.001	Yes
Ag-UV vs. Ag-Vis	0.0344	23.742	<0.001	Yes
Ag-UV vs. P25-Vis	0.0332	21.263	<0.001	Yes
P25-UV vs. Ag-UV	0.0134	9.237	<0.001	Yes
P25-Vis vs. Ag-Vis	0.00112	0.718	0.488	No

One Way Analysis of Variance Monday, November 25, 2019, 7:53:55 PM

Data source: DCF in Pharma

Normality Test (Shapiro-Wilk): Failed (P < 0.050)

Equal Variance Test (Brown-Forsythe): Passed (P = 0.568)

Group Name	**N**	**Missing**	**Mean**	**Std Dev**	**SEM**
P25-UV	4	0	0.119	0.0259	0.0130
P25-Vis	4	0	0.0146	0.00213	0.00106
Ag-P25-UV	3	0	0.0133	0.00366	0.00211
Ag-P25-Vis	4	0	0.0142	0.00253	0.00126

Source of Variation	**DF**	**SS**	**MS**	**F**	**P**
Between Groups	3	0.0324	0.0108	57.371	<0.001
Residual	11	0.00207	0.000188		
Total	14	0.0345			

The differences in the mean values among the treatment groups are greater than would be expected by chance; there is a statistically significant difference (P = <0.001).

Power of performed test with alpha = 0.050: 1.000

All Pairwise Multiple Comparison Procedures (Holm-Sidak method):

Overall significance level = 0.05

Comparisons for factor:

Comparison	Diff of Means	t	P	P<0.050
P25-UV vs. Ag-P25-Vis	0.105	10.819	<0.001	Yes
P25-UV vs. P25-Vis	0.105	10.782	<0.001	Yes
P25-UV vs. Ag-P25-UV	0.106	10.108	<0.001	Yes
P25-Vis vs. Ag-P25-UV	0.00132	0.126	0.999	No
Ag-P25-Vis vs. Ag-P25-UV	0.000967	0.0922	0.995	No
P25-Vis vs. Ag-P25-Vis	0.000358	0.0368	0.971	No

One Way Analysis of Variance Monday, November 25, 2019, 7:54:40 PM

Data source: ACE in Pharma

Normality Test (Shapiro-Wilk): Failed (P < 0.050)

Equal Variance Test (Brown-Forsythe): Passed (P = 0.218)

Group Name	N	Missing	Mean	Std Dev	SEM
P25-UV	4	0	0.167	0.00932	0.00466
P25-Vis	4	0	0.0397	0.00361	0.00180
Ag-UV	4	0	0.430	0.116	0.0578
Ag-Vis	4	0	0.0442	0.0101	0.00503

Source of Variation	DF	SS	MS	F	P
Between Groups	3	0.402	0.134	39.575	<0.001
Residual	12	0.0407	0.00339		
Total	15	0.443			

The differences in the mean values among the treatment groups are greater than would be expected by chance; there is a statistically significant difference (P = <0.001).

Power of performed test with alpha = 0.050: 1.000

All Pairwise Multiple Comparison Procedures (Holm-Sidak method):
Overall significance level = 0.05

Comparisons for factor:

Comparison	Diff of Means	t	P	P<0.050
Ag-UV vs. P25-Vis	0.391	9.489	<0.001	Yes
Ag-UV vs. Ag-Vis	0.386	9.381	<0.001	Yes
Ag-UV vs. P25-UV	0.264	6.408	<0.001	Yes
P25-UV vs. P25-Vis	0.127	3.081	0.028	Yes
P25-UV vs. Ag-Vis	0.122	2.973	0.023	Yes
Ag-Vis vs. P25-Vis	0.00442	0.107	0.916	No

One Way Analysis of Variance Monday, November 25, 2019, 7:55:18 PM

Data source: SMZ in Pharma

Normality Test (Shapiro-Wilk): Failed (P < 0.050)

Equal Variance Test (Brown-Forsythe): Passed (P = 0.131)

Group Name	N	Missing	Mean	Std Dev	SEM
P25-UV	4	0	0.488	0.130	0.0650
P25-Vis	4	0	0.0246	0.00496	0.00248
Ag-UV	4	0	0.923	0.0166	0.00828
Ag-Vis	4	0	0.0206	0.00289	0.00144

Source of Variation	DF	SS	MS	F	P
Between Groups	3	2.243	0.748	173.775	<0.001
Residual	12	0.0516	0.00430		
Total	15	2.295			

The differences in the mean values among the treatment groups are greater than would be expected by chance; there is a statistically significant difference (P = <0.001).

Power of performed test with alpha = 0.050: 1.000

All Pairwise Multiple Comparison Procedures (Holm-Sidak method):
Overall significance level = 0.05

Comparisons for factor:

Comparison	Diff of Means	t	P	P<0.050
Ag-UV vs. Ag-Vis	0.902	19.451	<0.001	Yes
Ag-UV vs. P25-Vis	0.898	19.364	<0.001	Yes
P25-UV vs. Ag-Vis	0.468	10.081	<0.001	Yes
P25-UV vs. P25-Vis	0.464	9.995	<0.001	Yes
Ag-UV vs. P25-UV	0.435	9.370	<0.001	Yes
P25-Vis vs. Ag-Vis	0.00402	0.0866	0.932	No

One Way Analysis of Variance Monday, November 25, 2019, 7:56:04 PM

Data source: eCBZ in Pharma

Normality Test (Shapiro-Wilk): Failed (P < 0.050)

Equal Variance Test (Brown-Forsythe): Passed (P = 0.301)

Group Name	N	Missing	Mean	Std Dev	SEM
P25-UV	4	0	0.0572	0.00117	0.000584
P25-Vis	4	0	0.00188	0.000133	0.0000665

Ag-UV	4	0	0.0277	0.000988	0.000494
Ag-Vis	4	0	0.00230	0.00136	0.000680

Source of Variation	**DF**	**SS**	**MS**	**F**	**P**
Between Groups	3	0.00825	0.00275	2615.463	<0.001
Residual	12	0.0000126	0.00000105		
Total	15	0.00826			

The differences in the mean values among the treatment groups are greater than would be expected by chance; there is a statistically significant difference (P = <0.001).

Power of performed test with alpha = 0.050: 1.000

All Pairwise Multiple Comparison Procedures (Holm-Sidak method):
Overall significance level = 0.05

Comparisons for factor:

Comparison	**Diff of Means**	**t**	**P**	**P<0.050**
P25-UV vs. P25-Vis	0.0553	76.272	<0.001	Yes
P25-UV vs. Ag-Vis	0.0549	75.693	<0.001	Yes
P25-UV vs. Ag-UV	0.0295	40.715	<0.001	Yes
Ag-UV vs. P25-Vis	0.0258	35.557	<0.001	Yes
Ag-UV vs. Ag-Vis	0.0254	34.978	<0.001	Yes
Ag-Vis vs. P25-Vis	0.000420	0.579	0.573	No

One Way Analysis of Variance Monday, November 25, 2019, 7:56:55 PM

Data source: NFLX in Pharma

Normality Test (Shapiro-Wilk): Passed (P = 0.058)

Equal Variance Test (Brown-Forsythe): Passed (P = 0.183)

Group Name	**N**	**Missing**	**Mean**	**Std Dev**	**SEM**
P25-UV	4	0	0.0604	0.00534	0.00267
P25-Vis	4	1	0.00409	0.000714	0.000412
Ag-P25 UV	4	0	0.0309	0.00398	0.00199
Ag-P25 Vis	4	0	0.00237	0.000233	0.000116

Source of Variation	**DF**	**SS**	**MS**	**F**	**P**
Between Groups	3	0.00852	0.00284	232.544	<0.001
Residual	11	0.000134	0.0000122		
Total	14	0.00865			

The differences in the mean values among the treatment groups are greater than would be expected by chance; there is a statistically significant difference (P = <0.001).

Power of performed test with alpha = 0.050: 1.000

All Pairwise Multiple Comparison Procedures (Holm-Sidak method):
Overall significance level = 0.05

Comparisons for factor:

Comparison	Diff of Means	t	P	P<0.050
P25-UV vs. Ag-P25 Vis	0.0581	23.508	<0.001	Yes
P25-UV vs. P25-Vis	0.0564	21.119	<0.001	Yes
P25-UV vs. Ag-P25 UV	0.0295	11.955	<0.001	Yes
Ag-P25 UV vs. Ag-P25 Vis	0.0285	11.553	<0.001	Yes
Ag-P25 UV vs. P25-Vis	0.0268	10.051	<0.001	Yes
P25-Vis vs. Ag-P25 Vis	0.00172	0.645	0.532	No

One Way Analysis of Variance Monday, November 25, 2019, 7:57:49 PM

Data source: TRIM in Pharma

Normality Test (Shapiro-Wilk): Failed (P < 0.050)

Equal Variance Test (Brown-Forsythe): Passed (P = 0.333)

Group Name	N	Missing	Mean	Std Dev	SEM
P25-UV	4	0	0.0495	0.00524	0.00262
P25-Vis	4	1	0.00201	0.000571	0.000329
Ag-UV	4	0	0.0994	0.00819	0.00409
Ag-Vis	4	0	0.00362	0.000663	0.000331

Source of Variation	DF	SS	MS	F	P
Between Groups	3	0.0241	0.00803	309.493	<0.001
Residual	11	0.000285	0.0000259		
Total	14	0.0244			

The differences in the mean values among the treatment groups are greater than would be expected by chance; there is a statistically significant difference (P = <0.001).

Power of performed test with alpha = 0.050: 1.000

All Pairwise Multiple Comparison Procedures (Holm-Sidak method):
Overall significance level = 0.05

Comparisons for factor:

Comparison	Diff of Means	t	P	P<0.050
Ag-UV vs. Ag-Vis	0.0958	26.600	<0.001	Yes
Ag-UV vs. P25-Vis	0.0974	25.039	<0.001	Yes
Ag-UV vs. P25-UV	0.0500	13.869	<0.001	Yes
P25-UV vs. Ag-Vis	0.0459	12.731	<0.001	Yes

P25-UV vs. P25-Vis	0.0475	12.199	<0.001	Yes
Ag-Vis vs. P25-Vis	0.00160	0.412	0.688	No

One Way Analysis of Variance Monday, November 25, 2019, 7:58:45 PM

Data source: SULFA in Pharma

Normality Test (Shapiro-Wilk): Passed (P = 0.923)

Equal Variance Test (Brown-Forsythe): Failed (P < 0.050)

Group Name	N	Missing	Mean	Std Dev	SEM
P25-UV	4	0	0.176	0.00753	0.00376
P25-Vis	4	0	0.0158	0.00414	0.00207
Ag-UV	4	0	0.0572	0.00669	0.00334
Ag-Vis	4	0	0.00797	0.000547	0.000274

Source of Variation	DF	SS	MS	F	P
Between Groups	3	0.0725	0.0242	814.122	<0.001
Residual	12	0.000356	0.0000297		
Total	15	0.0729			

The differences in the mean values among the treatment groups are greater than would be expected by chance; there is a statistically significant difference (P = <0.001).

Power of performed test with alpha = 0.050: 1.000

All Pairwise Multiple Comparison Procedures (Holm-Sidak method):
Overall significance level = 0.05

Comparisons for factor:

Comparison	Diff of Means	t	P	P<0.050
P25-UV vs. Ag-Vis	0.168	43.695	<0.001	Yes
P25-UV vs. P25-Vis	0.161	41.672	<0.001	Yes
P25-UV vs. Ag-UV	0.119	30.916	<0.001	Yes
Ag-UV vs. Ag-Vis	0.0492	12.779	<0.001	Yes
Ag-UV vs. P25-Vis	0.0414	10.755	<0.001	Yes
P25-Vis vs. Ag-Vis	0.00780	2.024	0.066	No

One Way Analysis of Variance Monday, November 25, 2019, 7:59:50 PM

Data source: MON in Pharma

Normality Test (Shapiro-Wilk): Passed (P = 0.648)

Equal Variance Test (Brown-Forsythe): Failed (P < 0.050)

Group Name	N	Missing	Mean	Std Dev	SEM
P25-UV	4	0	0.0585	0.00424	0.00212
P25-Vis	4	0	0.00243	0.000769	0.000385
Ag-UV	4	0	0.0452	0.00402	0.00201
Ag-Vis	4	0	0.00342	0.00104	0.000521

Source of Variation	DF	SS	MS	F	P
Between Groups	3	0.00992	0.00331	369.649	<0.001
Residual	12	0.000107	0.00000895		
Total	15	0.0100			

The differences in the mean values among the treatment groups are greater than would be expected by chance; there is a statistically significant difference (P = <0.001).

Power of performed test with alpha = 0.050: 1.000

All Pairwise Multiple Comparison Procedures (Holm-Sidak method):
Overall significance level = 0.05

Comparisons for factor:

Comparison	Diff of Means	t	P	P<0.050
P25-UV vs. P25-Vis	0.0561	26.505	<0.001	Yes
P25-UV vs. Ag-Vis	0.0551	26.038	<0.001	Yes
Ag-UV vs. P25-Vis	0.0427	20.199	<0.001	Yes
Ag-UV vs. Ag-Vis	0.0417	19.733	<0.001	Yes
P25-UV vs. Ag-UV	0.0133	6.306	<0.001	Yes
Ag-Vis vs. P25-Vis	0.000988	0.467	0.649	No

Solid phase extraction of Pharmaceuticals